

DESIGN OF AN ANTI-JERK CONTROLLER FOR BOTH LOCKED AND  
SLIPPING TORQUE CONVERTER CONDITIONS IN A VEHICLE

By

Syed Ahmad Nadeem

A THESIS

Submitted in partial fulfillment of the requirements for the degree of

MASTER OF SCIENCE

In Mechanical Engineering - Engineering Mechanics

MICHIGAN TECHNOLOGICAL UNIVERSITY

2020

© 2020 Syed Ahmad Nadeem



This thesis has been approved in partial fulfillment of the requirements for the Degree of MASTER OF SCIENCE in Mechanical Engineering - Engineering Mechanics.

Department of Mechanical Engineering - Engineering Mechanics

Thesis Co-advisor: *Dr. Mahdi Shahbakhti*

Thesis Co-advisor: *Dr. Darrell Robinette*

Committee Member: *Dr. Jeremy Worm*

Department Chair: *Dr. Dr. William W. Predebon*



# Contents

List of Figures . . . . .	xi
List of Tables . . . . .	xv
Preface . . . . .	xvii
Acknowledgments . . . . .	xix
Nomenclature . . . . .	xxi
List of Abbreviations . . . . .	xxvii
Abstract . . . . .	xxix
<b>1 Introduction . . . . .</b>	<b>1</b>
1.1 Motivation . . . . .	1
1.2 Technical terms used in this work . . . . .	5
1.3 Literature Review . . . . .	10
1.3.1 AJC torque shaping controllers . . . . .	11
1.3.2 Control oriented modeling of torque converter . . . . .	15

1.3.3	Model predictive control of drivetrain . . . . .	18
1.4	Research scope and Thesis organisation . . . . .	21
<b>2</b>	<b>Anti-Jerk controller development for locked torque converter in contact mode . . . . .</b>	<b>25</b>
2.1	Background . . . . .	26
2.2	State space model of the ROM . . . . .	28
2.2.1	Equations of motion from ROM . . . . .	28
2.2.2	State space model development . . . . .	31
2.2.3	Validation of the state space model . . . . .	33
2.3	Development of control strategy . . . . .	35
2.3.1	Realisation of the drivetrain dynamics . . . . .	37
2.3.1.1	Actuator dynamics under consideration . . . . .	37
2.3.1.2	Shuffle dynamics of drivetrain . . . . .	38
2.3.2	Design of Pre-compensator . . . . .	39
2.3.3	Design of feedback controller . . . . .	43
2.3.4	Analyses of the overall controller response . . . . .	48
2.4	Performance evaluation . . . . .	51
2.4.1	Processor-In-the-Loop (PIL) validation . . . . .	52
<b>3</b>	<b>Model-based feedforward and feedback control to meet requested torque during torque converter slip . . . . .</b>	<b>59</b>
3.1	Background . . . . .	62

3.2	Control strategy layout . . . . .	64
3.2.1	Anti-lag torque control (ALTC) . . . . .	66
3.3	Phase I: Driveline state space modeling with locked torque converter clutch . . . . .	67
3.3.1	State-space model development . . . . .	68
3.3.2	Validation of the state space model . . . . .	70
3.4	Phase II: Inversion of torque converter model . . . . .	72
3.4.1	Torque converter model assembly . . . . .	72
3.4.1.1	Friction path . . . . .	73
3.4.1.2	Fluid path - Speed Ratio, Torque Ratio and Capacity Factor (K-Factor lookup table model) . . . . .	74
3.4.1.3	Fluid path - Kotwicki model . . . . .	75
3.4.1.4	Determination of the Kotwicki coefficients . . . . .	79
3.4.1.5	Validation of Kotwicki model . . . . .	80
3.4.2	Inversion of torque converter model . . . . .	82
3.4.3	Comparison of inverted torque converter models . . . . .	85
3.5	Phase III: Controller development . . . . .	88
3.5.1	Feedforward path . . . . .	90
3.5.2	Feedback path . . . . .	92
3.6	Results, validation and limitations . . . . .	93
3.6.1	Processor-In-the-Loop validation . . . . .	97

<b>4</b>	<b>Model predictive control of TCC capacity and actuator torque to deliver requested torque during torque converter slip . . . . .</b>	<b>99</b>
4.1	Control Strategy . . . . .	101
4.2	Mathematical modeling of driveline with torque converter slipping .	102
4.2.1	Reduced order model with redistributed inertia . . . . .	103
4.2.2	Equations of motion . . . . .	106
4.2.3	Nonlinear torque converter model . . . . .	107
4.2.3.1	Kotwicki approximation . . . . .	108
4.2.4	Linearisation of the torque converter model . . . . .	109
4.2.5	Development of linearised mathematical model of driveline .	110
4.2.6	Performance comparison of nonlinear model with linear approximation . . . . .	112
4.3	Prediction based on developed linear model . . . . .	113
4.3.1	Overview . . . . .	113
4.3.2	Augmentation of the model under consideration . . . . .	115
4.3.3	Development of prediction matrices . . . . .	119
4.3.4	Unconstrained optimisation problem . . . . .	120
4.3.5	Results for unconstrained optimisation . . . . .	122
4.4	Constraints set-up . . . . .	124
4.4.1	Constraint on rate of input . . . . .	125
4.4.2	Constraint on magnitude of input . . . . .	127

4.4.3	Constraint on model impeller and turbine speeds . . . . .	130
4.5	Formulation of model predictive control problem . . . . .	135
4.5.1	Results and discussions . . . . .	138
4.5.2	Effect of transient fluid dynamics of torque converter . . . . .	140
<b>5</b>	<b>Conclusion and Future Work . . . . .</b>	<b>143</b>
5.1	Conclusion . . . . .	143
5.2	Future work . . . . .	150
	<b>References . . . . .</b>	<b>151</b>
	<b>A Validation of Kotwicki Model . . . . .</b>	<b>161</b>
	<b>B Software Versions . . . . .</b>	<b>169</b>
	<b>C Program and Data File Summary . . . . .</b>	<b>171</b>
C.1	Chapter 1 . . . . .	171
C.2	Chapter 2 . . . . .	172
C.3	Chapter 3 . . . . .	173
C.4	Chapter 4 . . . . .	174



# List of Figures

1.1	Sales of passenger cars in selected countries worldwide from 2005 to 2019 [1] . . . . .	2
1.2	US light truck retail sales from 1980 to 2019 (in 1000 units) [2] . . .	3
1.3	Contact and backlash mode . . . . .	7
1.4	3-part Torque converter assembly . . . . .	9
1.5	Approaches for torque converter modeling . . . . .	19
1.6	Layout of the thesis work . . . . .	23
2.1	Driveline performance with observed shuffle . . . . .	27
2.2	Schematic representation of reduced order model for contact mode .	29
2.3	Validation of the state space model with ROM - comparison of the output response . . . . .	34
2.4	Overall schematic of the designed AJC control strategy . . . . .	36
2.5	Bode response of the plant transfer function . . . . .	40
2.6	Step input response of the driveline with different pre-compensator designs . . . . .	42
2.7	Pole zero map of the driveline plant . . . . .	46

2.8	Block diagram analyses of the developed control strategy . . . . .	49
2.9	Bode response analyses of the controller . . . . .	50
2.10	Response comparison of driveline with and without AJC controller .	53
2.11	Schematic of the designed PIL setup . . . . .	54
2.12	Performance of the AJC controller in the PIL setup . . . . .	57
3.1	Response of AJC controlled driveline with slipping torque converter clutch . . . . .	61
3.2	Schematic of torque converter assembly with distinct torque flow paths . . . . .	63
3.3	Overall schematic of proposed control strategy . . . . .	65
3.4	Categorisation of the proposed control strategy . . . . .	66
3.5	Output comparison of proposed state space model with full-order model . . . . .	71
3.6	Torque ratio versus Speed Ratio . . . . .	76
3.7	Capacity factor versus Speed Ratio . . . . .	76
3.8	Fluid path torque band - Impeller . . . . .	77
3.9	Fluid path torque band - Turbine . . . . .	77
3.10	Kotwicky coefficients estimation for impeller fluid path torque . . .	81
3.11	Kotwicky coefficients estimation for turbine fluid path torque . . . .	81
3.12	Validation of the developed Kotwicky (Kot.) model . . . . .	83

3.13 Comparison of the Kotwicki based inverted torque converter model w.r.t. TR and $K_{cap}$ based inverted model. . . . .	87
3.14 Anti-lag torque control . . . . .	88
3.15 Anti-lag torque control - modified strategy layout . . . . .	90
3.16 Driveline response after implementing the designed model-based ALTC . . . . .	94
3.17 Controller performance evaluation - reference speed tracking and ac- tuator constraints . . . . .	96
3.18 Performance of the model-based ALTC in the PIL setup . . . . .	98
4.1 Schematic of MPC based control strategy . . . . .	101
4.2 Reduced order model with torque converter slipping . . . . .	103
4.3 Comparison of modified ROM with FOM for slipping TCC . . . . .	105
4.4 Comparison of the nonlinear model output with its linearised predic- tion at equilibrium points . . . . .	114
4.5 Unconstrained optimisation of inputs at a known equilibrium point	123
4.6 Designed MPC architecture for ALTC . . . . .	136
4.7 MPC controlled driveline response for slipping torque converter clutch	139
4.8 MPC response to torque converter with first order transient fluid dy- namics . . . . .	142
A.1 Results obtained for Test-case:1 . . . . .	162
A.2 Results obtained for Test-case:2 . . . . .	163

A.3	Results obtained for Test-case:3 . . . . .	164
A.4	Results obtained for Test-case:4 . . . . .	165
A.5	Results obtained for Test-case:5 . . . . .	166

# List of Tables

2.1	Characterstics of the considered actuator . . . . .	38
2.2	Lead compensator parameters . . . . .	48
2.3	Step input comparison of driveline performance with and without im- plemented AJC . . . . .	51
2.4	MicroAutoBox and PC Configurations . . . . .	55
2.5	PIL performance assessment . . . . .	56
3.1	Kotwicki coefficients for impeller torque . . . . .	80
3.2	Kotwicki coefficients for turbine torque . . . . .	81
3.3	PIL performance parameters . . . . .	97
4.1	Comparison of lumped inertia distribution for ROM with locked and slipping torque converter lockup clutch . . . . .	104
4.2	Percentage error for modified ROM validation . . . . .	106
4.3	Known parameters for equilibrium point . . . . .	122
4.4	Performance comparison of developed ALTC strategies . . . . .	140
A.1	Test cases considered for Kotwicki model validation . . . . .	167

A.2 Percentage error observed for the Kotwicki model for different test cases . . . . .	167
B.1 Software versions . . . . .	169
C.1 Figure files - Chapter 1 . . . . .	171
C.2 Figure files - Chapter 2 . . . . .	172
C.3 Simulink and Amesim model files - Chapter 2 . . . . .	172
C.4 Matlab script and dataset files - Chapter 2 . . . . .	173
C.5 Figure files - Chapter 3 . . . . .	173
C.6 Simulink and Amesim model files - Chapter 3 . . . . .	174
C.7 Matlab script and dataset files - Chapter 3 . . . . .	174
C.8 Figure files - Chapter 4 . . . . .	175
C.9 Simulink and Amesim model files - Chapter 4 . . . . .	175
C.10 Matlab script and dataset files - Chapter 4 . . . . .	176

# Preface

The work in this thesis is developed on the work done in the past by Prince Lakhani [3], Prithvi Reddy[4] and Kaushal Darokar [5]. The Full order model used in this work was developed in [4]. Further, the reduced order model used in Sections 2.2.1, 3.3 and 4.2 of this work were built upon the work done by Prithvi Reddy and Kaushal Darokar in [4] and [5]. The Anti-jerk controller related work presented in Chapter 2 of this thesis is done in collaboration with Prithvi Reddy. The tabulated data for the torque converter empirical model data was provided by Ford Motor Company. Dr. Maruthi Ravichandran and Dr. Jeffrey Doering from Ford Motor Company provided their insights on the AJC development for shuffle control in contact mode, as mentioned across Chapter 2. Dr. Mahdi Shahbakhti provided his constant guidance throughout the course of this project.



## Acknowledgments

First of all I would like to thank Dr. Mahdi Shahbakhti and Dr. Darrell Robinnette for providing me with this golden opportunity to work on this interesting project. There constant guidance and support has helped me become an enthusiastic learner both in technically and socially. Next, I wanted to thank Dr. Jeremy Worm for accepting my request to be a member of my defense committee.

I would also like to take this opportunity to thank Dr. Maruthi Ravichandran and Dr. Jeffrey Doering from Ford Motor Company for their valuable technical insights during the initial phases of this work.

I am thankful to Prince and Kaushal whose contribution in this project established the stepping stone for the work done during the course of this thesis. I also wanted to specially thank Prithvi for his patience and guidance as his inputs have been of great value addition to this work.

Next, I would like to thank Divyaditya, Utkarsh, Shivam and Himanshu for being constantly supportive and making a relaxed environment around, during the course of this work.

At last, a special thanks to my parents, Sabiha and Nadeem, whose love and support

for me has made me what I am, and my sister Aqsa whose constant faith in me knows no bounds.

# Nomenclature

$\alpha_{1,act}$	I <sup>st</sup> coeff. of Kotwicki eq. for impeller torque [ $Nm/(rad/s)^2$ ]
$\alpha_{2,act}$	II <sup>2nd</sup> coeff. of Kotwicki eq. for impeller torque [ $Nm/(rad/s)^2$ ]
$\alpha_{3,act}$	III <sup>rd</sup> coeff. of Kotwicki eq. for impeller torque [ $Nm/(rad/s)^2$ ]
$\alpha_{1,tu}$	I <sup>st</sup> coeff. of Kotwicki eq. for impeller torque [ $Nm/(rad/s)^2$ ]
$\alpha_{2,tu}$	II <sup>2nd</sup> coeff. of Kotwicki eq. for impeller torque [ $Nm/(rad/s)^2$ ]
$\alpha_{3,tu}$	III <sup>rd</sup> coeff. of Kotwicki eq. for impeller torque [ $Nm/(rad/s)^2$ ]
$\Delta T_{act}^*$	Commanded change in the actuator torque [ $Nm$ ]
$\Delta T_{act}$	Change in the actuator torque [ $Nm$ ]
$\Delta T_c^*$	Commanded change in the TCC capacity [ $Nm$ ]
$\Delta T_c$	Change in the TCC capacity [ $Nm$ ]
$\theta_{act}$	Angular position of actuator [ $rad$ ]
$\dot{\theta}_{act}$	Angular velocity of actuator [ $rad/s$ ]
$\dot{\theta}_{act}^*$	Reference/commanded angular velocity of actuator/impeller [ $rad/s$ ]
$\ddot{\theta}_{act}$	Angular acceleration of actuator [ $rad/s^2$ ]
$\theta_{fd}$	Angular position of lumped rotational inertia $J_2$ [ $rad$ ]
$\dot{\theta}_{fd}$	Angular velocity of lumped rotational inertia $J_2$ [ $rad/s$ ]
$\ddot{\theta}_{fd}$	Angular acceleration of lumped rotational inertia $J_2$ [ $rad/s^2$ ]
$\theta_{imp}$	Angular position of impeller [ $rad$ ]

$\dot{\theta}_{\text{imp}}$	Angular velocity of impeller [ $rad/s$ ]
$\ddot{\theta}_{\text{imp}}$	Angular acceleration of impeller [ $rad/s^2$ ]
$\theta_{\text{tu}}$	Angular position of turbine [ $rad$ ]
$\dot{\theta}_{\text{tu}}$	Angular velocity of turbine [ $rad/s$ ]
$\ddot{\theta}_{\text{tu}}$	Angular acceleration of turbine [ $rad/s^2$ ]
$\dot{\theta}_{\text{tu}}^*$	Reference angular turbine velocity from locked TCC ROM [ $rad/s$ ]
$\theta_{\text{w}}$	Angular position of lumped rotational inertia $J_3$ [ $rad$ ]
$\dot{\theta}_{\text{w}}$	Angular velocity of lumped rotational inertia $J_3$ [ $rad/s$ ]
$\ddot{\theta}_{\text{w}}$	Angular acceleration of lumped rotational inertia $J_3$ [ $rad/s^2$ ]
$\theta_1$	Actuator side angular position of lumped propeller shaft [ $rad$ ]
$\theta_2$	Wheel side angular position of the lumped shaft [ $rad$ ]
$\dot{\theta}_1$	Actuator side angular velocity of lumped propeller shaft [ $rad/s$ ]
$\dot{\theta}_2$	Wheel side angular velocity of the lumped shaft [ $rad/s$ ]
$\mu$	Coefficient of friction between clutching elements of TCC [–]
a	Zero added by the compensator [–]
b	Pole added by the compensator [–]
$c_s$	Damping coefficient of lumped propeller shaft [ $Nm/(rad/s)$ ]
$c_w$	Damping coefficient of lumped axle shaft [ $Nm/(rad/s)$ ]
$F_1$	road load resistances [ $Nm$ ]
$f_p$	Pass band frequency of butterworth low pass filter [ $Hz$ ]
$f_s$	Stop band frequency of butterworth low pass filter [ $Hz$ ]

$i_t$	Transmission gear ratio $[-]$
$i_{fd}$	final drive ratio $[-]$
$J_{imp}$	Impeller rotational inertia $[kg.m^2]$
$J_{tu}$	Turbine rotational inertia $[kg.m^2]$
$J_{act}$	Actuator rotational inertia $[kg.m^2]$
$J_{tc}$	Total torque converter rotational inertia $[kg.m^2]$
$J_{tc,1}$	Impeller rotational inertia of torque converter $[kg.m^2]$
$J_{tc,2}$	Turbine rotational inertia of torque converter $[kg.m^2]$
$J_{trans}$	Transmission assembly rotational inertia $[kg.m^2]$
$J_{propshaft}$	FOM propeller shaft rotational inertia $[kg.m^2]$
$J_{fd}$	rotational inertia of the final drive $[kg.m^2]$
$J_{tire}$	Tire rotational inertia $[kg.m^2]$
$J_{axle}$	Axle shaft rotational inertia $[kg.m^2]$
$J_{wheel}$	Wheel rotational inertia $[kg.m^2]$
$k_c$	lead compensator gain $[-]$
$K_{cap}$	Capacity Factor for torque converter model $[(rad/s)/(\sqrt{Nm})]$
$k_i$	integral gain of the PI controller $[-]$
$k_p$	proportional gain of the PI controller $[-]$
$k_s$	stiffness coefficient of lumped propeller shaft $[Nm/rad]$
$k_w$	stiffness coefficient of lumped axle shaft $[Nm/rad]$
$M$	Mass of the vehicle $[kg]$

$N$	Normal reaction between the clutching elements [ $Nm$ ]
$N_c$	Control horizon $[-]$
$N_p$	Prediction horizon $[-]$
$R_{\text{eff}}$	effective radius of clutch [ $mm$ ]
$r_T$	Radius of the tire [ $m$ ]
$SR$	Speed ratio for torque converter model $[-]$
$TR$	Torque ratio for torque converter model $[-]$
$T_{\text{act}}$	Delivered actuator torque [ $Nm$ ]
$T_{\text{act}}^*$	Commanded actuator torque [ $Nm$ ]
$T_{\text{act},1}^*$	Pre-compensator based commanded actuator torque [ $Nm$ ]
$T_{\text{act},2}^*$	lead compensator based commanded actuator torque [ $Nm$ ]
$T_c$	Commanded clutch capacity [ $Nm$ ]
$T_{\text{dr}}^*$	Driver requested torque [ $Nm$ ]
$T_{\text{feedforward}}^*$	Feedforward commanded torque for model based ALTC [ $Nm$ ]
$T_{\text{feedback}}^*$	feedback commanded torque for model based ALTC [ $Nm$ ]
$T_{\text{imp,fluid}}$	Impeller fluid path torque of torque converter [ $Nm$ ]
$T_{\text{load}}$	Road load resistive torque [ $Nm$ ]
$T_{\text{res}}$	load on turbine [ $Nm$ ]
$T_s$	Lumped propeller shaft torque from ROM [ $Nm$ ]
$\dot{T}_s$	Lumped propeller shaft torque derivative from ROM [ $Nm$ ]
$T_{\text{shaped,cm}}$	contact mode shaped torque by AJC [ $Nm$ ]

$T_{tu}$	Torque at turbine [ $Nm$ ]
$T_{tu}^*$	Shaped AJC torque at turbine during TCC slip [ $Nm$ ]
$T_{tu,fluid}$	Turbine fluid path torque of torque converter [ $Nm$ ]
$T_w$	Lumped axle shaft torque from ROM [ $Nm$ ]



## List of Abbreviations

ALTC	Anti-lag torque controller
AJC	Anti-Jerk Controller
EV	Electric vehicle
FOM	Full order model
GUI	Graphical user interface
HEV	Hybrid electric vehicle
HIL	Hardware-In-Loop
ICE	Internal combustion engine
LQR	Linear Quadratic Regulator
MABx	Microautobox
MPC	Model predictive control
NVH	Noise vibration and harshness
PFA	Piece-wise affine
PI	Proportional integrator
PIL	Processor-In-Loop
ROM	Reduced order model
RTI	Real time implementation
SS	State space

TCC

Torque converter clutch

## Abstract

With the advancement in the automotive technologies, the customer scrutiny on the ride comfort of automobiles has come to light. Vehicle drivability is one of the important aspects that defines the ride comfort for a vehicle. Drivability of a vehicle is a qualitative measure and may differ from person to person, however, researches have come up to highlight a few parameters that can categorise the drivability performance of a vehicle into good or bad for a majority of the targeted audience. One of those parameters include shuffle, which is defined as the longitudinal oscillations that occurs in the drivetrain when a sudden demand for torque rise or drop is made. Another such parameter is the sluggishness in the delivery of torque at wheels against the requested torque by the driver. This can exist due to the shift in the dynamics during the drivetrain operation from locked torque converter clutch to slipping torque converter clutch.

This work addresses both the drivability related issues, namely, shuffle and torque lag mentioned in the preceding para. Initially, the shuffle oscillations generated in a vehicle are analysed when subjected to a sudden positive to positive driver torque tip-in request. Further, a pre-compensator and feedback controller based control scheme is designed to damp those shuffle oscillations while keeping the torque delivery response fast. This control approach shapes the actuator torque (i.e., an engine or

an e-motor) in such a way that the desired response is achieved. Next, the problem of sluggish torque response at wheels due to slipping of the torque converter clutch is addressed. Initially, a model-based feedforward and feedback controller is developed to control the actuator torque such that when the torque converter slips, an extra compensatory torque from the actuator is applied. This compensation torque ensures that the torque response at the turbine and succeeding driveline components up till the wheels is maintained as desired. However, the actuator has some physical limitations in terms of the maximum magnitude and rate of the torque delivery. So, at some instances, the torque request generated by the controller may not be feasible for the actuator to follow. This problem is addressed when another controller, based on model predictive control approach, is proposed. This controller is based on the approach that continuously updates the controller of the torque delivery of the actuator. The controller solves an optimisation problem over the defined constraints of the actuator and plant, and further finds the most feasible response for the actuator to follow within its defined operating range. Later, A comparison between the two controllers showed model predictive controller to be 15.3% better in terms of the propeller shaft torque response than the feedforward and feedback controller, for the problem under discussion.

# Chapter 1

## Introduction

### 1.1 Motivation

With the unprecedented upsurge in the number of automobiles on road today, the buyers have been at the luxury of choosing the vehicle of their choice, almost exactly, if not perfectly, aligning with the features that they wish for in an ideal vehicle. A statistic from a survey conducted by the Organisation Internationale des Constructeurs d'Automobiles (OICA), [1], showcases the trend in the sales of the passenger cars worldwide over the past decade and a half (see Figure 1.1). The figure shows that countries like China have marked a number in the passenger car sales of around 22 million units in recent times. In the US, this number is around 5 million. However,

Fig

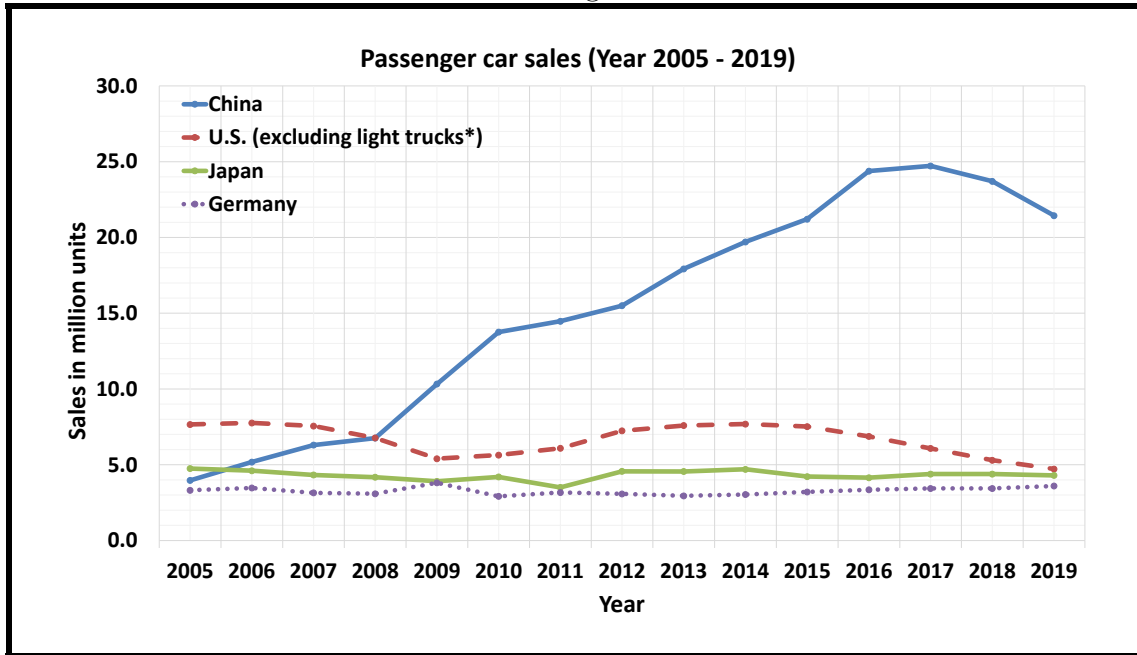


**Figure 1.1:** Sales of passenger cars in selected countries worldwide from 2005 to 2019 [1]

a report on US automotive market [6] shows that the market is inclined towards the light duty truck sales as it mentions a statistic for year 2018 where the light duty truck sales showed a rise of 7.7 percent, approximating to 11.98 million units - a number that has never been reached by the car sales. The study in reference [2] also showcases this by demonstrating a trend for the retail sales of the light duty truck in the US auto market (see Figure 1.2).

As the advancement in the technologies equipped in a modern day automobile is realised, the customer's perspective of exploring the performance and comfort aspect of a vehicle has come into light. Earlier, during the 80s and 90s, safety and fuel economy used to be the prime criteria while making the selection for a car. However,

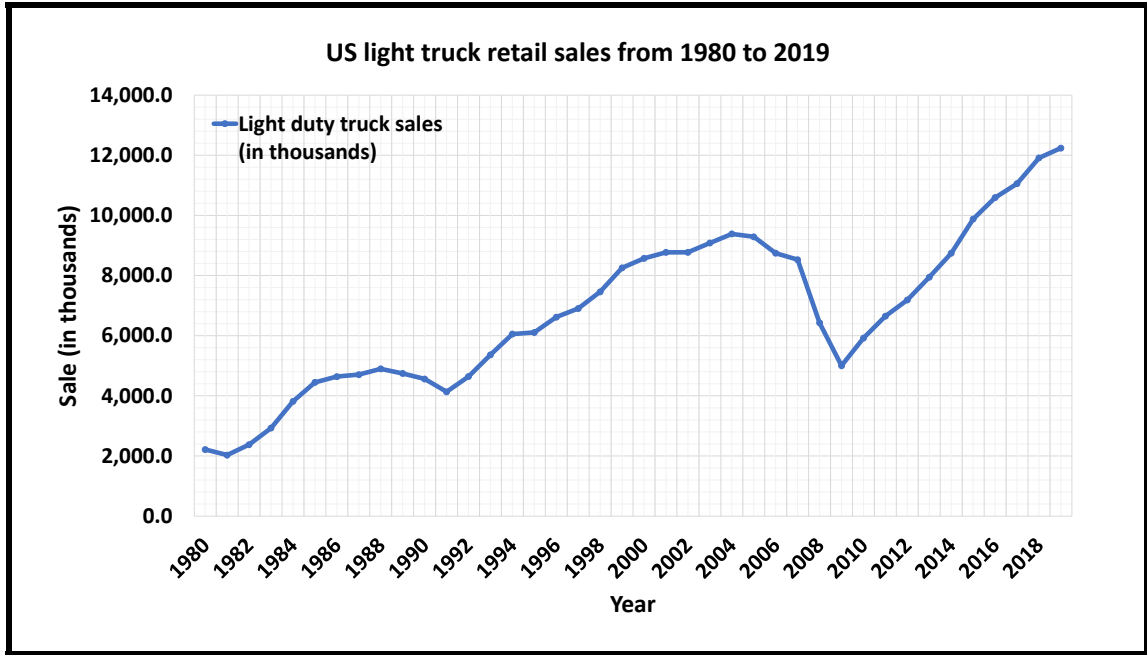


**Figure 1.2:** US light truck retail sales from 1980 to 2019 (in 1000 units) [2]

with the advent of the modernisation in the automotive technologies, such as hybridisation, electrification, automation etc., almost all the vehicles competing within a similar price range and application segment, are likely to offer approximately same fuel economy meeting the safety norms set by the respective governing organisations, [7]. Hence, the focus of the customer has now shifted on other characteristics of the vehicle such as performance and comfort. As a result, this change in the customer's perception is the new addition to the Original Equipment Manufacturer's (OEMs) reality.

A few of the characteristics that are looked upon by customers today on a broader level while purchasing a passenger vehicle are listed in [8]. One such parameter is the drivability performance of the vehicle. Further, as mentioned in [9], vehicle drivability

is evolving as a key decisive factor for the marketability and competitiveness among the passenger vehicles. Drivability can be understood as a combination of two words - 'drive' and 'able'. Jointly, the word is comprehended as the ability of the vehicle to propel while augmenting upon characteristics like, vehicle jerks, torque lag at wheels, pedal response, actuator oscillations (engine and/or motor) in terms of its speed and torque, smooth gear shifts etc. The study in reference [5] lists a few major criterion considered under the drivability assessment of the vehicle. As can be apprehended through these parameters, drivability is a rather qualitative terminology unlike other quantifiable vehicle characteristics like fuel economy, safety standard, cost etc.

The noise mask of the actuator that was earlier present in an internal combustion engine (ICE)-only vehicle is bound to reduce in an electric vehicle or the one comprised of a hybrid electric drivetrain. Sandberg et. al., in [10], show a comparison of noise levels for a hybrid electric vehicle (HEV), operated in electric vehicle (EV) mode, with two ICE only operated vehicles and accentuate the lower noise generation in EV. Also, the torque delivery response of a motor is faster than that of an engine, thus increasing the possibility of induction of higher amplitude jerks while driving with sudden acceleration demands. Furthermore, the recent trend in the electric vehicle industry from the year 2014 to 2018 is showcased in [11]. It mentions that there is a 59% growth in the global light EV sales year on year since 2014. This trend in electric vehicles, which are comparatively quieter, further underlines the need to focus on an improved drivability response.

Moreover, in recent times a major research focus in the automotive industry is towards the driverless or the autonomous vehicles. With the addition of autonomy in the vehicles, the passenger is expected to continue through their routine tasks while the vehicle is driving on its own. A major factor in the execution of this plan is the implementation of comfortable, smooth, noiseless and jerk-free ride. This again entails the need to look towards a smooth and lag-free driveline response, hence the motivation for this work.

All the factors mentioned in this section demand for a feature that controls such induced anomalies to an ideal drivability response. Initially, this work addresses the problem of the vehicle jerks induced, when the driver requests for a sudden increase in the actuator delivered torque, demanding a rise from lower positive acceleration to a higher positive acceleration. Further, this work also emphasizes on the overcoming of a torque lag in the drivability response observed when the torque converter clutch is made to slip. All these issues, if not addressed, can generate a repulsive or unpleasant impression while driving.

## **1.2 Technical terms used in this work**

This section defines the basic terminologies used in this work and further discusses the problem statements considered in this work with the intention of helping the reader

to understand this work in a better way.

An automotive driveline consists of multiple elements and sub-assemblies where each of them play an important role in deciding the drivability of the vehicle. A discussion about a few such elements and sub-assemblies is provided, that shall aid in analysing the drivability parameter at best.

A **gearbox** is a sub-assembly within the driveline with a multiple number of gear pairs incorporated within. There can be various ways these gear pairs are assembled and engaged, leading to one of the criteria for its classification. However, the primary purpose of each gear pair is to modify either the torque or the angular speed across its input and output at the expense of the other. Since, the torque and angular speeds rated for the actuator are not sufficient enough to propel the vehicle in all conditions, a gearbox provide a feature to widen this torque and speed band of the source and hence allow the vehicle to maneuver across various scenarios.

In order to allow a smooth rotation of the gears in a gear pair, slight clearance is provided in the gear geometry between the two adjacent teeth of a gear. This clearance, known as **backlash**, allows the mating gear tooth to rotate seamlessly, transmitting torque across without any interference. Also, due to this clearance lubricant is allowed to flow through the gap during the gear meshing, allowing the heat generated due to friction to escape. This prevents the overheating of the gear that can further lead to its damage.

When operating without the presence of any torque from the source or during the torque reversal scenarios (tip-in and/or tip-out), this backlash region allows a play between the teeth of the two mating gears. Under the action of the actuator torque, the contact between these two gear teeth in mesh tends to make and break. When such meshing gear teeth elements are in contact during vehicle propagation, this is referred to as **contact mode** operation of the driveline. Further, when the connection between the meshing elements tend to break for the traversal of backlash, this mode is referred to as **backlash mode**. Figure 1.3 shows the contact and backlash modes existing in a gear pair.

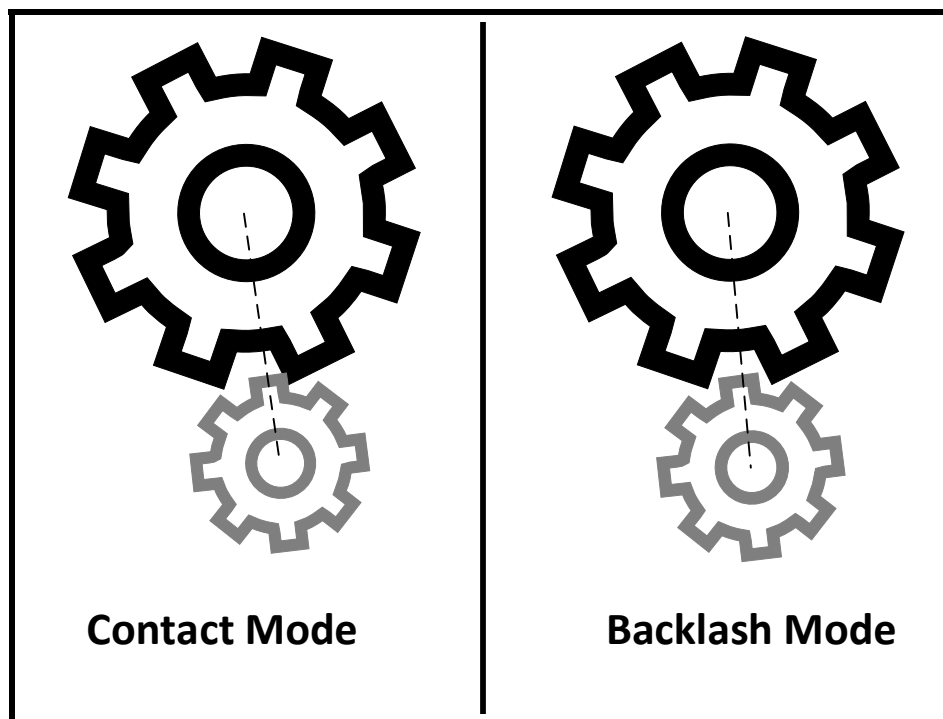


**Figure 1.3:** Contact and backlash mode

Another important element of a drivetrain is its shafts. Shafts are the monolithic

(single-piece) rotating components responsible for the transmission of the torque (and angular rotation) from its one end to another. However, by the virtue of the compliance property (i.e., the property of elasticity), they tend to twist while acting under a rotational load at one end i.e. any external torque, when the other end is connected to some inertial load. This phenomena of shaft twisting under an active torque and an inertial load often leads to oscillations when the acting load varies in magnitude or direction or both, like for the cases of vehicle tip-in. Such oscillations induced in the half shafts or axles in the drivetrain can have negative effects on the drivability experience and are studied under the noise, vibration and harshness (NVH) analyses of the drivetrain. These longitudinal oscillations pertaining in the driveline are referred to as **shuffle** and are addressed in this work.

Another important aspect of this work focuses on the **torque converter** assembly of the drivetrain. A torque converter is a device that transfers the torque from its one end to another by the virtue of involved hydraulic coupling or fluid coupling. The torque converter is composed of three sub elements, namely, **pump** or **impeller**, **turbine** and a **stator**. The pump is connected to the actuator shaft and is responsible for the application of torque on the turbine through the fluid coupling. The stator is connected to a one way clutch that intermediately fixes its position with respect to the impeller and turbine. This allows the torque to amplify while propagating from the impeller to turbine. Figure 1.4 shows the basic elemental structure of a 3 part (i.e., impeller, turbine and stator) torque converter assembly.

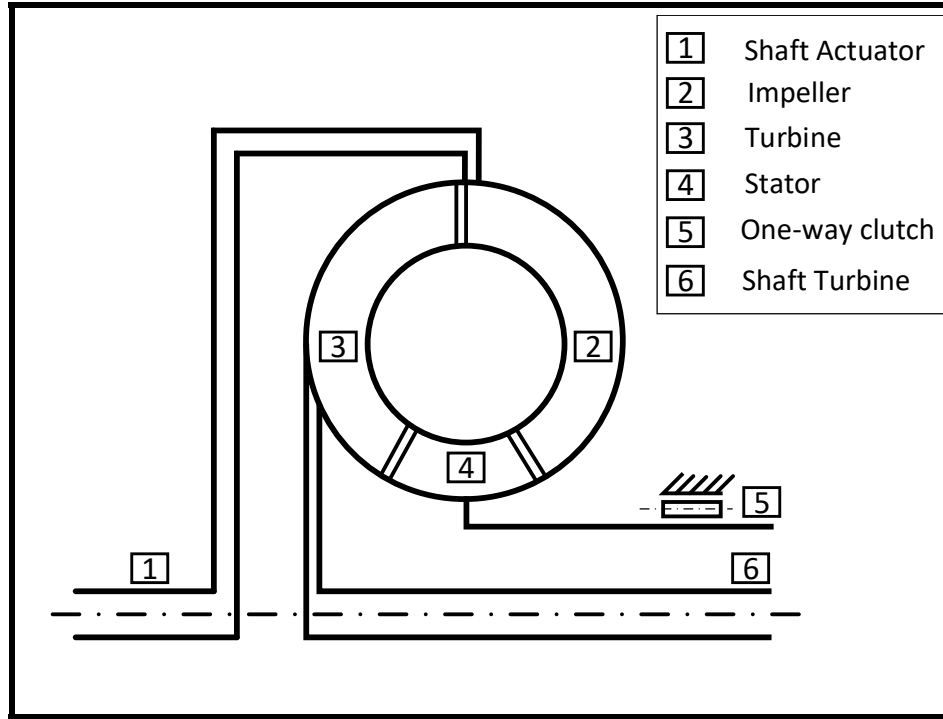


**Figure 1.4:** 3-part Torque converter assembly

The torque converter assembly is also equipped with a **lockup clutch**. This torque converter clutch (TCC) locks the impeller and turbine sides when the speeds between the two becomes almost equal. The locking of the two ensures the torque transfer through the mechanical friction path via TCC and eliminates the power loss that exists during the fluid coupling. On the other hand, due to the reasons like restricting undesirable vibrations at low speed combustions from passing through, as listed in [12] and [13], the TCC is made to slip. However, as the TCC slips a lag in the torque delivery at the turbine is observed. This lag in the torque propagates to the wheels and further makes the drivability response sluggish. This torque lag is also addressed to overcome through this work.

## 1.3 Literature Review

This section provides an overview of some of the researches that have been published till date on the areas that are of interest and motivation behind this work. The development of strategies and their testing and validation to avoid jerks during the propagation of vehicle is of prime interest to the researchers since long. There are various approaches that have been chosen for the development of an anti-jerk control (AJC) based torque shaping of the actuator, which is shown in this section. Further, in the context of refinement to the drivability response, the control of the torque converter clutch slip has been a source of research interests for some. However, not much literature is found with a specific focus on controlling of the actuator torque to maintain the desired performance of the driveline during the slipping of torque converter clutch. This marks the novelty of the work done as a part of this thesis.

This section is divided into three subsections. The first part gives an overview of the research conducted on the development of control strategies of an anti-jerk controller. The second part discusses the research in the field of modeling of the torque converters. The third and the final part of this section discusses about the research in the field of model predictive control and its application in the powertrain segment.

### 1.3.1 AJC torque shaping controllers

As mentioned at the beginning of this section, the mitigation of shuffle induced in the driveline in order to ensure a smooth maneuver of the vehicle is a point of interest for many researchers. Robert A. Krenz is noted to be amongst the first few to focus on this performance aspect of the drivetrain through [14]. He discussed about the rudimentary experimental and analytical techniques to address the clunk and shuffle induced.

Lagerberg et. al., through their works in [15], [16], [17], [18] and [19], are noted to be amongst the primary researchers on the development of anti-jerk control strategies. Their work extensively involved the designing of the control strategies for automotive driveline with backlash. The author in [15] provided a literature survey on control of backlash containing automotive powertrains. Further, in [17] and [19], the authors showcase the backlash state estimation methods for automotive powertrains. In [18], the authors discussed a model predictive controller. The study in reference [16] provides a detailed discussion on modeling, estimation and control of powertrains with backlash.

Templin and Egardt worked on the development of an LQR based torque compensator with backlash handling through [20] and [21]. One of the key highlights of their work

was that there was no state reference trajectories involved as the concerned output - the driveshaft torque derivative, was always required to be 0. Also, in their work, the cost function for optimization involved the difference between the driver's torque request and the controller output. The developed controller was tested on a Volvo heavy duty truck.

Karikomi et. al., in [22], and Kawamura et. al., in [23], developed a shaking vibration control approach for electric vehicles. The designed controller comprised a feedforward compensator, to suppress the vibration induced by the motor output torque, and a feedback controller, to suppress the vibrations due to disturbances and modeling errors. It incorporated the transfer function approach to design the compensators. The results with (positive to positive motor torque) and without (negative to positive motor torque) gear backlash consideration were shown. Due to the modeling error (no backlash consideration), the results showed the need of using the feedback controller along with the feedforward controller.

Ravichandran et. al., in [24], developed a controller that shaped the actuator torque for both the contact and backlash modes. For contact mode, the authors developed a pre-compensator (feedforward) and lead compensator (feedback) based controller. Further, for the backlash mode, they proposed a bang-bang controller. The switching between the two controllers is based on the estimation of the backlash position that is done by a state estimator.

Baumann et. al., in [25], discuss the development of a robust controller for anti-jerk control based on the  $H_\infty$  approach. The authors developed a 2 degree of freedom (DOF) driveline state space model for contact mode whose parameters were identified using measurement data. The controlled variable realised was the measured difference between the engine speed and the wheel speed, representing the driveline oscillations. The command variable was zero, corresponding to the ideal shuffle free response. The controller output provided a correction torque to be subtracted from the driver request.

Baumann et al., in [26], used the same 2 DOF model from [25], to develop a model based predictive controller through smith predictive control approach. The controller is implemented in the feedback loop. The authors used the technique of root locus to develop the controller. Similar to [25], good controller performance was emphasized for low engine speed and high requested torque considering it to be the most critical jerking configuration. Both the proposed controllers in [25] and [26] are tested on a Siemens automotive drive test vehicle.

Lagerberg et. al, in [18], developed an offline model predictive controller (MPC) using the powertrain dynamics as piece-wise affine (PFA) systems. The affine dynamics are considered separately for each of positive contact, backlash traversal and negative contact mode. Further, the framed MPC problem involves the consideration of constraint on the engine delivered torque. The author also defines the target sets

for two distinct phases of operation of powertrain. The first phase ends when the engine side and wheel side of backlash are almost in contact. At this instant, the shaft displacement is required to be within lash, and the engine torque and shaft displacement relative velocity should almost be 0. The second phase ends when a steady state value of acceleration is achieved for the contact mode. At the end of phase 2, the speed difference and acceleration difference between engine and wheel sides should be within the required limits. For this approach, the MATLAB based Multi-Parametric toolbox is used.

Formentini et. al., in [27], developed a switch based model predictive controlling strategy, where the model was developed with a similar piece-wise affine dynamics as in [18]. First, the model for three affine dynamics is defined dividing it into positive, negative and in-lash modes. Further, the authors divided the contact mode state space model on the basis of positive or negative contact and define separate MPC controllers for the two. Next, they defined two more MPC controllers for the backlash mode each for positive or negative direction lash traversal. Later, a switching strategy based on the estimated lash position is framed to switch between the designed MPC controllers.

Reddy, in [4], showed the detailed evolution of the AJC controller over the period of time. Also, he provides a comprehensive summary on the different anti-jerk control approaches discussed. He also provided a comparative study of the AJC controllers

that were based on  $H_\infty$ , MPC, and LQR approaches.

Further, control models are usually developed with separate strategies, each for contact mode and backlash mode. In order to switch between these two modes during the vehicle operation, lash estimators are used. The study in reference [28] and [29] proposes methods to estimate the backlash size and backlash position for automotive powertrain operation.

### **1.3.2 Control oriented modeling of torque converter**

This subsection reviews publications and research work conducted on the torque converter's mathematical modeling. It is relevant to this work as it provides an overview about the development of a torque converter model which shall later be used to define the control strategies in order to control the actuator torque while the slipping is induced in the TCC, thus improving the drivability performance during the slip. Also, this shall help developing an insight on the consideration of the effect of TCC slip on the desired performance and further its improvement as discussed in Chapters 3 and 4 of this work.

Ishihara and Emori, in [30], were amongst the first of the researchers to work on the modeling of the torque converter. The authors proposed a torque converter model represented by three first-order differential equations for pump, impeller and energy

conservation. These equations were derived from fundamental equations of motion and energy conservation principles.

Hrovat and Tobler, in [31], provided a detailed derivation of the torque converter's dynamic model. In this work, they derived four first-order differential equations to present the torque converter dynamics in the form of a mathematical model. The authors further used these equations to develop a bond graph model. Tsangarides and Tobler in [32], further built their research from the work done in [31]. They highlighted the effect of a by-pass clutch used in combination with a hydraulic torque converter on the drivability performance. Their work included computer-based simulations that were run on the developed mathematical models and showed how locking up of the by-pass clutch affected the torsional vibrations and tip-in response of the drivetrain.

Adibi Asl et. al., in [33] presented the math-based model of a torque converter using the same equations derived in [31], and further implements the model in the MapleSim<sup>®</sup> modeling environment. Also, [34] and [35], are among other literature that notifies the use of four first order differential equations discussed in [31].

However, such modeling of torque converter with the nonlinear differential equations have found to be computationally cumbersome and a need was realised for the use of computationally light control oriented model representation of the torque converter.

Allan J. Kotwicki in [36] discussed a methodology to develop a simplified control

oriented torque converter model. First, he deduced the physics based model equations for the torque converter and later extended it to propose a simplified analytical model. The simplified model was for two distinct operating modes of the torque converter and was represented using simple quadratic equations. The coefficients for these equations were determined using the regression fit of the model with the experimental data available. The Kotwicki based modeling is found to be among the most effective approaches in terms of building computationally light control strategies. Studies in references [37], [38], [39] and [40] are some of the notable literature using this approach that are referred to for this work.

Another control oriented modeling approach involves the application of K-factor lookup table method, where the speed ratio, torque ratio and capacity factor based lookup tables are used for torque converter modeling. Their relation is obtained through experimental analysis. Hebbale et. al., in [37], used this method to develop a torque converter clutch slip control approach.

Adibi Asl et. al., in [40], showed a flow diagram of the torque converter modeling approaches with increasing complexity. The study showed that the empirical relations based modeling is least complex and the Computational fluid dynamics (CFD) based modeling is the most complex approach. Further, in [41], the author mentions that the Kotwicki based and the lookup table based approaches are fairly suitable for model-based control designing.

Among other approaches of torque converter modeling were, Li and Wang in [42], where they demonstrated a torque converter mathematical model by considering the converter to be a torsional spring-damper assembly with pump and turbine as the end side inertia elements. Though this makes the model simpler, it still is not completely relevant for the control oriented use, as the stiffness and damping factors are liable to change under operation. Yang et. al., in [43] grouped the torque converter performance into 2 modes, traction and stall based on whether the vehicle is propelling or braking respectively. The torque converter model used for their analysis is based on a second degree polynomial equation for the capacity factor that closes the experimental values. Also, the torque ratio defined is deduced to be a first order polynomial equation dependent on the speed ratio. The coefficients in the polynomial equation for capacity factor varied with modes.

Figure 1.5 shows a comparative study of different approaches used for the modeling of torque converter.

### **1.3.3 Model predictive control of drivetrain**

In this work, the MPC approach was used to control the actuator torque and the clutch capacity in order to overcome the torque lag during the slipping of torque converter. Although, no directly related literature could be found on a similar work,

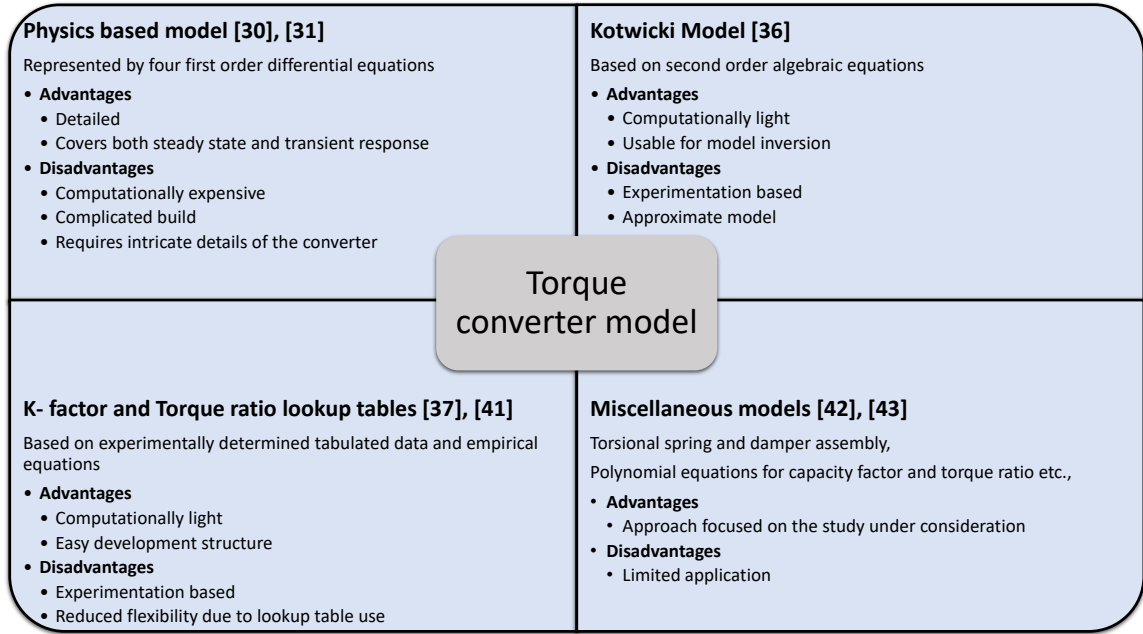


**Figure 1.5:** Approaches for torque converter modeling

this subsection reviews the literature on different model prediction and optimization based approaches implemented in powertrain controls domain, that were found useful for this work.

Earlier, the MPC approach was majorly restricted to the industrial sector for process optimization but in past decade a rise has been observed in its application to automotive controls. Qin and Badgewell in [44] tabulates a survey study on the application share of MPC in different industrial domains.

Atabay et. al., in [45], discusses the development of an MPC controller to attenuate the longitudinal shuffle oscillations induced in the drivetrain. The authors deduce a 3-DOF model and further uses it to frame an MPC based controller to control

the engine brake torque accordingly. This controller in conjunction with a feedback proportional controller is used to attenuate the shuffle oscillations.

Wang and Sun, in [46], provides a slip control approach for a torque converter clutch. They develop an optimization problem for slipping of the torque converter clutch with the objective of minimising the power loss across the torque converter due to fluid damping. For development of the powertrain model, they used the Kotwicki based quadratic equations of the torque converter as were discussed in Subsection 1.3.2.

Bemporad et al., in [47], discusses the development of a supervisory controller using the MPC approach. The authors used a linear prediction model and further framed an optimization problem to develop the MPC supervisory controller with the objective of modifying the reference to track driver requested axle torque while simultaneously optimising the fuel economy.

Bemporad et al., in [48], discusses the development of a torque tracking MPC controller with optimised fuel consumption designed for transient and steady state operation of gasoline turbocharged engines. The control approach involved setting up of multiple MPC controllers, where, system identification based linear models were obtained for each MPC controller.

Raut et al., in [49] develops a control oriented model and an MPC for a reactivity controlled compression ignition (RCCI) engine. The dynamic model is developed

using a combination of physics-based equations and empirical models. The MPC has a 5-cycle prediction horizon and is developed and implemented on an experimental setup of an RCCI engine. The authors develop a switched MPC setup where 4 different set of MPCs were defined over the range of dual-fuel premixed ratio and start of injection timing.

Caruntu et al., in [50] and [51], develops an MPC to control driveline oscillations improving the drivability and ride comfort performance of a vehicle. The authors developed a novel state space piece wise affine drivetrain model with three inertia elements along with the driveshafts and clutch flexibility. Further, The authors developed the MPC for a single prediction horizon window using flexible Lyapunov functions.

## **1.4 Research scope and Thesis organisation**

This work is a continuation to the work done by Lakhani [3], Reddy [4], and Darokar [5]. This is an extension of an Alliance project between Michigan Technological University and Ford Motor Company. The work conducted in this thesis can be segmented into three phases. In the first phase, the shuffle oscillations observed in the driveline are addressed. Further, in this phase, a control strategy is developed to particularly address the shuffle oscillations during the positive to positive torque

tip-ins in the contact mode. In order to observe and control these shuffle oscillations effectively, the torque converter lockup clutch is considered locked. Next, in the second and third phases of this work, the problem of torque lag occurring specifically due to the torque converter lockup clutch slipping is addressed. In these phases, the driveline is considered in contact mode. In the second phase, a model based feedforward and feedback anti-lag torque controller (ALTC) is developed to overcome the observed lag. Later, in the third phase, the constraints of the actuator were included and further a model prediction based ALTC controller with the constraints is set up.

This thesis is organised as shown in Figure 1.6. The following chapter, Chapter 2, includes the details of the development of the torque shaping control methodologies and simulation based evaluation of the developed controller for contact mode. It also briefly explains about the physics based equations involved and the mathematical model developed with respect to the reduced order model prepared and validated in [4] and [5]. Chapter 3 discusses about the torque converter slipping scenarios and the development of a model based feedforward-feedback ALTC to overcome the observed torque deviation during the converter slip. Later, Chapter 4 introduces an MPC based ALTC to overcome the torque deviation while maintaining the actuation commands within the known physical constraints of the actuators. Also, this chapter discusses the performance comparison of the two developed ALTCs from Chapters 3 and 4. The final chapter provides conclusions drawn from this thesis work and presents the future work planned.

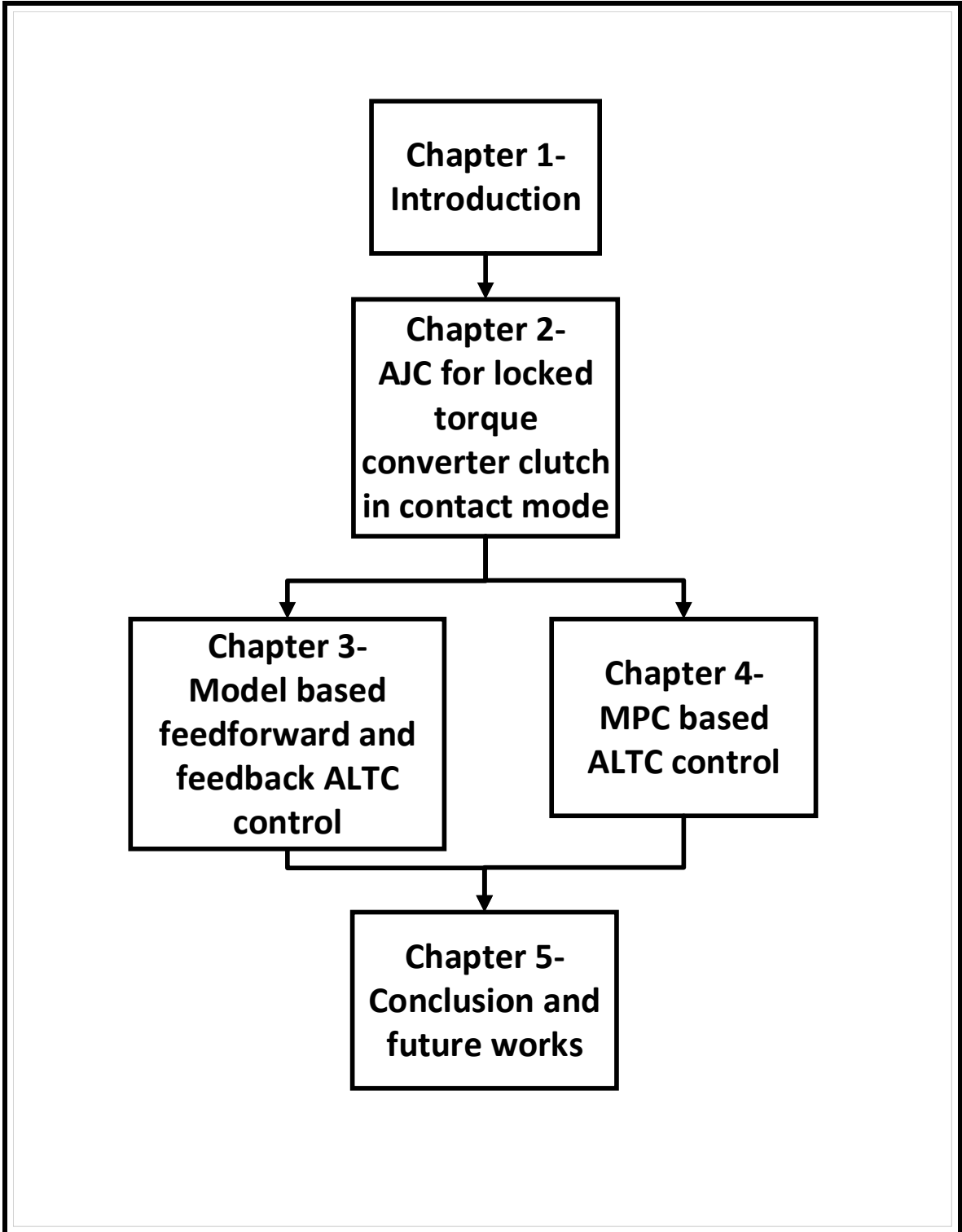


Figure 1.6: Layout of the thesis work



# Chapter 2

## Anti-Jerk controller development for locked torque converter in contact mode

This chapter deals with the development of an anti-jerk control (AJC) strategy and its implementation, specifically during the contact mode. This work is a continuation of the control-oriented reduced order model (ROM) development, and parameter and state estimator development done in [4] and [5]. The discussion in this chapter begins with understanding the problem statement which is the observation of shuffle in the driveline. Then the chapter discusses the ROM that was derived from a detailed full-order model (FOM) in [4], capturing the shuffle response of the actual driveline

from a test vehicle. Next, the development of the state space model from the ROM is discussed in detail. In the later parts of this chapter, the development and implementation of the control strategy is discussed. Finally, evaluation of the controller performance is conducted.

## 2.1 Background

This work uses the FOM from [4] that was developed in Amesim and was experimentally validated for simulating the shuffle dynamics of a passenger vehicle. A detailed layout of the FOM is provided in [4] and [5]. When the vehicular drivetrain is subjected to an unshaped torque request from the driver, by the virtue of the property of compliance of the shaft elements involved (i.e., propeller shaft and axle shaft), the drivetrain's torque response is observed to oscillate for a while and die out eventually. The driveshafts connected to wheels when subjected to such torques tend to twist and untwist over a period of time, and propagate shuffle response to the wheels. This can be seen in Figure 2.1. An unshaped driver requested torque is provided to the actuator which delivers torque to the FOM as shown in Figure 2.1(a). In Figure 2.1(b) and 2.1(c), the shuffle oscillations in the transmission input torque (also the torque at turbine of the torque converter) and the propeller shaft torque are shown, respectively. The typical range of shuffle oscillation frequency for passenger cars lies in between 1 Hz to 15 Hz, as mentioned in [52].

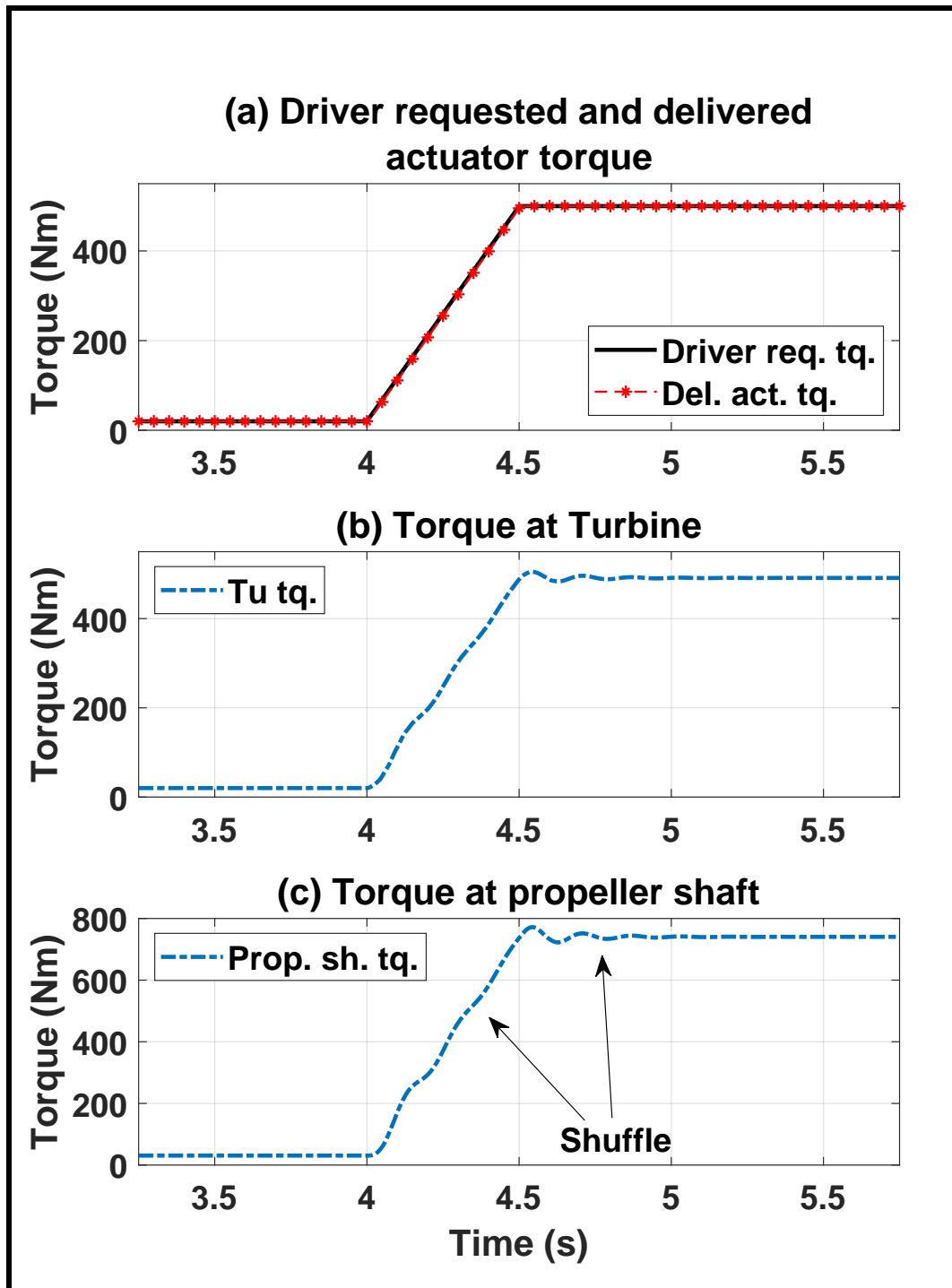


Figure 2.1: Driveline performance with observed shuffle

## 2.2 State space model of the ROM

This section describes the development of a state space model of the drivetrain obtained from the ROM. As mentioned in the introduction of this chapter, The control oriented ROM was developed from the FOM to capture the essential shuffle dynamics. Both the FOM and ROM were developed in Amesim, as discussed in detail in [4] and [5]. Further, in this section, the equations of motion are explained at the beginning. Later, these equations are used to develop the state space model. Finally, a discussion on the validation of the obtained state space model is done in this section.

### 2.2.1 Equations of motion from ROM

Figure 2.2 shows the schematic representation of the ROM used for this work. Note that the ROM considered is only for the contact mode and is updated from the ROM developed in [4] and [5] by disregarding the backlash element. This model, which is a simplified version of the FOM, is developed with the mindset that being computationally lighter it shall prove advantageous in the development of control strategy. To initiate the state space model development, the equations of motion are realised from the ROM as discussed.

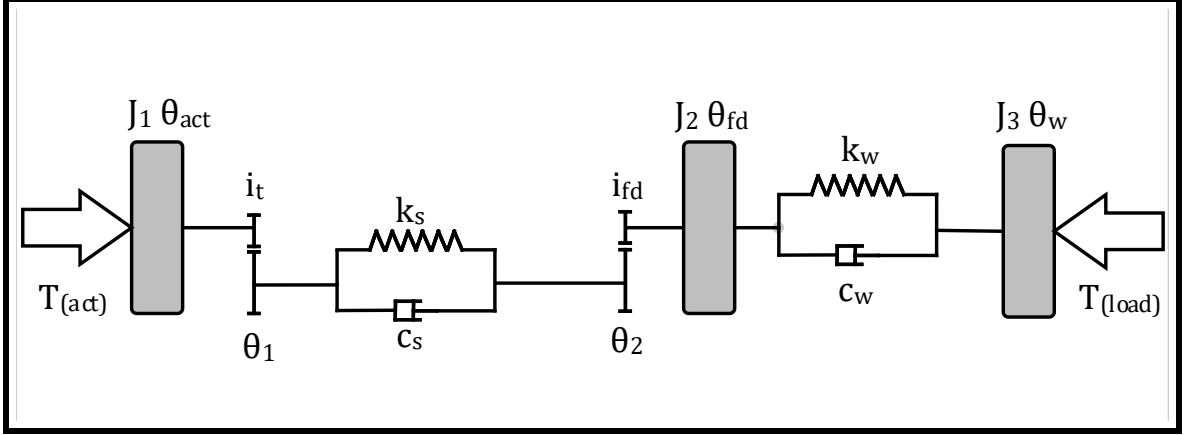


**Figure 2.2:** Schematic representation of reduced order model for contact mode

### Equations of motion

The equations of motion derived from the ROM are formulated using the Newton's laws of motion as shown below. Each of the inertia and compliance element from Figure 2.2 is subjected to the free body analysis and the mentioned equations are obtained. The discussion on the free body analyses of the individual elements of ROM is done below.

Applying equations of motion for the lumped inertia  $J_1$  yields:

$$T_{\text{act}} - \frac{T_s}{i_t} = J_1 \ddot{\theta}_{\text{act}}, \quad (2.1)$$

$$\theta_1 = \frac{\theta_{\text{act}}}{i_t}, \quad (2.2)$$

where,  $T_{\text{act}}$  represents the applied torque from the actuator,  $T_s$  represents lumped

shaft torque,  $\ddot{\theta}_{\text{act}}$  denotes the angular acceleration of the actuator side lumped inertia,  $J_1$  and  $i_t$  is the transmission gear ratio.

Next, applying equations of motion on the lumped compliance element constituting torque converter, propeller shaft and axle shaft yields:

$$T_s = k_s(\theta_1 - \theta_2) + c_s(\dot{\theta}_1 - \dot{\theta}_2), \quad (2.3)$$

$$\theta_2 = \theta_{\text{fd}} i_{\text{fd}}, \quad (2.4)$$

where,  $k_s$  is the stiffness of the lumped shaft and  $c_s$  is its damping coefficient.  $\theta_1$ ,  $\dot{\theta}_1$ ,  $\theta_2$  and  $\dot{\theta}_2$  represents the angular positions and angular speeds at the two ends of the lumped shaft respectively. Note that the lumped shaft torque,  $T_s$ , is representative of the propeller shaft torque from the FOM.

Furthermore, applying equations of motion on lumped inertia  $J_2$ , following is obtained:

$$T_s i_{\text{fd}} - T_w = J_2 \ddot{\theta}_{\text{fd}}, \quad (2.5)$$

where  $T_w$  denotes the torque of the shaft with lumped axle and tire compliances,  $\ddot{\theta}_{\text{fd}}$  is the angular acceleration of inertia  $J_2$ .

Applying the equations of motion on the lumped compliance element comprising axle

and tires yields:

$$T_w = k_w(\theta_{fd} - \theta_w) + c_w(\dot{\theta}_{fd} - \dot{\theta}_w), \quad (2.6)$$

where  $k_w$  and  $c_w$  represents stiffness and damping coefficients respectively, of the shaft lumped with axle and tire compliances and,  $\theta_{fd}$ ,  $\theta_w$ ,  $\dot{\theta}_{fd}$ ,  $\dot{\theta}_w$  are the angular position and angular velocity of inertia  $J_2$  side and  $J_3$  side of shaft respectively.

Further the equations of motion were applied on lumped wheel inertia  $J_3$  and the vehicle motion and following equations were obtained:

$$T_w - F_l r_T = (J_3 + M r_T^2) \ddot{\theta}_w. \quad (2.7)$$

where  $F_l$  is road load resistance,  $r_T$  is the tire radius. The term  $F_l r_T$  represents the  $T_{load}$  from Figure 2.2. Further,  $M$  is the vehicle mass, and  $\ddot{\theta}_w$  is the angular acceleration of lumped inertia  $J_3$ .

### 2.2.2 State space model development

The equations developed above from the ROM for the contact mode (Equations (2.1) - (2.7)), are represented in the form of a state space model as shown

$$\dot{\mathbf{x}} = \mathbf{A}\mathbf{x} + \mathbf{B}\mathbf{u}, \quad (2.8)$$

$$\mathbf{y} = \mathbf{C}\mathbf{x} + \mathbf{D}\mathbf{u}, \quad (2.9)$$

where

$$\mathbf{x} = \left[ \dot{\theta}_{\text{act}} \quad (\theta_{\text{fd}} - \theta_{\text{w}}) \quad \dot{\theta}_{\text{fd}} \quad \dot{\theta}_{\text{w}} \quad T_{\text{s}} \right]^{\text{T}}, \quad (2.10)$$

$$\mathbf{y} = \left[ T_{\text{s}} \right], \quad (2.11)$$

$$\mathbf{u} = \begin{bmatrix} T_{\text{act}} \\ F_1 \end{bmatrix}, \quad (2.12)$$

where  $\dot{\theta}_{\text{act}}$ , is the angular velocity of the lumped actuator inertia,  $J_1$ ,  $(\theta_{\text{fd}} - \theta_{\text{w}})$ , is the wheel side twist angle,  $\dot{\theta}_{\text{fd}}$ , is the angular velocity of inertia  $J_2$ ,  $\dot{\theta}_{\text{w}}$ , is the angular velocity of inertia  $J_3$ , and  $T_{\text{s}}$  is the lumped propeller shaft torque. Furthermore, the matrices A, B, C and, D are as shown

$$\mathbf{A} = \begin{bmatrix} 0 & 0 & 0 & 0 & \frac{-1}{J_1 i_t} \\ 0 & 0 & 1 & -1 & 0 \\ 0 & -\frac{k_{\text{w}}}{J_2} & -\frac{c_{\text{w}}}{J_2} & \frac{c_{\text{w}}}{J_2} & \frac{i_{\text{fd}}}{J_2} \\ 0 & \frac{k_{\text{w}}}{b} & \frac{c_{\text{w}}}{b} & -\frac{c_{\text{w}}}{b} & 0 \\ \frac{k_{\text{s}}}{i_t} & \frac{c_{\text{s}} k_{\text{w}} i_{\text{fd}}}{J_2} & \left( -k_{\text{s}} i_{\text{fd}} + \frac{c_{\text{s}} c_{\text{w}} i_{\text{fd}}}{J_2} \right) & -\frac{c_{\text{s}} c_{\text{w}} i_{\text{fd}}}{J_2} & -\left( \frac{c_{\text{s}}}{J_1 i_t^2} + \frac{c_{\text{s}} i_{\text{fd}}^2}{J_2} \right) \end{bmatrix}, \quad (2.13)$$

$$\mathbf{B} = \begin{bmatrix} \frac{1}{J_1} & 0 & 0 & 0 & \frac{c_s}{J_1 i_t} \\ 0 & 0 & 0 & \frac{-r_T}{b} & 0 \end{bmatrix}^T, \quad (2.14)$$

$$\mathbf{C} = \begin{bmatrix} 0 & 0 & 0 & 0 & 1 \end{bmatrix}, \quad (2.15)$$

$$\mathbf{D} = \begin{bmatrix} 0 \end{bmatrix}, \quad (2.16)$$

where

$$b = J_3 + Mr_T^2.$$

### 2.2.3 Validation of the state space model

The developed state space model is validated by comparing its output with that of the Amesim based ROM. Figure 2.3 shows the comparison of the lumped shaft torque outputs from the state space model and from the ROM, as shown in Figure 2.3(b). These outputs are obtained when two models are subjected to the actuator torque shown in Figure 2.3(a). The lumped shaft torque outputs from the two models match with each other with an average error of 1.3%.

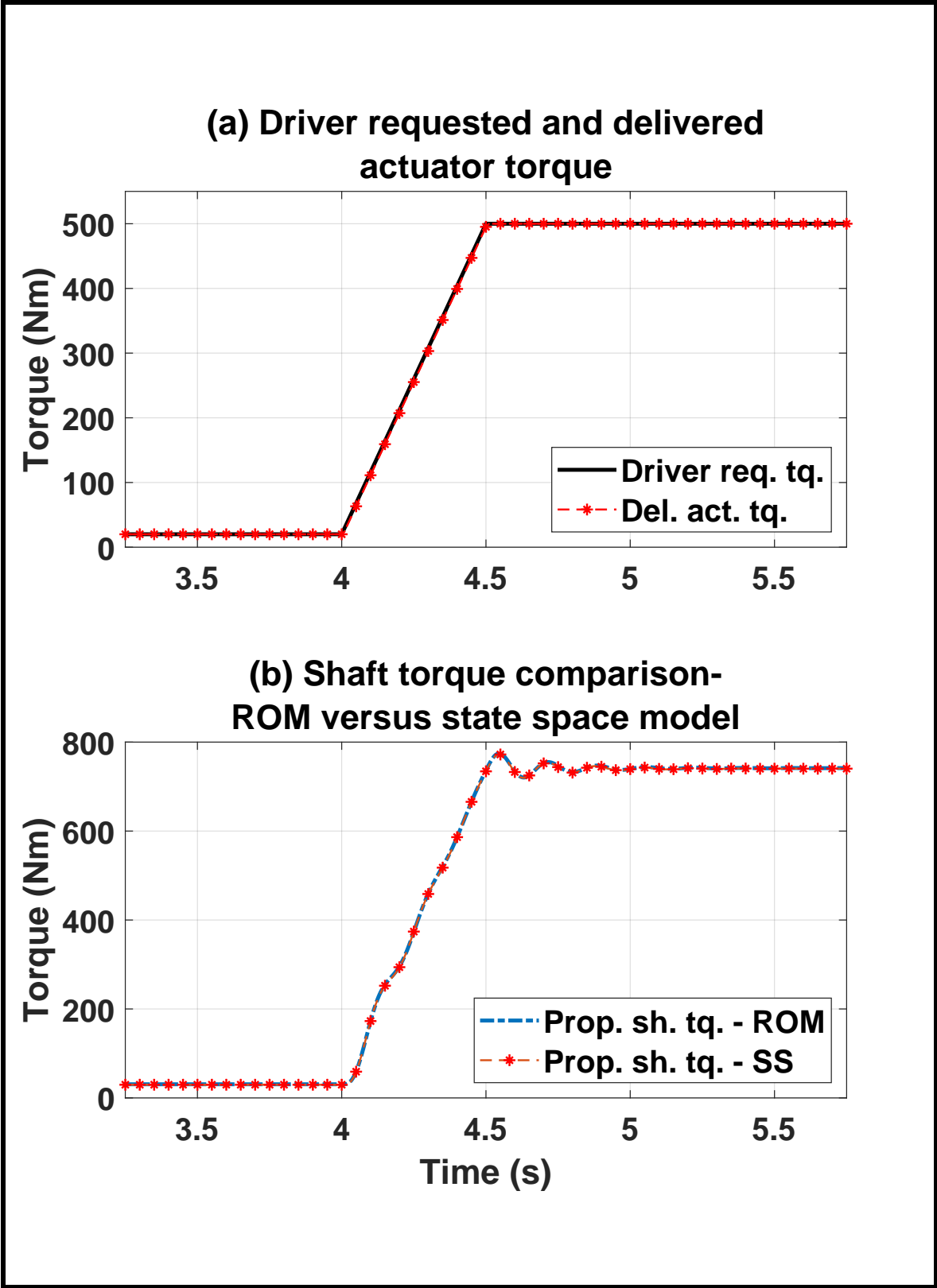


Figure 2.3: Validation of the state space model with ROM - comparison of the output response

## 2.3 Development of control strategy

As discussed in Section 2.1, when a drivetrain is subjected to an unshaped torque request from the driver, it experiences oscillatory response (shuffle) by the virtue of compliance property of the shaft elements comprising it. To overcome this effect physically would mean to have increased stiffness of these elements, but that could lead to the rise in the brittleness of the elements or infeasible design requirements. Hence, there exists a need to design a control strategy to overcome the shuffle oscillations for the drivetrain comprising of compliant elements. In this section, a control strategy is developed to overcome/reduce the shuffle phenomenon by shaping the driver requested torque appropriately.

In order to overcome the shuffle oscillations, the actuator delivered torque is required to act within one shuffle period of the driveline oscillations when subjected to a step input torque request, as mentioned in [24], where this rule was based on subjective testing. This objective of actuator torque delivery acting within one shuffle period, is achieved utilising a pre-compensator and feedback controller based control strategy as shown in Figure 2.4.

Initially, the proposed control strategy involves the development of a pre-compensator that is required to shape the driver requested torque in order to eliminate any sharp

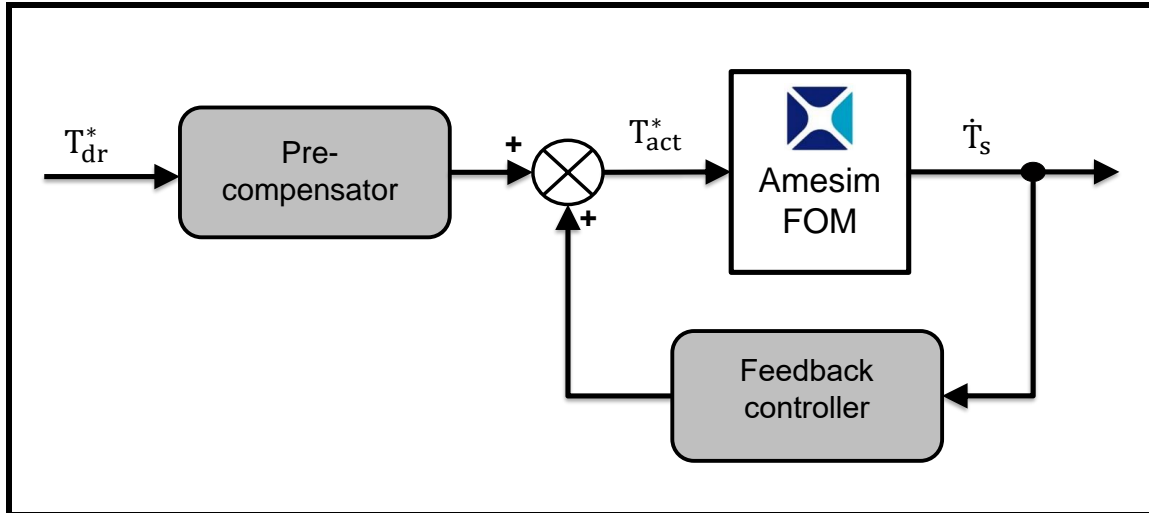


**Figure 2.4:** Overall schematic of the designed AJC control strategy

rises and drops, and to further filter the requested torque in such a way that it does not excite the shuffle response of the driveline.

Next, the oscillations existing in the drivetrain are to be monitored by a feedback controller, whose function is to receive this oscillatory response and accordingly shape the torque request adding damping to the driveline oscillations. The two individually shaped torque requests are combined further to generate the commanded actuator torque.

In order to implement the mentioned control strategy, first, the shuffle dynamics of the drivetrain system under consideration is realised in this section. Later, the explanation on designing of the pre-compensator and the feedback controller is provided in detail.

### 2.3.1 Realisation of the drivetrain dynamics

The dynamics of the drivetrain under consideration can be divided into two parts. The first part involves the dynamics of the actuator considered for this work. The second part involves the dynamics of the drivetrain that is represented through the ROM and subsequently through the state space model developed in Section 2.2. Each of the two dynamic subsystems are discussed as follows.

#### 2.3.1.1 Actuator dynamics under consideration

The actuator considered for this work is assumed to have the characteristics mentioned in Table 2.1. Further, the actuator is assumed to follow first order dynamics with a time constant of 5 ms. Mathematically, this is represented as

$$\frac{T_{\text{act}}}{T_{\text{act}}^*} = \frac{1}{0.005 \text{ s} + 1}. \quad (2.17)$$

**Table 2.1**  
Characteristics of the considered actuator

Parameter	Value
Max. delivered torque	500 Nm
Min. delivered torque	0 Nm
Max. torque delivery rate	$6000 \frac{\text{Nm}}{\text{s}}$
Min. torque delivery rate	$-6000 \frac{\text{Nm}}{\text{s}}$

### 2.3.1.2 Shuffle dynamics of drivetrain

In this subsection, a discussion is conducted on the consideration of the dynamics of the drivetrain that captures the shuffle oscillations of the system.

The state space model developed in Section 2.2 is used to frame a transfer function equation that takes the actuator delivered torque,  $T_{\text{act}}$ , as input and delivers the lumped propeller shaft torque,  $T_s$ , as the output. The obtained transfer function equation is shown as

$$\frac{T_s}{T_{\text{act}}} = \frac{0.1827 s^4 + 2606 s^3 + 5.845e05 s^2 + 1.7e07 s - (2.248e - 07)}{s^5 + 227.8 s^4 + 1.159e04 s^3 + 3.948e05 s^2 + 1.148e07 s + 5.207e - 08}, \quad (2.18)$$

Further, the transfer function representing the overall plant dynamics with the commanded actuator torque,  $T_{\text{act}}^*$ , as input and the lumped propeller shaft torque,  $T_s$ , as

the output can be obtained from Equations (2.17) and (2.18) as shown

$$\frac{T_s}{T_{act}^*} = \frac{1}{0.005s + 1} \cdot \frac{T_s}{T_{act}} \quad (2.19)$$

The shuffle frequency of the drivetrain can be determined using the transfer function, representing the overall drivetrain dynamics (Equation 2.19), under the Bode plot analysis. Figure 2.5 shows the frequency response of the plant. It can be seen that the plant shows an excitation tip in the magnitude plot at around 5.9 Hz input frequency. This excitation in the frequency response of the plant is accredited to its natural frequency or shuffle frequency. This shuffle is under focus for elimination by the AJC controller.

### 2.3.2 Design of Pre-compensator

As mentioned at the beginning of this section, the pre-compensator is required to smoothen the sharp rises and drops in the torque request generated by the driver, filtering it to avoid excitation of shuffle oscillations in the driveline. However, in doing so the lag of the pre-compensator's shaped torque is needed to be kept at minimum such that the overall shaped torque request is applicable within the one shuffle period. In this subsection, a detailed discussion on the design selection of the pre-compensator

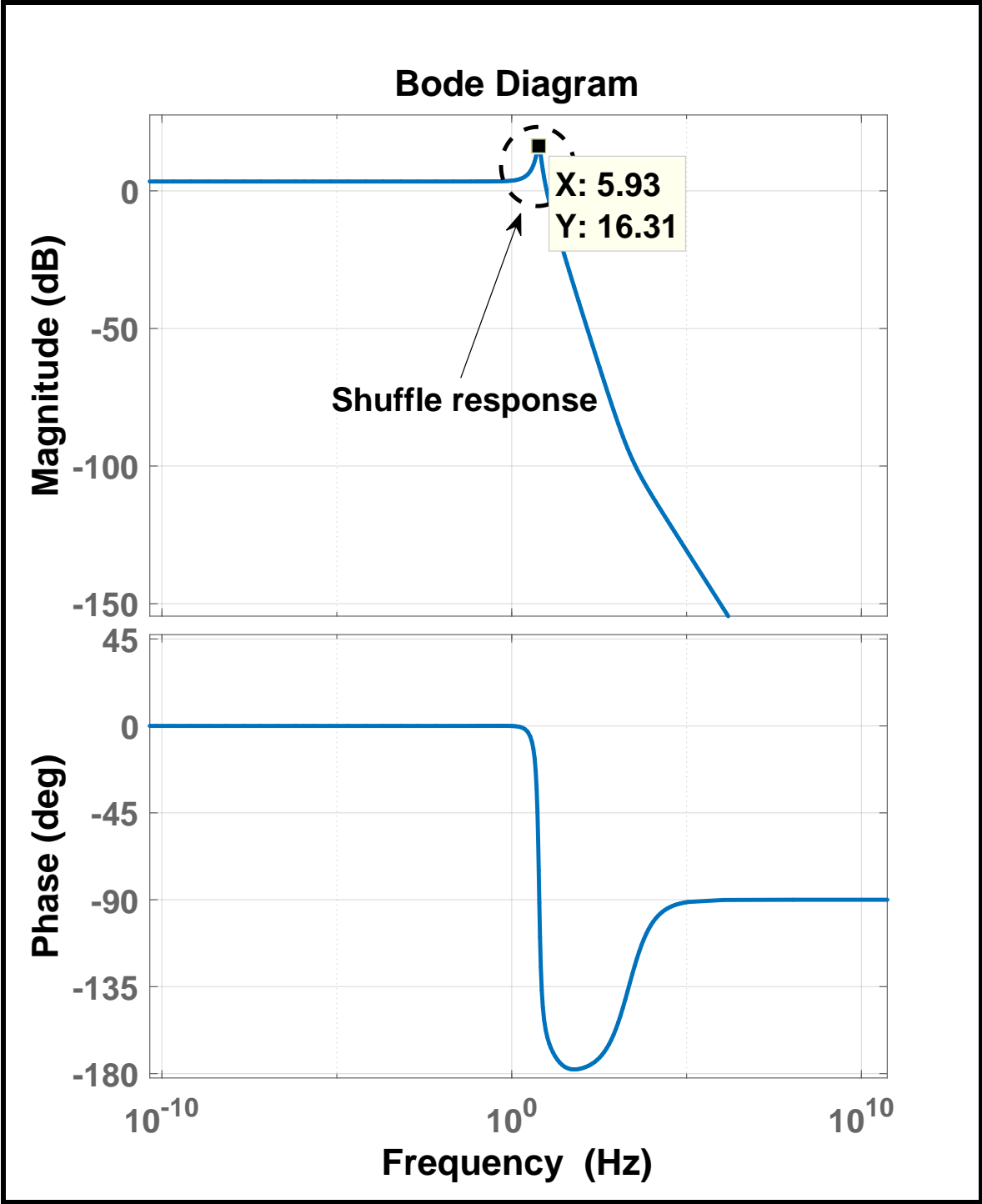


Figure 2.5: Bode response of the plant transfer function

is provided.

Considering the above mentioned objectives, the pre-compensator was chosen to be a low-pass filter. Among the various available options of low-pass filters such as chebyshev, cauer, butterworth etc., priority was given to the one that offered a low pass band ripple and a fairly steep roll-off. Thus, butterworth low-pass filter was chosen for the pre-compensator design.

The designing of the butterworth filter was based on the selection of pass band and stop band frequencies. These frequencies were chosen to be in the vicinity of the drivetrain's shuffle frequency. This was required in order to filter the input torque in proximity of the natural frequency of the plant, while simultaneously avoiding the sluggish torque response.

Therefore, for the standard pass band and stop band ripple limits, various viable combinations of pass band and stop band frequencies for the butterworth filter were used to study the response of the step input to the driveline plant as shown in Figure 2.6. The driveline plant considered was given by Equation 2.18.

Figure 2.6 shows the step input excitation response of the driveline plant in combination with different butterworth filters with different passband and stopband frequencies. From the Figure 2.6, the filter performance corresponding to the pass band frequency,  $f_p = 1$  Hz, and stop band frequency,  $f_s = 5$  Hz was considered for the

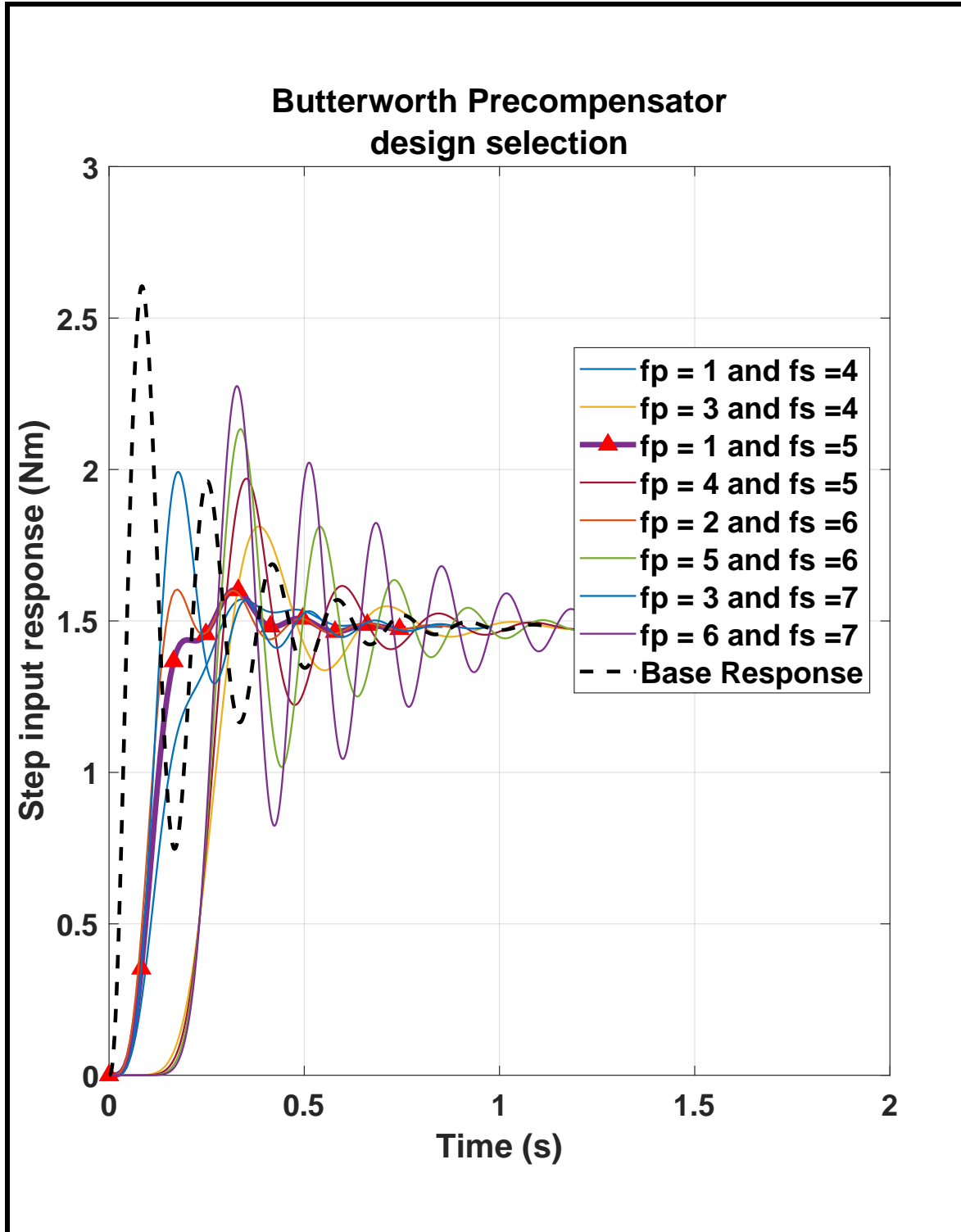


**Figure 2.6:** Step input response of the driveline with different precompensator designs

designed butterworth filter.

Moreover, a zero was added to the chosen filter to overcome the sluggishness due to introduced filter dynamics, thus, improving the rise time response of the shaped torque while not effecting the other performance specifications. This zero was obtained using the MATLAB's control system designer toolbox where its position was tuned to obtain an optimum step input response.

Thus, the designed overall butterworth filter based pre-compensator, is represented in the form of a transfer function equation as

$$PC = \frac{T_{act,1}^*}{T_{dr}^*} = \frac{10.57 s + 201.4}{s^2 + 20.07 s + 201.5} \quad (2.20)$$

where  $T_{act,1}^*$ , is the pre-compensator based output torque command, and  $T_{dr}^*$  is the driver requested torque.

### 2.3.3 Design of feedback controller

This section discusses the criteria followed to design the feedback controller shown in Figure 2.4. It is important to recall that the feedback controller is required to monitor the propeller shaft oscillations of the drivetrain and further shape the driver

requested torque to provide damping to the shuffle response.

In order to control the shuffle oscillations in the driveline response, the derivative of the propeller shaft torque is considered as the input to the feedback controller. During the simulation runs, this propeller shaft torque derivative is obtained from the FOM based actuator and wheel speeds, using the Equations (2.2), (2.3) and (2.4), as

$$\dot{T}_s = k_s \left( \frac{\dot{\theta}_{\text{act}}}{i_t} - \dot{\theta}_{\text{fd}} i_{\text{fd}} \right) + c_s \left( \frac{\ddot{\theta}_{\text{act}}}{i_t} - \ddot{\theta}_{\text{fd}} i_{\text{fd}} \right), \quad (2.21)$$

where  $\dot{T}_s$ , is the propeller shaft torque derivative,  $\left( \frac{\dot{\theta}_{\text{act}}}{i_t} - \dot{\theta}_{\text{fd}} i_{\text{fd}} \right)$  represents the relative angular velocity between the two ends of the propeller shaft, and  $\left( \frac{\ddot{\theta}_{\text{act}}}{i_t} - \ddot{\theta}_{\text{fd}} i_{\text{fd}} \right)$  represents the relative angular acceleration between the two ends of the propeller shaft.

However, while designing the feedback controller, this propeller shaft torque derivative can be represented through the derivative of the lumped propeller shaft torque from Equation 2.18 as

$$\frac{\dot{T}_s}{T_{\text{act}}^*} = \frac{s T_s}{T_{\text{act}}^*}, \quad (2.22)$$

where the term  $\frac{T_s}{T_{\text{act}}^*}$ , is the plant transfer function obtained from Equation (2.18).

Recall that this equation is obtained from the developed state space model in Section

2.2. Further, this transfer function with lumped shaft torque derivative as the output, obtained through the Equation (2.22), is used for the shuffle response analyses of the plant and hence to further design the feedback controller.

The plant transfer function under consideration (Equation 2.22), is observed to have the following set of poles and zeros.

**poles:**

$$p_1 = -170.5 + 0.0j, \quad p_2 = -46.9 + 0.0j, \quad p_3 = -5.0 + 37.6j, \quad p_4 = -5.0 - 37.6j, \\ p_5 = 0.0 + 0.0j, \quad p_6 = -200.0 + 0.0j.$$

**zeros:**

$$z_1 = 0 + 0.0j, \quad z_2 = -14035 + 0.0j, \quad z_3 = -193.1 + 0.0j, \quad z_4 = -34.3 + 0.0j, \\ z_5 = 0.0 + 0.0j.$$

Furthermore, Figure 2.7 shows the pole zero map of the plant transfer function from Equation 2.22. As can be observed clearly, the poles,  $p_3$  and  $p_4$ , form a conjugate pair of lightly damped poles that lie close to the imaginary axis. Thus, they can be accredited to contribute majorly to the shuffle oscillations of the plant. Therefore, the objective of the feedback controller is to bring these poles closer to the real axis, enhancing the damping of the overall response of the plant. In other words, the feedback controller is required to add phase to the closed loop poles of the considered

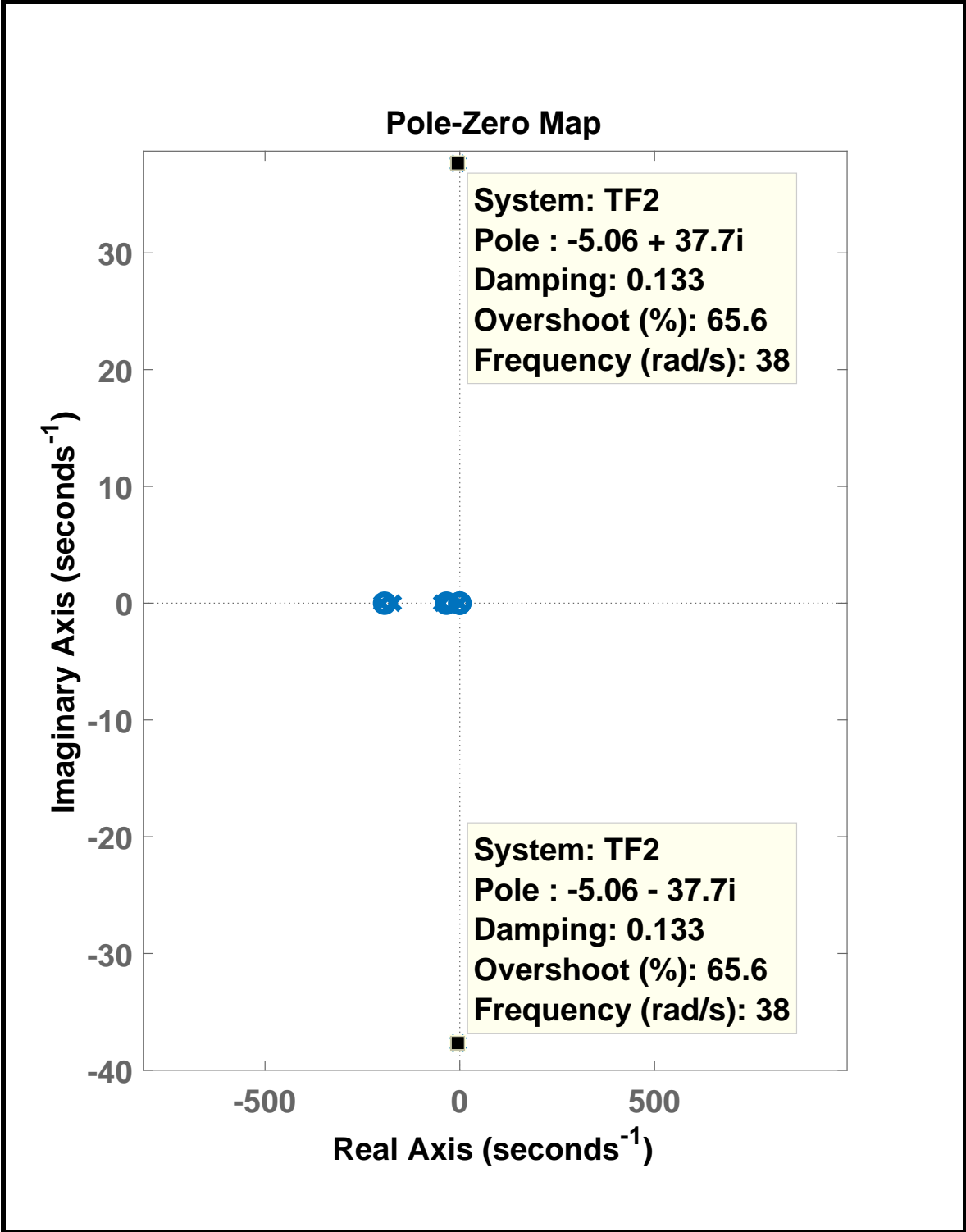


Figure 2.7: Pole zero map of the driveline plant

plant, so that the damping in the closed loop performance of the plant is increased.

This is ensured by considering the feedback controller to be a lead compensator where it is provided with the error signal between lumped propeller shaft torque derivative, that is output from the plant, and its ideal reference of 0. The 0 ideal reference indicates the shuffle free propeller shaft torque response. This is implemented as shown in the feedback loop of Figure 2.8.

The structure of the feedback lead compensator in the form of a transfer function is given as

$$\text{LC} = \frac{T_{\text{act},2}^*}{-\dot{T}_s} = k_c \frac{(s - a)}{(s - b)}, \quad (2.23)$$

where  $k_c$  is the compensator gain,  $a$  is the zero added by the compensator, and  $b$  is the pole added by the compensator. To obtain the desired lead compensator, the plant transfer function (Equation 2.22) was used in the MATLAB's control system designer toolbox where its closed loop performance was analysed and simultaneously the feedback lead compensator was tuned to attain the desired damped closed loop response of the plant. The attained lead compensator parameters are shown in Table 2.2.

**Table 2.2**  
Lead compensator parameters

parameter	value
compensator gain ( $k_c$ )	0.013
zero (-a)	-20.85
pole (-b)	-26.45

### 2.3.4 Analyses of the overall controller response

The overall shaped actuator torque command,  $T_{act}^*$ , can be obtained from the sum of the individual torque commands output from each of the pre and lead compensators (Equations 2.20 and 2.23) as

$$T_{act}^* = T_{act,1}^* + T_{act,2}^* \quad (2.24)$$

Figure 2.8 shows the overall block diagram layout of the developed control scheme. This block diagram is used to analyse the controller performance by framing a transfer function equation for the controller. The output of this transfer function is considered to be the actuator torque command,  $T_{act}^*$ , and the input is the driver requested torque,  $T_{dr}^*$ . Mathematically, this transfer function can be shown as

$$\frac{T_{act}^*}{T_{dr}^*} = \frac{PC}{1 + (LC)G} \quad (2.25)$$

where  $G$  denotes the plant transfer function given by Equation 2.22 and, PC and LC, are the respectively the designed pre-compensator and lead compensator transfer functions.

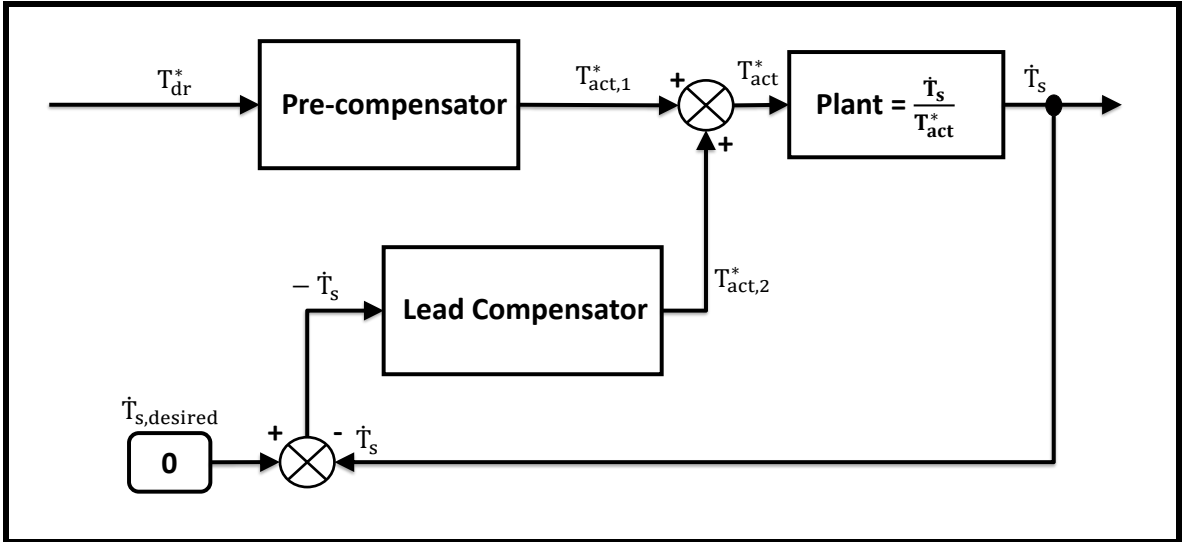


**Figure 2.8:** Block diagram analyses of the developed control strategy

Figure 2.9 shows the bode plot response of the transfer function representing the controller response as given by Equation 2.25. As can be seen in the figure, the dip in the magnitude response of the bode plot for the controller lies around the same region where the shuffle frequency of the plant was observed (as shown in Figure 2.5). This dip represents the controller performance where it tries to suppress the plant shuffle oscillations. This allows the driveline to follow damped shuffle response.

The results obtained after the implementation of the developed AJC control strategy with the FOM model are discussed in the following section.

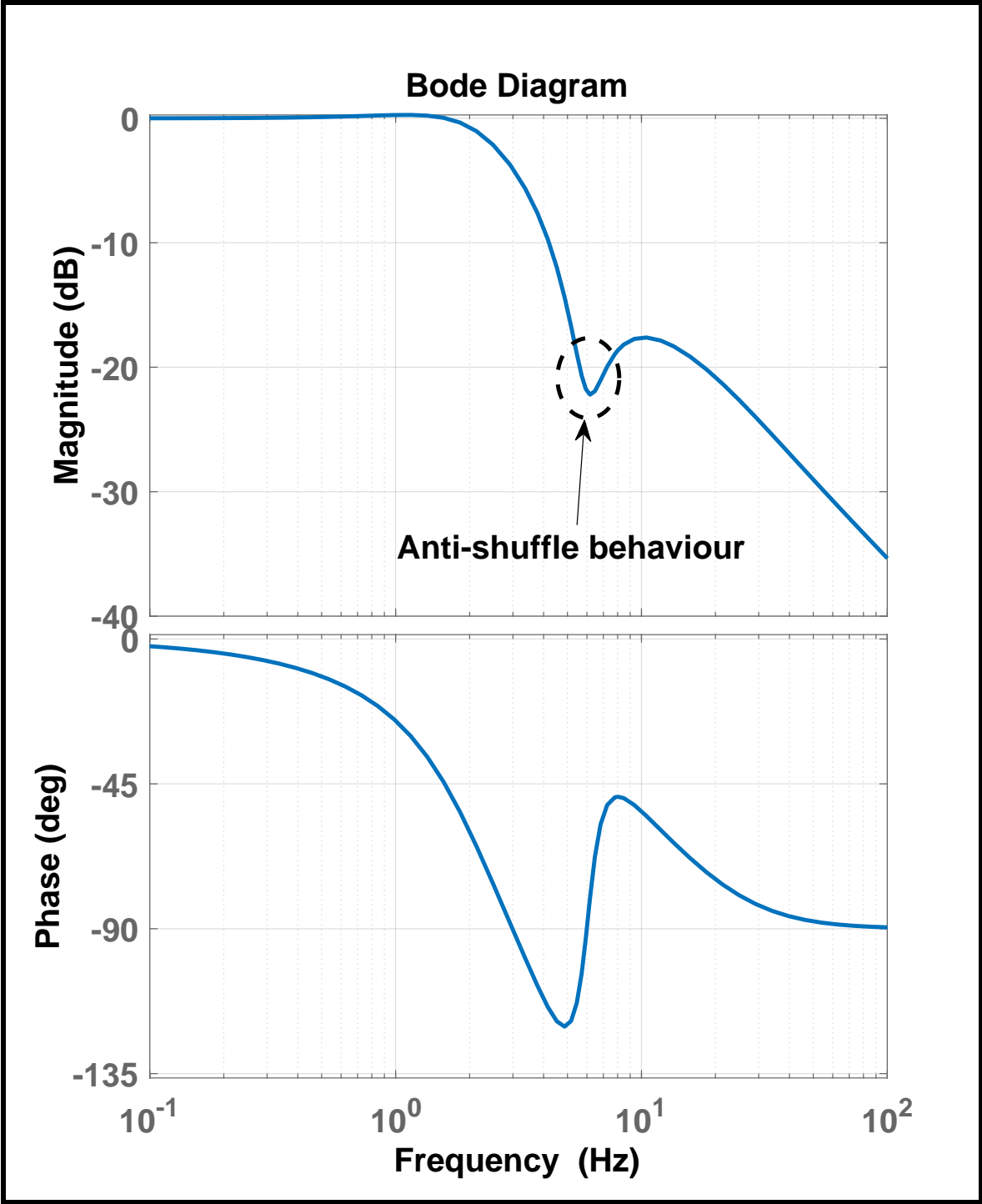


Figure 2.9: Bode response analyses of the controller

## 2.4 Performance evaluation

This section compares the performance of the driveline with the proposed controller to that without any control. Firstly, Table 2.3 shows the performance parameters for propeller shaft torque for the two cases, for a step input driver request. Later, the Figure 2.10 is obtained to show the performance improvement of the driveline for the test case discussed in Section 2.1.

Table 2.3 compares the % overshoot, rise time and settling time of the propeller shaft torque response of the driveline when subjected to a step input torque request by the driver. In Table 2.3, the maximum overshoot percentage was determined w.r.t. the steady state value. Further, the rise time and settling time were determined for the 90% of the steady state value and within 2% of the steady state value, respectively.

**Table 2.3**  
Step input comparison of driveline performance with and without implemented AJC

Parameter	Driveline response	
	Without AJC	With AJC
% Max. overshoot	58.0%	7.2 %
90% Rise time	0.04 s	0.14 s
2% Settling time	0.45 s	0.37 s

Figure 2.10 shows the performance comparison of the driveline with and without the implementation of the developed AJC, corresponding to the same driver requested

torque in Section 2.1. When the said driver requested torque is directly passed without any shaping to the drivetrain, a resulting shuffle is observed at the turbine, as shown in Figure 2.10(b) and the propeller shaft torque, in Figure 2.10(c). However, as the AJC is implemented, the driver requested torque is shaped as shown by ‘shaped act. tq.’ in Figure 2.10(a). Corresponding to this shaped torque, the turbine torque and propeller shaft torque response are observed to be shuffle free as seen in Figure 2.10(b) and 2.10(c), respectively. Further on comparing the 2% settling time for this test case (from the starting of the torque tip-in request), the propeller shaft torque with AJC implementation was observed to settle at a 10.8% reduced settling time compared to when no AJC was implemented. Thus, it can be said that the implementation of the developed Anti-jerk control is able to damp the shuffle in the drivetrain and has improved the drivability performance.

#### **2.4.1 Processor-In-the-Loop (PIL) validation**

The designed AJC controller is implemented in a processor in the loop (PIL) setup to validate operation of the controller in real-time. Figure 2.11 shows a schematic diagram of the PIL setup. The plant used for the validation is the computationally efficient Amesim based ROM discussed in the introduction and further in Section 2.2 of this chapter. The MATLAB-Amesim based model, containing the plant and the controller, is converted into suitable code using dSPACE tools for implementation on

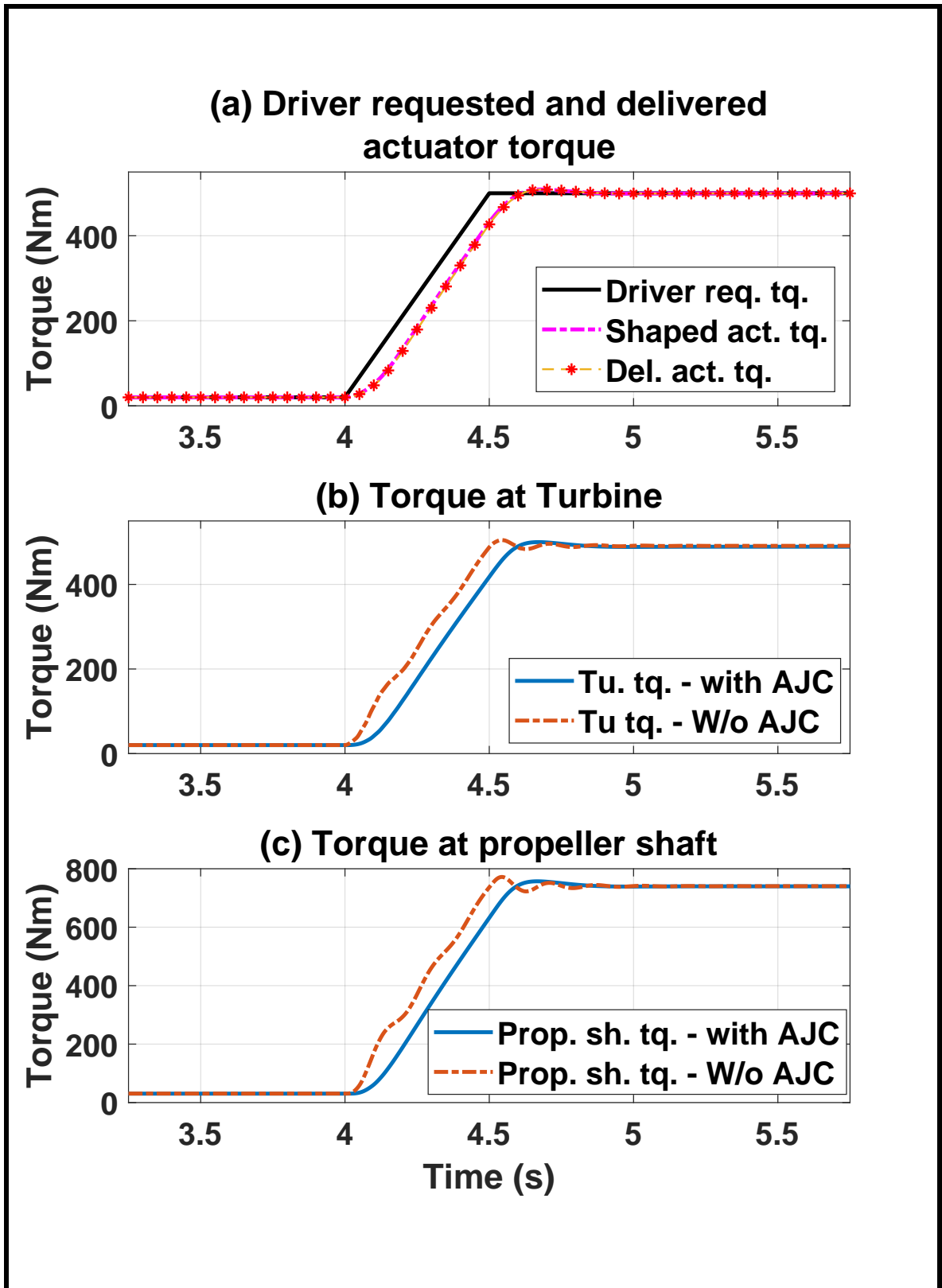
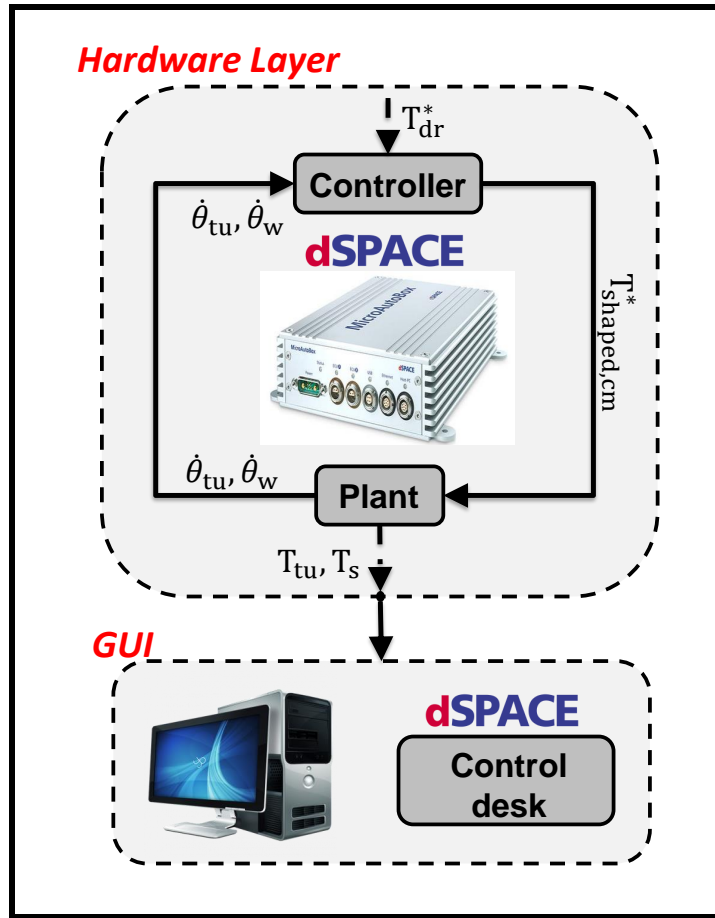


Figure 2.10: Response comparison of driveline with and without AJC controller

dSPACE MicroAutobox (MABx). Further, the built code is flashed in MABx.



**Figure 2.11:** Schematic of the designed PIL setup

The driver requested torque is provided through the model's built-in signal builder block. The controller inside MABx receives the requested torque and provides a shaped output torque command to the plant model (also inside the MABx) as shown in Figure 2.11. Simultaneously, the turbine and wheel speed signals are taken from the plant model to the controller, to compute the propeller shaft torque derivative. Parallely, the propeller shaft torque and turbine torque values were received and recorded by the Control Desk graphical user interface (GUI) as the output from

the plant model running inside MABx. The specifications of dSPACE MABx and computer system used for this work are mentioned in Table 2.4

**Table 2.4**  
MicroAutoBox and PC Configurations

System parameter	Description
<b>Computer system specifications</b>	
Computer Processor	Intel® Core™ i7-8750H CPU @2.20 GHz, 2208Mhz
RAM	16.0 GB
System type	x64 - based PC
<b>dSPACE hardware specifications</b>	
MicroAutoBox II	1401/1511/1514
Processor	IBM PPC 750GL, 900Mhz (incl. 1MB level 2 cache)
Memory	16 MB + 6 MB + 16 MB

The results for the PIL validation are shown in Figure 2.12. Results obtained through the PIL setup are compared with the ones obtained from the simulink model. The average error between the two ‘shaped torque requests’, as shown in Figure 2.12(a), is observed to be 0.6 %. Next, the average errors between the ‘turbine and propeller shaft torques’ w.r.t. their counterparts from the simulink model, as shown in Figure 2.12(b) and 2.12(c), are also found to be 0.6 % each, respectively.

Further, Table 2.5 tabulates the processing performance parameters obtained for the simulation run. Note that during this PIL validation, The sample time used for running the controller is 10 ms. This was done to verify the real-time performance capability of the controller. Further, note that the term ‘Turn-around time’ used in Table 2.5 refers to the average processing time taken by the processor from receiving

the input driver requested torque signal to providing the processed results of propeller shaft and turbine torque at the Control Desk interface, for one cycle run.

**Table 2.5**  
PIL performance assessment

<b>Parameter</b>	<b>Value</b>
Controller sample time	10 ms
Turn-around time	0.04 ms
Run time	7 s

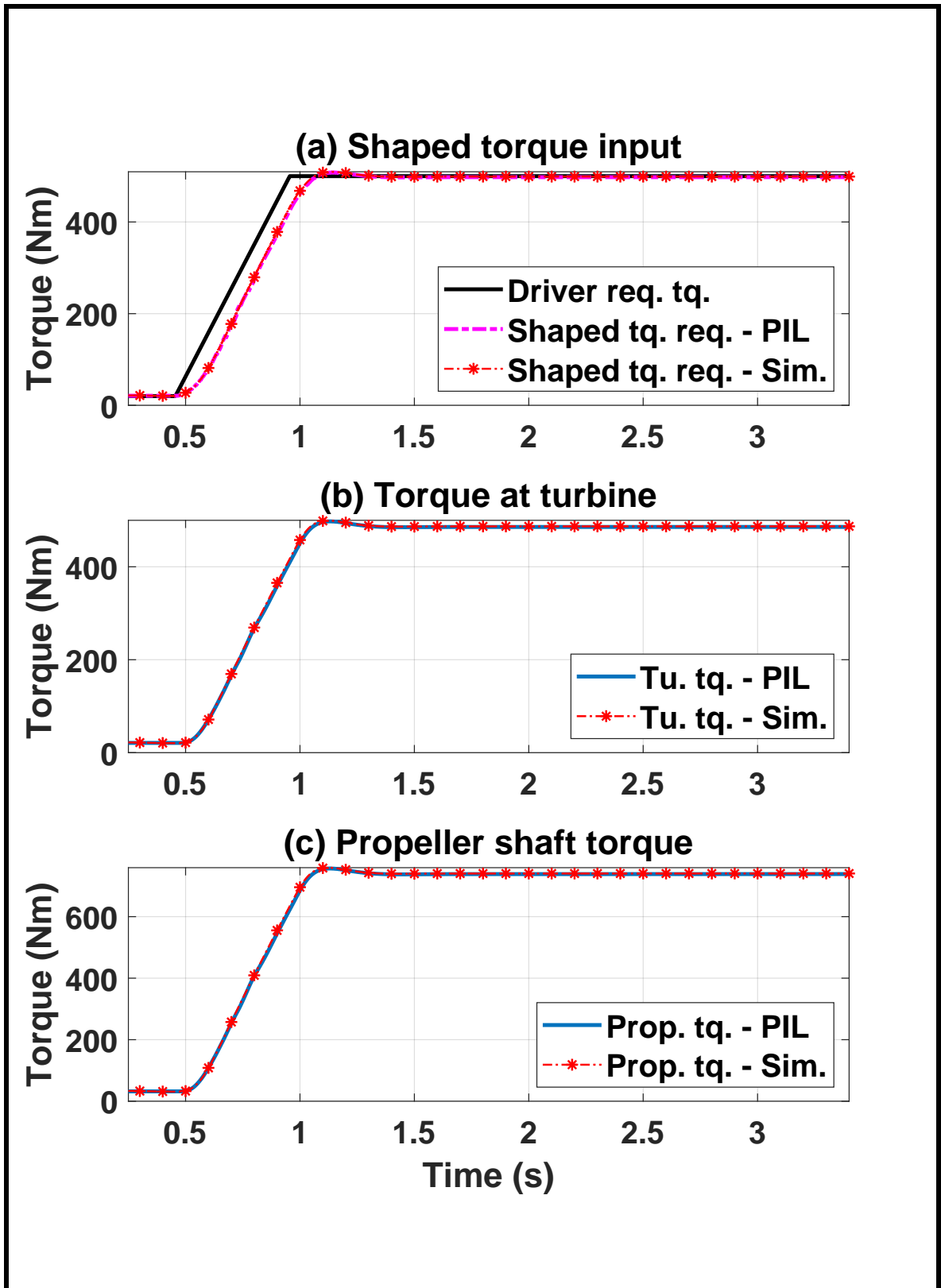


Figure 2.12: Performance of the AJC controller in the PIL setup



# Chapter 3

## Model-based feedforward and feedback control to meet requested torque during torque converter slip

Chapter 2 discussed the design and development of a torque shaping controller for the driveline in the contact mode with a locked torque converter. However, there are certain scenarios while driving where the slipping of torque converter is necessary. For instance, while running at low engine speeds the noise and vibration performance of the driveline become prominent and requires the actuator's oscillations to be cut-off from propagating to the driveline. The study in [13] mentions the disadvantages of the system in terms of noise and vibration due to torque fluctuation produced in the

engine being transmitted directly to drivetrain. Further, as mentioned in [53], the low frequency torsional oscillations due to slower combustion rate may resonate with and further excite the oscillations in other components of the vehicle. These unwanted oscillations can be reduced by slipping the torque converter clutch (TCC), as in that case the involved fluid damping will not allow the oscillations to pass through to the drivetrain. However, in such a situation where the torque converter clutch is slipping, because of the involved fluid coupling dynamics, a certain amount of deviation is observed between the torque at the impeller and the corresponding torque at the turbine (see Figure 3.1(b)). This will lead to the delivered torque deviating from the desired torque profile and causing a sluggish response from the driveline. This sluggishness in the driveline response can be observed at the propeller shaft torque, as shown in Figure 3.1(c), and at wheels.

In this chapter, a detailed discussion on the development of an anti-lag torque controlling (ALTC) technique is conducted where an attempt has been made to overcome this torque gap generated due to the slipping torque converter clutch.

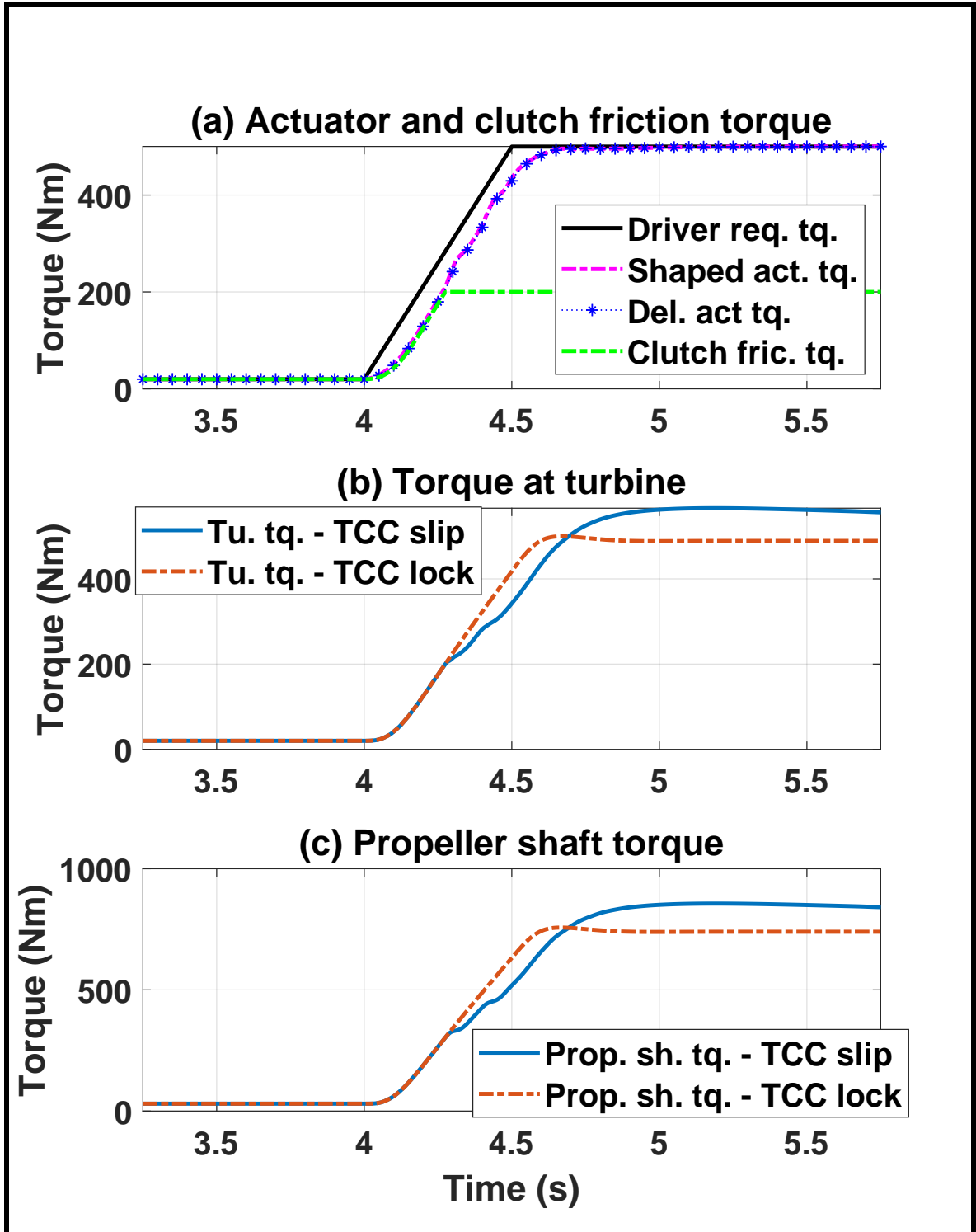


Figure 3.1: Response of AJC controlled driveline with slipping torque converter clutch

## 3.1 Background

The torque converter assembly with a lockup clutch incorporates two torque travel paths, one, through the mechanical friction coupling of the lockup clutch which connects and disconnects the impeller with the turbine via physical contact ([1](#) in Figure 3.2) and, two, through the hydrodynamic fluid coupling between the impeller and the turbine ([2](#) in Figure 3.2). The slipping or locked state of the torque converter is governed by the lockup clutch which is generally operated hydraulically or pneumatically. When the commanded torque capacity of the clutch is more than or equal to the torque delivered by the actuator, i.e., an engine or a motor, the clutch is locked and all of the torque from the source is transmitted across the lockup clutch to the drivetrain. However, for the case of slipping torque converter the commanded clutch capacity is lower than the actuator delivered torque. This clutch capacity is controlled by controlling the normal reaction between the two friction elements. Equation (3.1) shows a general relation of the clutch capacity with the normal reaction between the clutching elements as:

$$T_c = \mu NR_{\text{eff}}, \quad (3.1)$$

where  $T_c$  is the commanded clutch capacity,  $\mu$  is the coefficient of friction,  $N$  is the normal reaction between the clutching elements and  $R_{\text{eff}}$  is the effective radius of clutch. For this work, the clutch actuation dynamics is assumed to be of first order

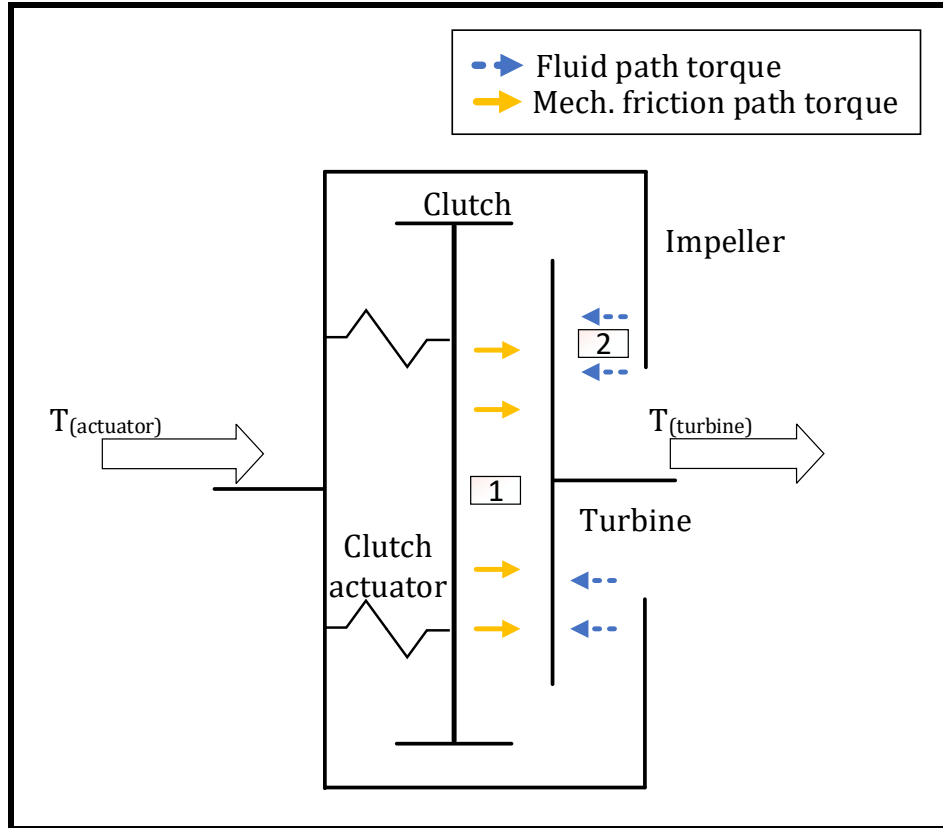


**Figure 3.2:** Schematic of torque converter assembly with distinct torque flow paths

with a time constant of 50 ms. This assumption was based on hydraulic dynamics involved in actuation of the clutching system [54].

From Figure 3.2, it can be seen that when the torque converter is locked, it allows the torque delivered by the actuator to directly pass through the lockup clutch to the transmission assembly (path 1), as has been mentioned before. But, when the torque converter clutch slips, the torque across the converter assembly passes through the fluid path (path 2) along with the friction path (path 1). This passage of torque is linear for the friction path but attains nonlinearity for the part that passes through

the fluid path.

## 3.2 Control strategy layout

This section discusses the control scheme designed to perform the desired task of making the turbine side of the converter to follow the shaped torque request overcoming the torque gap between the impeller and turbine due to converter's clutch slip. Figure 3.3 shows the overall schematic of control strategy including the AJC with the anti-lag torque control. The control scheme is showcased to work in conjunction with the AJC. Here, a detailed discussion on the highlighted portion in the figure, that showcases the proposed ALTC control strategy is provided.

As shown in Figure 3.3, the shaped torque command out of the AJC in contact mode is passed through the ALTC, which modifies the commanded torque further so that the said torque gap can be overcome. Note that the slipping of torque converter only takes place once the backlash has traversed (i.e., in the contact mode), as it is required to prevent the low speed torsional oscillations to transmit to the driveline from the primary actuator. Therefore, the converter's lockup clutch begins slipping in the contact mode and the ALTC is expected to modify the actuator torque in this mode.

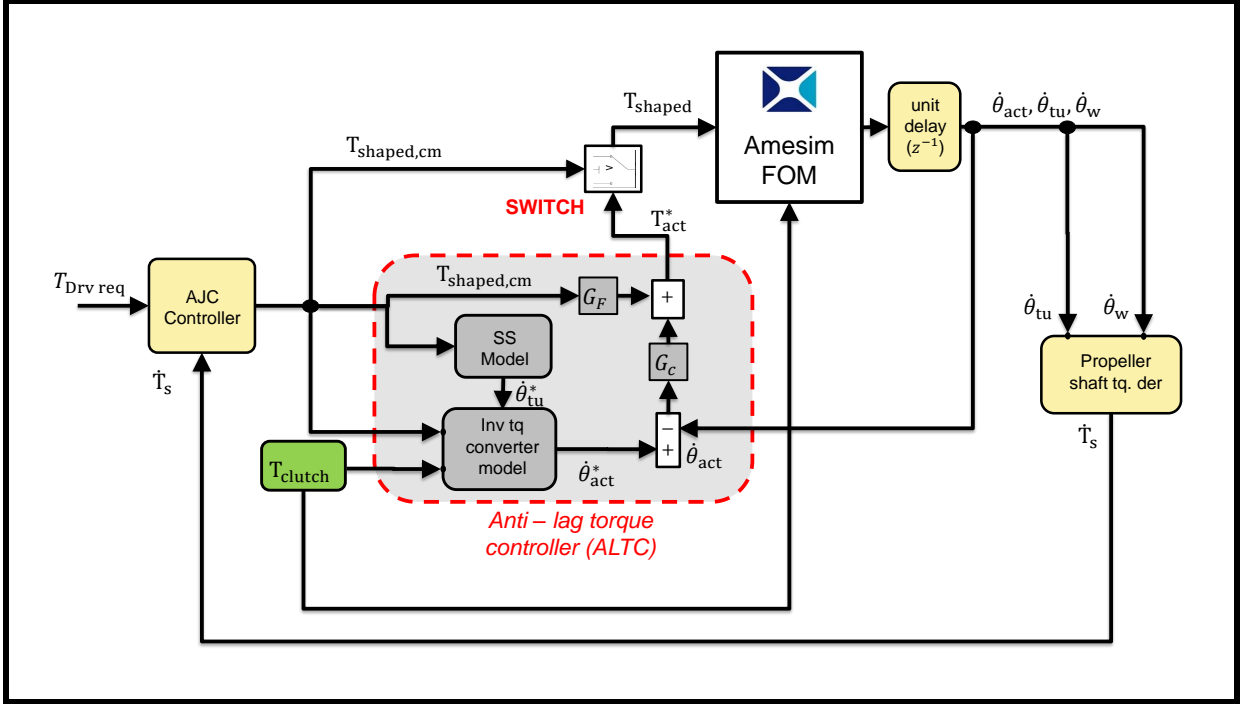


**Figure 3.3:** Overall schematic of proposed control strategy

The shaped torque command out of the ALTC (specifically for when the converter slips),  $T_{act}^*$ , is then provided as an input to the actuator of the Amesim based FOM, and the available measured signal of impeller speed (which is also the actuator speed),  $\dot{\theta}_{act}$  is taken as feedback to the ALTC. Further, note that the clutch capacity input,  $T_{clutch}$ , for the ALTC is assumed to be known for this work.

In the following sections of this chapter, a detailed discussion has been done on the development of each of the different controller element, shown inside the highlighted section of Figure 3.3.

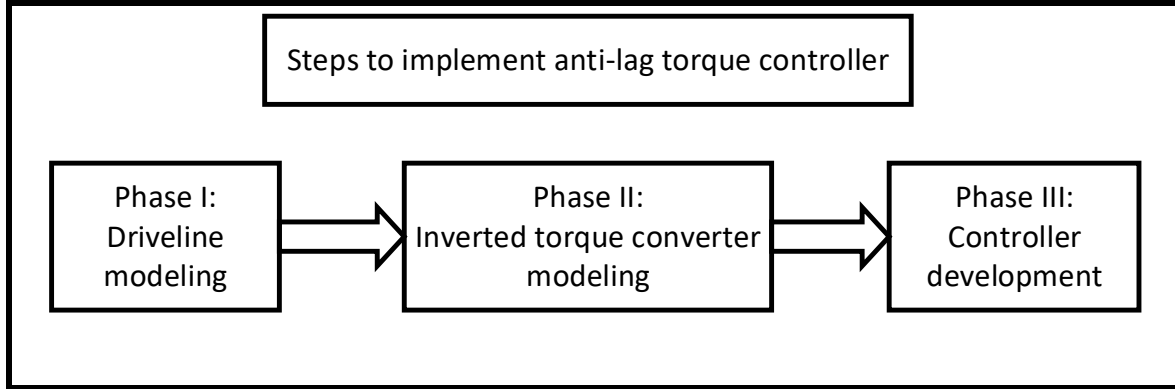


**Figure 3.4:** Categorisation of the proposed control strategy

### 3.2.1 Anti-lag torque control (ALTC)

The developed control scheme relies on the generation of a reference impeller speed signal,  $\dot{\theta}_{act}^*$ , that the actuator is required to follow in order to reach the desired torque performance at the turbine. This shall be realised along the course of this chapter.

The proposed control scheme can be categorised into three phases. The first phase involves the development of a state space model corresponding to the driveline with locked torque converter clutch. The second phase involves the development of an inverted torque converter model, whose function is to provide a reference impeller speed signal based on the known fluid path turbine torque and the turbine speed determined from the first phase. The third phase of this strategy involves the development of a combined feedforward and feedback controller to make the plant follow the reference impeller speed signal generated from the second phase. The three phases to design the proposed ALTC are shown in Figure 3.4.

### 3.3 Phase I: Driveline state space modeling with locked torque converter clutch

Based on the control strategy layout discussed above (Section 3.2), it is intended to develop a mathematical model representation of the driveline with locked torque converter. The shaped torque request output from the contact mode AJC controller,  $T_{\text{shaped,cm}}$ , is the input to the driveline model along with the road load torque,  $T_{\text{load}}$ . The speed of the turbine,  $\dot{\theta}_{\text{tu}}^*$ , and wheel speed,  $\dot{\theta}_{\text{w}}$ , are the outputs. The wheel speed output of the state space model is only required to compute the road load torque.

It is important to note that with the locked torque converter driveline, the impeller speed and turbine speed are considered equal. The actuator or turbine speed output of state space model for driveline with locked torque converter is taken as an input by the inverted torque converter model to generate the desired reference impeller speed during the converter clutch slip.

In this section, the state space model development has been discussed, similar to one discussed in Section 2.2.2 but with a different set of outputs. In the later half of this section, the validation of the attained outputs by comparing them with the respective counterparts from the FOM has been done.

### 3.3.1 State-space model development

Similar to Section 2.2.2, the state space model for the driveline with locked torque converter has been developed based on the reduced order model previously shown in Figure 2.2. This state space model is shown below: , as shown

$$\dot{\mathbf{x}} = \mathbf{A}_{lc}\mathbf{x} + \mathbf{B}_{lc}\mathbf{u} + \mathbf{G}_{lc}\mathbf{d}, \quad (3.2)$$

$$\mathbf{y} = \mathbf{C}_{lc}\mathbf{x} + \mathbf{D}_{lc}\mathbf{u}, \quad (3.3)$$

where the subscript lc indicates the locked torque converter clutch state. Moreover,

$$\mathbf{x} = \left[ \left( \frac{\theta_{act}}{i_t} - \theta_{fd}i_{fd} \right) \quad \dot{\theta}_{tu}^* \quad (\theta_{fd} - \theta_w) \quad \dot{\theta}_{fd} \quad \dot{\theta}_w \right]^T, \quad (3.4)$$

$$\mathbf{y} = \begin{bmatrix} \dot{\theta}_{tu}^* \\ \dot{\theta}_w \end{bmatrix}, \quad (3.5)$$

$$\mathbf{u} = \left[ T_{shaped,cm} \right], \quad (3.6)$$

$$\mathbf{d} = \left[ F_1 \right], \quad (3.7)$$

In the above equations (3.4 - 3.7),  $\left( \frac{\theta_{act}}{i_t} - \theta_{fd}i_{fd} \right)$  represents the twist angle on the actuator side,  $\dot{\theta}_{tu}^*$  is the angular speed of the turbine and also of the actuator in this case,  $(\theta_{fd} - \theta_w)$  is the twist angle on the wheel side,  $\dot{\theta}_{fd}$  is the angular speed of the final

drive,  $\dot{\theta}_w$  is the angular speed of the wheel,  $T_{\text{shaped,cm}}$  is the shaped torque request by the AJC controller, and  $T_{\text{load}}$  is the road load acting on the vehicle. Furthermore, the matrices  $\mathbf{A}_{\text{lc}}$ ,  $\mathbf{B}_{\text{lc}}$ ,  $\mathbf{C}_{\text{lc}}$ ,  $\mathbf{D}_{\text{lc}}$  and  $\mathbf{G}_{\text{lc}}$  in equation (3.2) and (3.3) are given by

$$\mathbf{A}_{\text{lc}} = \begin{bmatrix} 0 & \frac{1}{i_t} & 0 & -i_{\text{fd}} & 0 \\ -\frac{k_s}{J_1 i_t} & -\frac{c_s}{J_1 i_t^2} & 0 & \frac{c_s i_{\text{fd}}}{J_1 i_t} & 0 \\ 0 & 0 & 0 & 1 & -1 \\ \frac{k_s i_{\text{fd}}}{J_2} & \frac{c_s i_{\text{fd}}}{J_2 i_t} & -\frac{k_w}{J_2} & -\frac{(c_s i_{\text{fd}}^2 + c_w)}{J_2} & \frac{c_w}{J_2} \\ 0 & 0 & \frac{k_w}{b} & \frac{c_w}{b} & -\frac{c_w}{b} \end{bmatrix}, \quad (3.8)$$

$$\mathbf{B}_{\text{lc}} = \begin{bmatrix} 0 & \frac{1}{J_1} & 0 & 0 & 0 \end{bmatrix}^{\text{T}}, \quad (3.9)$$

$$\mathbf{C}_{\text{lc}} = \begin{bmatrix} 0 & 1 & 0 & 0 & 0 \\ 0 & 0 & 0 & 0 & 1 \end{bmatrix}, \quad (3.10)$$

$$\mathbf{D}_{\text{lc}} = \begin{bmatrix} 0 \\ 0 \end{bmatrix}, \quad (3.11)$$

$$\mathbf{G}_{\text{lc}} = \begin{bmatrix} 0 & 0 & 0 & 0 & \frac{-r_{\text{T}}}{b} \end{bmatrix}^{\text{T}}. \quad (3.12)$$

where  $b = J_3 + Mr_T^2$ .

Moreover, all other notations used in the model are same as those mentioned in Section 2.2.1.

### 3.3.2 Validation of the state space model

The developed state space model is validated by comparing its outputs with the Amesim based FOM prepared in [4]. For this validation, the AJC shaped torque for a ramp torque command was provided as an input to both the models, and the corresponding turbine and wheel speeds were compared. Figure 3.5 shows the comparison of the turbine and wheel speed outputs from the developed state space model with their respective counterparts from FOM. As can be observed in the figure, the turbine speed and wheel speeds of both the models are in good agreement with an average error of 2.2% and 2.3%, respectively. For the development of a control strategy, a computationally efficient model is required. This helps in control applications, where the processors computation time is of importance. Therefore, this validation allows us to consider the error bounds as acceptable and use the state space model for developing the control strategy.

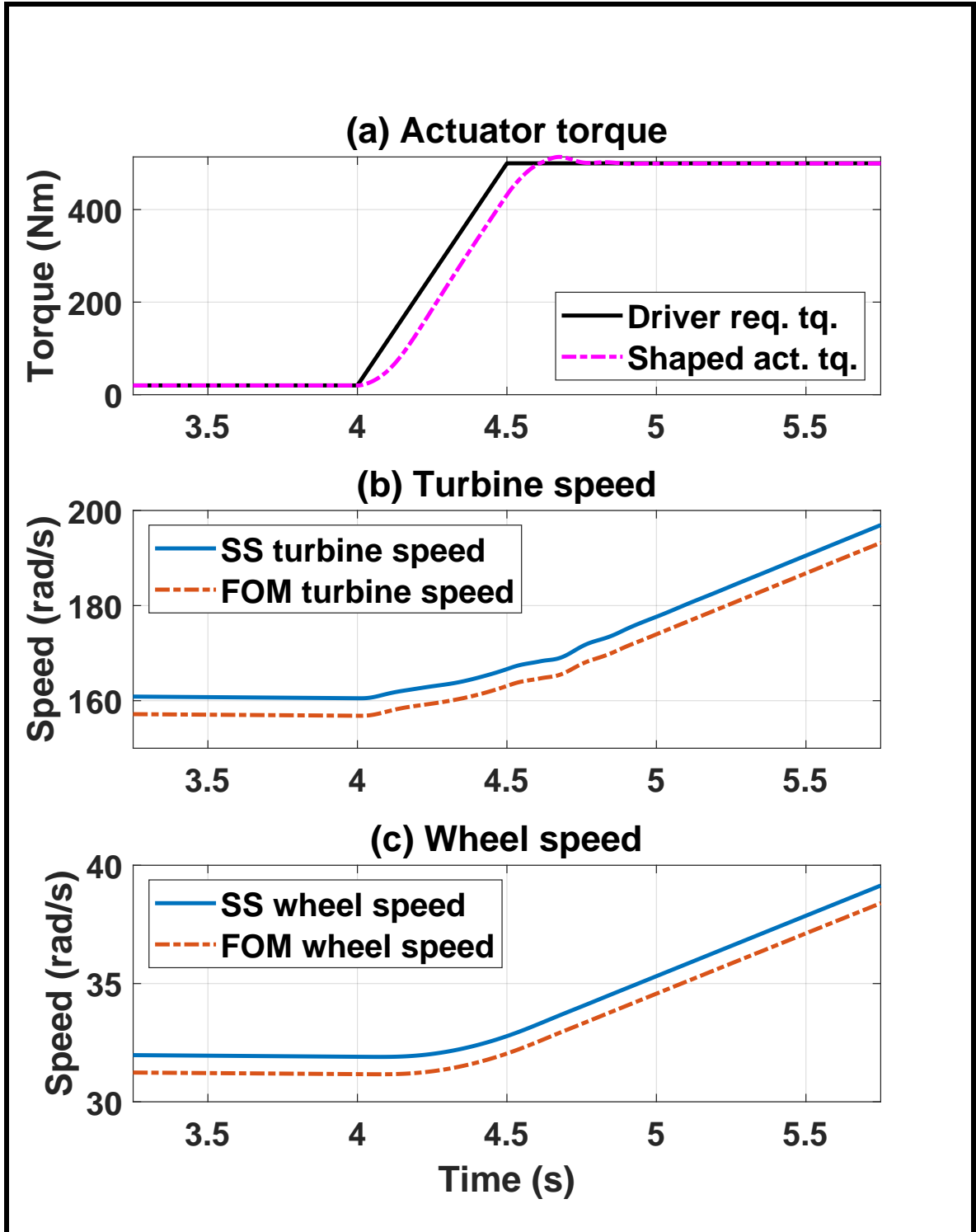


Figure 3.5: Output comparison of proposed state space model with full-order model

## **3.4 Phase II: Inversion of torque converter model**

Once the state space model is developed in phase 1 (Section 3.3), the next task is to set up the inverted torque converter model, as can be followed from Figure 3.3. This section discusses the stage wise development of the inverted torque converter model. First stage involves a discussion on torque converter models and showcases the mathematical relations based on Newton's laws of motion and empirical equations (Section 3.4.1). Further, in this stage, a Kotwicki model from the available K-factor lookup table data is developed. Next, in second stage, the inverted torque converter models are prepared based on the two considered modeling approaches (Section 3.4.2), and compared for their performances.

### **3.4.1 Torque converter model assembly**

This section discusses the model of the torque converter used for Amesim based FOM development in [4] and for designing of the control scheme in this work. The representations of the two torque paths across the torque converter assembly, mentioned in Section 3.1 are discussed in detail below.

### 3.4.1.1 Friction path

Through torque converter lockup clutch , the torque passes via the clutch friction element, and is dependent on the normal reaction and coefficient of friction between the elements in contact, as represented by Equation 3.1. Mathematically, the torque flow across the assembly can be represented using the Newton's laws of motion on both the impeller and the turbine.

**Torque balancing at impeller:**

$$T_{\text{act}} - T_c - T_{\text{imp,fluid}} = J_{\text{imp}}\ddot{\theta}_{\text{imp}}, \quad (3.13)$$

**Torque balancing at turbine:**

$$T_c + T_{\text{tu,fluid}} - T_{\text{res}} = J_{\text{tu}}\ddot{\theta}_{\text{tu}}, \quad (3.14)$$

where  $T_c$  represents the clutch capacity for the lock up clutch. Furthermore,  $T_{\text{act}}$  is the torque delivered by the actuator on the impeller,  $T_{\text{res}}$  is the load on turbine,  $J_{\text{imp}}$  is the rotational inertia of the impeller,  $J_{\text{tu}}$  is the rotational inertia of the turbine,  $\ddot{\theta}_{\text{imp}}$  is the angular acceleration of the impeller and,  $\ddot{\theta}_{\text{tu}}$  is the angular acceleration of the turbine of the torque converter. Further,  $T_{\text{imp,fluid}}$  and  $T_{\text{tu,fluid}}$  represents the fluid path torque on impeller and turbine respectively. The two fluid path torques

are discussed below.

### 3.4.1.2 Fluid path - Speed Ratio, Torque Ratio and Capacity Factor (K-Factor lookup table model)

This section shows the empirical relation between the impeller and turbine torque through fluid path. The relation is dependent on the speed ratio (SR), torque ratio (TR) and capacity factor ( $K_{\text{cap}}$ ) as shown in the following equations:

$$\text{SR} = \frac{\dot{\theta}_{\text{tu}}}{\dot{\theta}_{\text{imp}}}, \quad (3.15)$$

$$\text{TR} = \frac{T_{\text{tu,fluid}}}{T_{\text{imp,fluid}}}, \quad (3.16)$$

$$K_{\text{cap}} = \frac{\left(\frac{60}{2\pi}\right)\dot{\theta}_{\text{imp}}}{\sqrt{T_{\text{imp,fluid}}}}, \quad (3.17)$$

where  $\dot{\theta}_{\text{tu}}$  and  $\dot{\theta}_{\text{imp}}$  represents the turbine and impeller angular speeds in RPM, respectively. Using above set of equations (3.15 - 3.17), torque via fluid path at impeller side of the converter is deduced by

$$T_{\text{imp,fluid}} = \frac{\left(\frac{60}{2\pi}\right)^2 \dot{\theta}_{\text{imp}}^2}{K_{\text{cap}}(\text{SR})}, \quad (3.18)$$

and the torque at the turbine acting via fluid path can be obtained by

$$T_{tu,fluid} = \frac{\left(\frac{60}{2\pi}\right)^2 \dot{\theta}_{imp}^2 TR(SR)}{K_{cap}(SR)}, \quad (3.19)$$

where  $TR$  and  $K_{cap}$  are functions of  $SR$  and their relation in general is determined through experimental analysis of the torque converter. For the torque converter under consideration, these experimental details were provided by the project sponsor. The relation of  $TR$  and  $K_{cap}$  with  $SR$  is shown in Figure 3.6 and 3.7 respectively.

Figures 3.8 and 3.9 show the fluid path torque band of the torque converter at impeller and turbine for a range of operating impeller speeds. The shown torque converter operation is in the torque multiplication mode ( $SR \leq 0.95$ ), which is discussed in following sections. The figure projects the dependency of fluid path torque on the impeller speed and speed ratio.

### 3.4.1.3 Fluid path - Kotwicki model

As discussed in Section 1.3.2 of Chapter 1, a Kotwicki model of torque converter is based on simple algebraic equations and hence is more flexible for inversion when compared to the model developed through the K-Factor lookup table approach (see Figure 1.5). Thus, the algebraic equations based Kotwicki model is discussed in this section. A Kotwicki based empirical model of the torque converter represents the

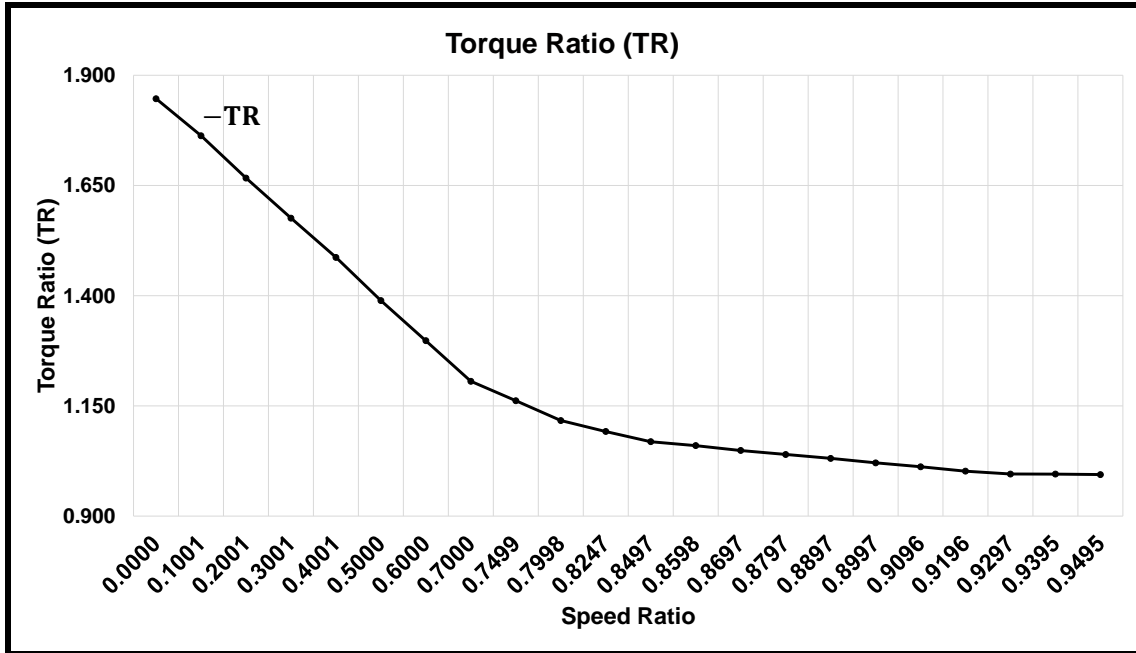


Figure 3.6: Torque ratio versus Speed Ratio

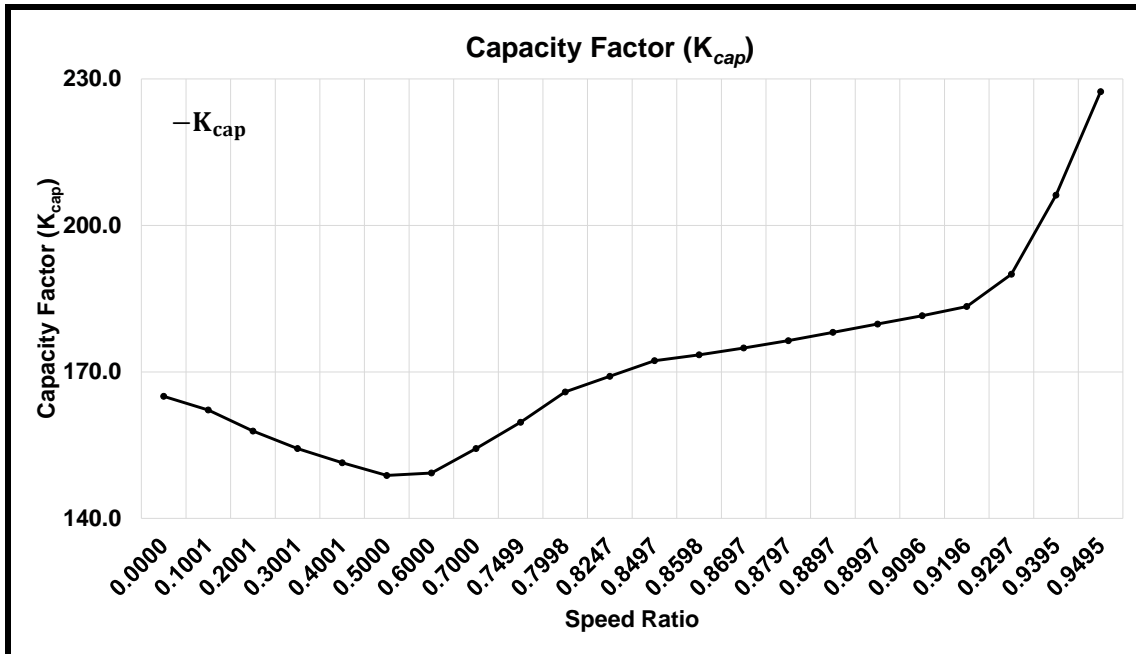


Figure 3.7: Capacity factor versus Speed Ratio

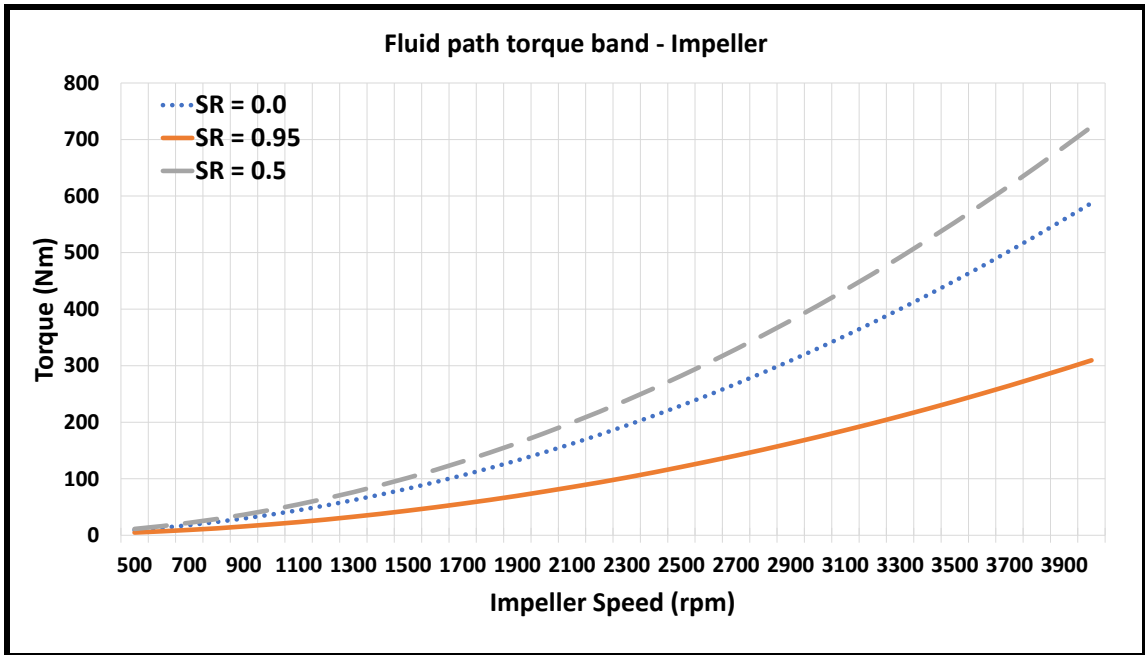


Figure 3.8: Fluid path torque band - Impeller

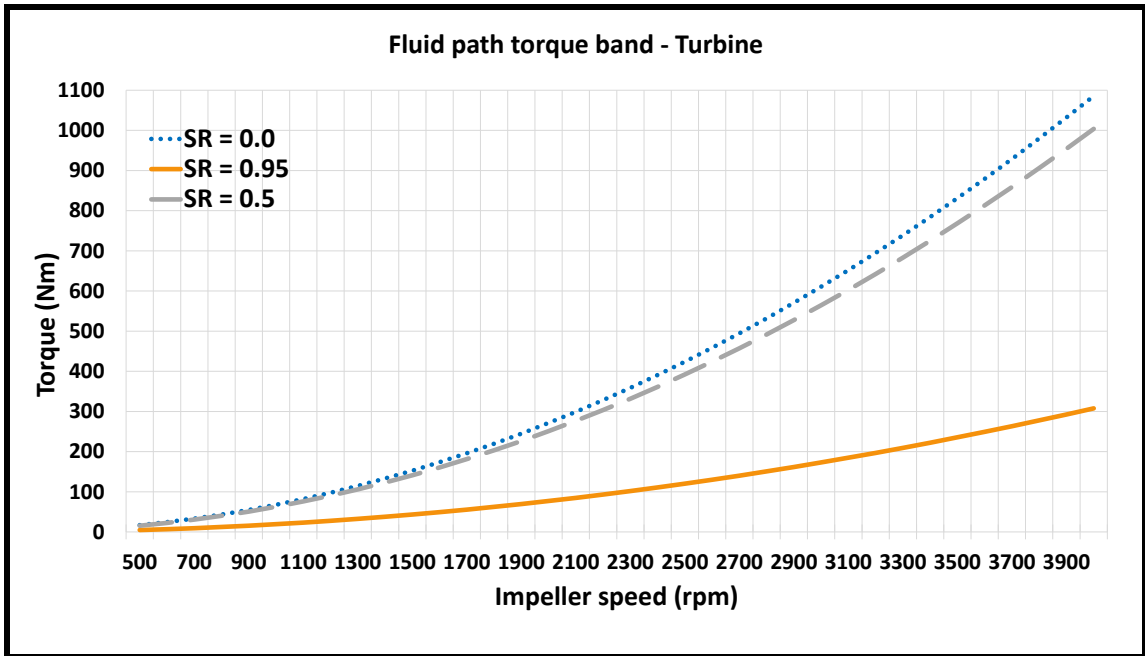


Figure 3.9: Fluid path torque band - Turbine

fluid path torques as quadratic equations in terms of the impeller and turbine speeds.

The functioning of torque converter is categorised into two distinct modes. The first mode is the **torque multiplication** mode, where the stator inside the torque converter is fixed w.r.t. the impeller and turbine via a one-way clutch. As the fluid flows from impeller across the stator to turbine, amplification of torque occurs. For the torque converter under consideration, this mode pertains over the range of speed ratio,  $0 \leq SR \leq 0.95$ . The second mode is **fluid coupling** mode where there isn't any torque amplification as the stator rotates freely and the impeller and turbine have nearly equal torques.

Based on the empirical relations proposed by Kotwicki, the torque of impeller and turbine can be represented mathematically for the two distinct modes as

**Torque multiplication mode:**

$$T_{\text{imp,fluid}} = \alpha_{1,\text{act}} \dot{\theta}_{\text{act}}^2 + \alpha_{2,\text{act}} \dot{\theta}_{\text{act}} \dot{\theta}_{\text{tu}} + \alpha_{3,\text{act}} \dot{\theta}_{\text{tu}}^2, \quad (3.20)$$

$$T_{\text{tu,fluid}} = \alpha_{1,\text{tu}} \dot{\theta}_{\text{act}}^2 + \alpha_{2,\text{tu}} \dot{\theta}_{\text{act}} \dot{\theta}_{\text{tu}} + \alpha_{3,\text{tu}} \dot{\theta}_{\text{tu}}^2, \quad (3.21)$$

**Fluid coupling mode:**

$$T_{\text{imp,fluid}} = T_{\text{tu,fluid}} = \alpha_{1,\text{fc}} \dot{\theta}_{\text{act}}^2 + \alpha_{2,\text{fc}} \dot{\theta}_{\text{act}} \dot{\theta}_{\text{tu}} + \alpha_{3,\text{fc}} \dot{\theta}_{\text{tu}}^2, \quad (3.22)$$

where  $\alpha_{i,j}$ , (for  $i = 1, 2, 3$  and  $j = \text{act, tu, fc}$ ) represents the coefficients of the Kotwicki model equations of the impeller (actuator) and turbine for torque multiplication and fluid coupling mode.  $\dot{\theta}_{\text{act}}$  is the impeller or actuator angular speed and,  $\dot{\theta}_{\text{tu}}$  is the angular speed of the turbine.

In this work, an attempt was made to come up with a torque converter model based on Kotwicki approximations derived from the available details on the speed ratio, torque ratio and capacity factor as discussed in Section 3.4.1.2. However, as the data was only available for the torque multiplication mode, i.e., up till speed ratio 0.95, the Kotwicki model was prepared for torque multiplication mode and post this ratio the torque converter assembly was assumed locked as the torque of impeller and turbine became equal.

#### **3.4.1.4 Determination of the Kotwicki coefficients**

The coefficients from equations (3.20) and (3.21) were determined using a parameter estimation approach. A virtual experimental set up was prepared in Simulink. Simultaneously, the Amesim based FOM model was run for different test cases and the corresponding impeller speed, turbine speed, impeller torque and turbine torque signals were recorded. Further, for each set of known impeller and turbine speeds, the output of the Kotwicki model was made equal to the known output of the available

torque converter model, while concurrently estimating the coefficients of the Kotwicki model equations. The layout for this virtual experimentation process is shown in Figures 3.10 and 3.11. To carry out the estimation process, the parameter estimation tool of MATLAB was used.

Note that in this procedure the empirical model details (SR, TR and  $K_{cap}$ ) were only available for torque multiplication mode. Hence, the experimental setup focused on running the torque converter in this mode and determining the concerned Kotwicki model coefficients for this mode only.

The Kotwicki coefficients for impeller torque Equation (3.20) and turbine torque Equation (3.21) are given in Table 3.1 and Table 3.2, respectively.

**Table 3.1**  
Kotwicki coefficients for impeller torque

Coefficients	Values in $\left(\frac{\text{Nm}}{(\text{rad/s})^2}\right)$
$\alpha_{1,\text{act}}$	$0.77 \times 10^{-3}$
$\alpha_{2,\text{act}}$	$12.44 \times 10^{-3}$
$\alpha_{3,\text{act}}$	$-11.52 \times 10^{-3}$

#### 3.4.1.5 Validation of Kotwicki model

Figure 3.12 compares the output of estimated Kotwicki model with the output calculated from the available torque converter model. Figure 3.12(a) projects the known

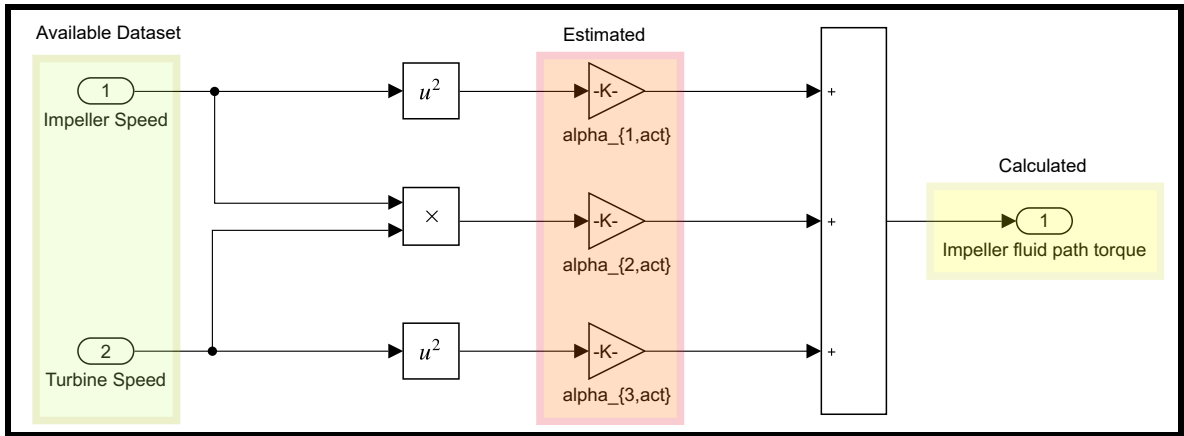


**Figure 3.10:** Kotwicky coefficients estimation for impeller fluid path torque

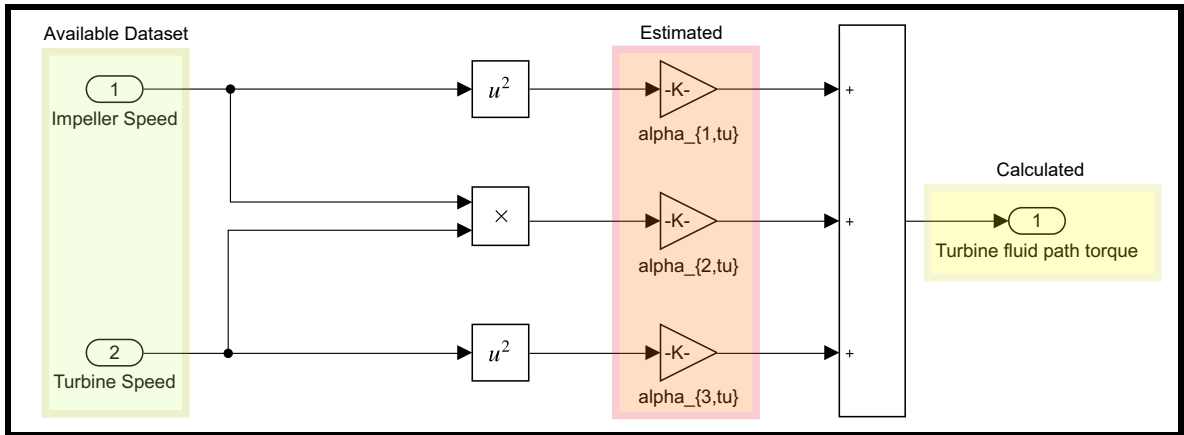


**Figure 3.11:** Kotwicky coefficients estimation for turbine fluid path torque

**Table 3.2**  
Kotwicky coefficients for turbine torque

Coefficients	Values in $\left(\frac{\text{Nm}}{(\text{rad/s})^2}\right)$
$\alpha_{1,tu}$	$5.04 \times 10^{-3}$
$\alpha_{2,tu}$	$6.36 \times 10^{-3}$
$\alpha_{3,tu}$	$-9.94 \times 10^{-3}$

recorded values of the impeller and turbine speed signals for a test case. Figure 3.12(b) shows the comparison of the impeller side fluid path torque. The two computed outputs are in close proximity with an average percentage error of 1.3%. Hence, the estimated coefficients for Equation (3.20) are validated. Similarly, from Figure 3.12(c), the Kotwicki coefficients for turbine torque Equation (3.21), are validated as the average percentage error computed between the two is 1.2%.

### 3.4.2 Inversion of torque converter model

Based on the control strategy discussed in Section 3.2, the requirement in order to overcome the torque deviation is to compute a desired impeller speed reference,  $\dot{\theta}_{act}^*$ , for a known reference of turbine fluid path torque,  $(T_{tu}^* - T_c)$ , and known turbine speed,  $\dot{\theta}_{tu}^*$ . Note that the torque reference,  $T_{tu}^*$ , is the reference torque command generated by the AJC controller. For the locked torque converter clutch, the reference torque from the AJC is referred to as  $T_{shaped,locked}$  and is acted at the actuator while for the slipping torque converter clutch, the same torque reference from AJC, is addressed as  $T_{tu}^*$  and is considered to act at the turbine in order to attain the desired driveline performance. To attain this desired performance at the turbine, the inverse torque converter model is required to generate the reference impeller speed signal that the actuator shall follow. Therefore, to compute the reference for impeller speed, relations between impeller and turbine fluid path torques and speeds, discussed in

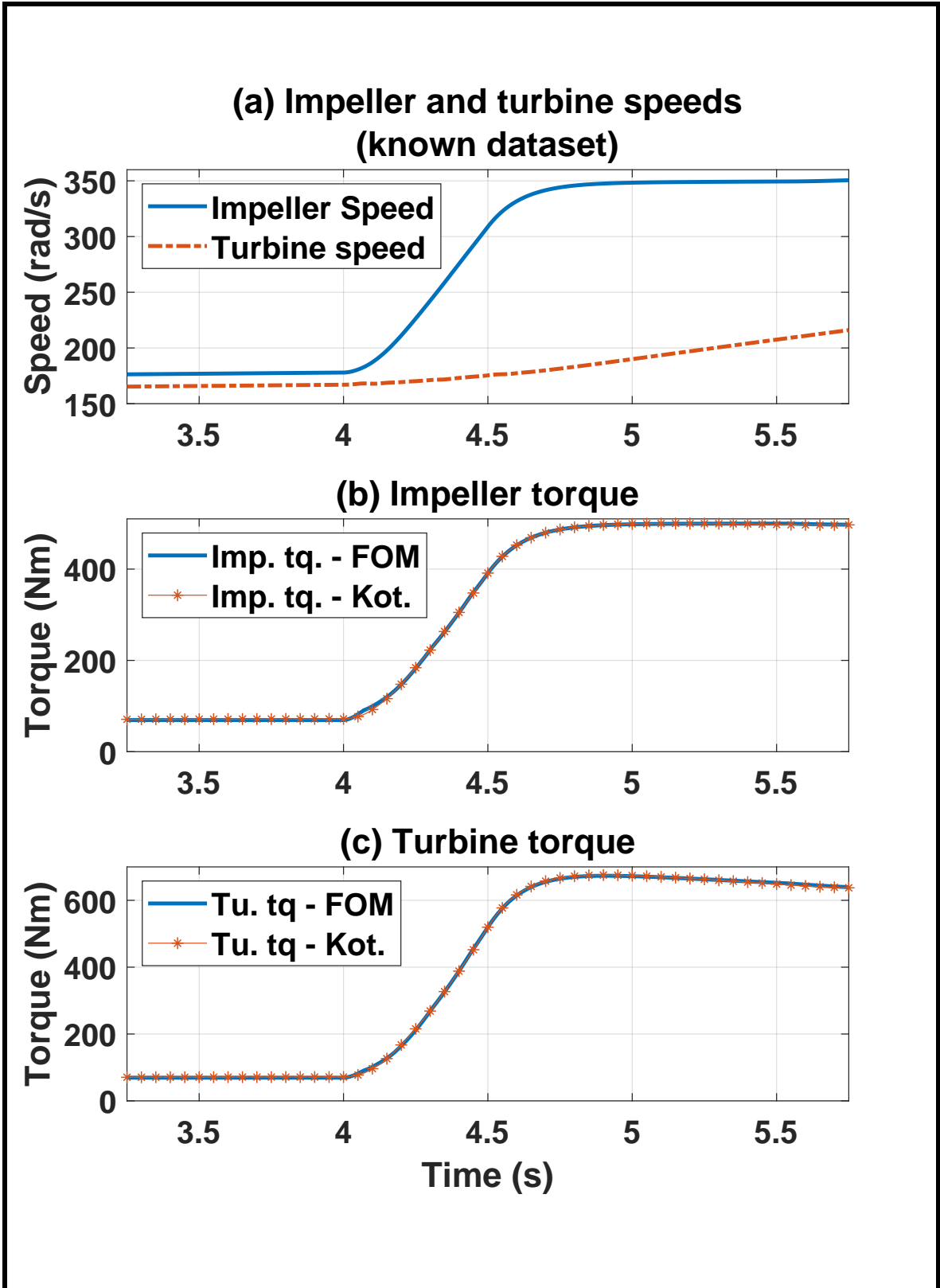


Figure 3.12: Validation of the developed Kotwicky (Kot.) model

Sections 3.4.1.2 and 3.4.1.3, can be used.

By re-framing Equation (3.19), the desired impeller speed reference signal can be obtained as

$$\dot{\theta}_{act}^* = \frac{K_{cap}(SR)\sqrt{(T_{tu}^* - T_c)}}{\sqrt{TR(SR)}}, \quad (3.23)$$

where,  $SR = \frac{\dot{\theta}_{tu}^*}{\dot{\theta}_{act}^*}$ , from equation (3.15). It can be seen that equation 3.23 is an implicit equation as it contains an algebraic loop. Hence, the direct computation of impeller speed reference,  $\dot{\theta}_{act}^*$ , using this equation was not possible. Initially, an approximated computation algorithm was set to overcome the algebraic loop, as shown,

$$\dot{\theta}_{act, k+1}^* = \frac{K_{cap}(SR_k)\sqrt{(T_{tu,k}^* - T_{c,k})}}{\sqrt{TR(SR_k)}}, \quad (3.24)$$

where subscript k denotes the respective signal value at k<sup>th</sup> time step. However, even with this approximation, to attain the refined impeller speed signal significant amount of manual calibration of the speed ratio limit was required for each of the test cases. Therefore, a more feasible approach of using the Kotwicki model approximations was taken into consideration instead.

In order to deduce the impeller speed reference,  $\dot{\theta}_{act}^*$ , for a known reference of turbine fluid path torque,  $(T_{tu}^* - T_c)$ , and turbine speed,  $\dot{\theta}_{tu}^*$ , the Kotwicki model based quadratic equation (3.21) is used. This equation is solved for non-negative real  $\dot{\theta}_{act}^*$ , to get

$$\dot{\theta}_{act}^* = \frac{-\alpha_{2,tu}\dot{\theta}_{tu}^* + \sqrt{((\alpha_{2,tu}\dot{\theta}_{tu}^*)^2 - 4\alpha_{3,tu}\alpha_{1,tu}\dot{\theta}_{tu}^{*2} + 4\alpha_{1,tu}(T_{tu}^* - T_c))}}{2\alpha_{1,tu}}. \quad (3.25)$$

The mathematical validity of the developed inverse torque converter model can be derived from equation 3.25 to be,

$$\dot{\theta}_{act}^* \in \mathbb{R} \geq 0, \forall (T_{tu}^* \geq T_c), \quad (3.26)$$

where the condition ( $T_{tu}^* > T_c$ ) is always true for the slipping torque converter.

Further, the obtained impeller speed signal is considered as the reference for the generation of the desired performance at the turbine.

### 3.4.3 Comparison of inverted torque converter models

In this section, a comparison and validation of the obtained desired impeller speed using the two different approaches from Equations (3.24) and (3.25), has been demonstrated. For designing of controller later in this chapter, the impeller speed obtained through the Kotwicki based inverted model is used as reference.

Figure 3.13 shows the comparison of two reference impeller speeds generated from the two inverted torque converter models shown by Equations (3.24) and (3.25). As

can be seen in Figure 3.13(a), when the delivered actuator torque exceeds the clutch capacity, i.e., when the torque converter clutch begins to slip, a reference impeller speed signal,  $\dot{\theta}_{act}^*$ , shown in Figure 3.13(b) is generated. This  $\dot{\theta}_{act}^*$  signal signifies that if the impeller of the torque converter runs at this speed, the turbine side performance will be as desired, i.e., close to desired shaped torque request.

For the two generated speed references shown in Figure 3.13(b), notice that the initial part of each reference speed profile has a nearly linear profile. This is accredited to a saturation limit that was implemented on the generated signal so that the torque coupling mode is ensured (i.e.  $SR \leq 0.95$ ) at all times that the torque converter clutch is slipping. However, this initial saturation limit is higher for the case of reference speed signal generated using the tabulated data for TR and  $K_{cap}$  (Equation 3.23). As mentioned earlier, this is attributed to the comprehensive tuning required for the reference speed generation using this approach, which forced the generated signal for this case to undergo a higher saturation limit.

Thus, from the two available sources of reference impeller speed signal, the one generated through Kotwicki approach is chosen as a more feasible option for implementation of the control scheme.

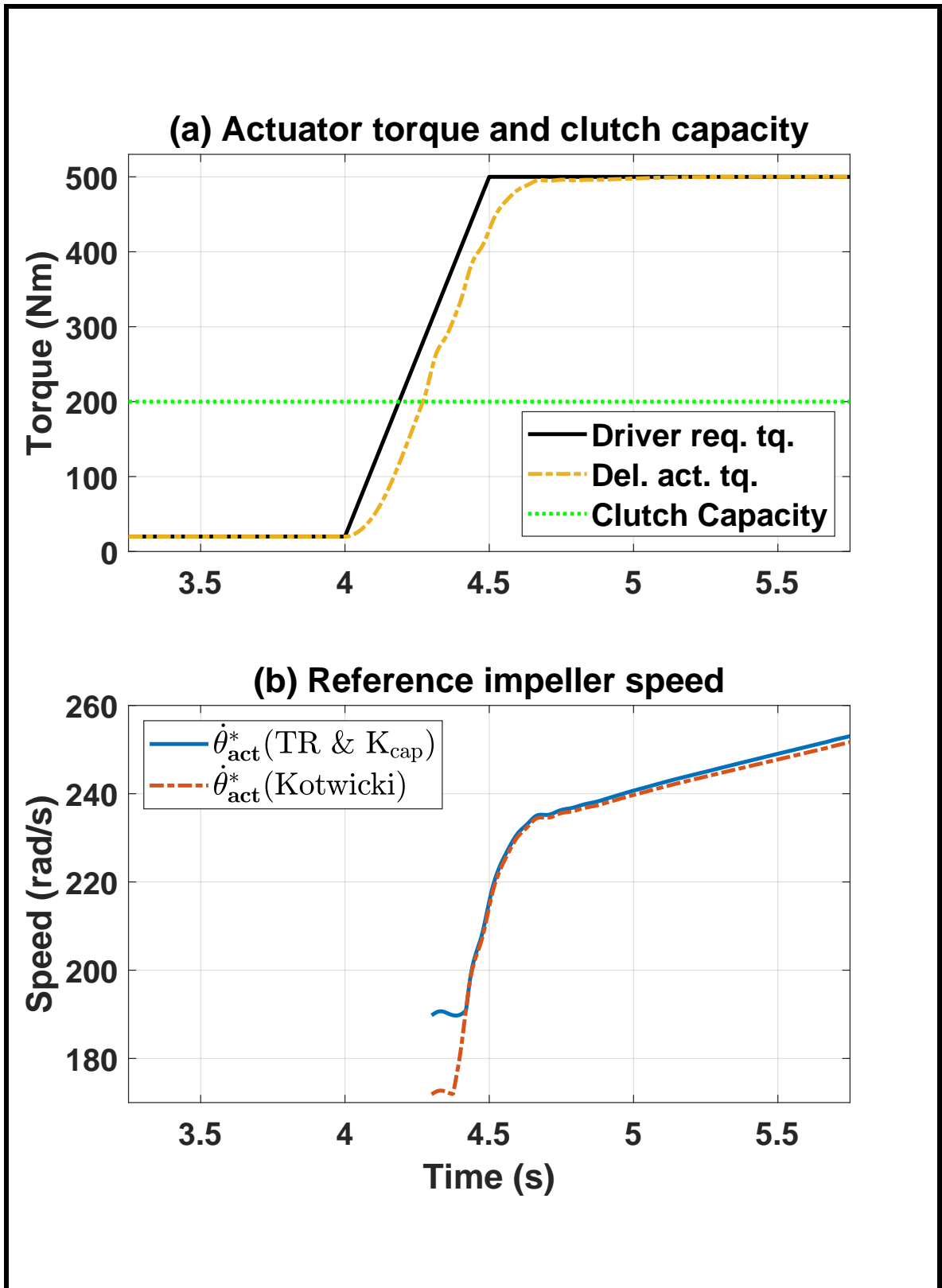


Figure 3.13: Comparison of the Kotwicki based inverted torque converter model w.r.t. TR and  $K_{cap}$  based inverted model.

### 3.5 Phase III: Controller development

In this section, the control strategy for Anti-lag torque control (Figure 3.3), are discussed in detail. Figure 3.14 shows the ALTC strategy from Figure 3.3. A short block diagram study was conducted to further simplify the shown control strategy layout.

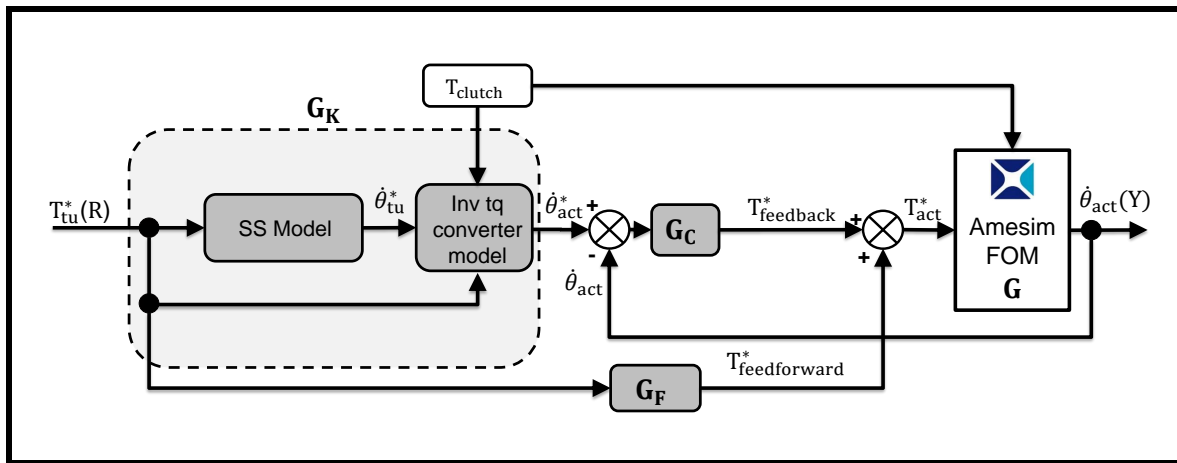


Figure 3.14: Anti-lag torque control

#### Block diagram analysis:

Consider the block  $\mathbf{G}_K$ , in Figure 3.14, to be a transfer function block that takes the reference  $\mathbf{R}$  as an input and provides the output as reference impeller speed,  $\dot{\theta}_{act}^*$ . Furthermore, for the sake of simplicity of the block diagram analysis, the clutch capacity input is assumed to be zero. Next, the requirement of the control scheme was realised to match the FOM impeller speed,  $\dot{\theta}_{act}$ , with the reference impeller speed,

$\dot{\theta}_{act}^*$ . This can be written in the form of a control objective as

$$\mathbf{Y} - \mathbf{R}\mathbf{G}_K = 0, \quad (3.27)$$

and the control law from Figure 3.14 can be framed as

$$((\mathbf{R}\mathbf{G}_K - \mathbf{Y})\mathbf{G}_C + \mathbf{R}\mathbf{G}_F)\mathbf{G} = \mathbf{Y}, \quad (3.28)$$

where  $\mathbf{Y}$  is the plant output,  $\dot{\theta}_{act}$ ,  $\mathbf{G}_F$  is the feedforward path controller with input as the reference  $\mathbf{R}$  and output as a feedforward path torque command  $T_{feedforward}^*$ ,  $\mathbf{G}_C$  is the feedback path controller with the error between the reference and FOM impeller speeds as input and feedback path torque command,  $T_{feedback}^*$ , as output, and  $\mathbf{G}$  is the Amesim based plant with the overall actuator torque command,  $T_{act}^*$ , as input and the FOM impeller speed,  $\mathbf{Y}$ , as the output.

On simplifying the Equation (3.28) the relation for the feedforward controller can be observed as

$$\mathbf{G}_F = \mathbf{G}_K\mathbf{G}^{-1}. \quad (3.29)$$

Based on the results obtained through the block diagram analysis from Figure 3.14 (Equation 3.29), a modified control scheme was realised as shown in Figure 3.15.

This control schematic realises  $G_{FF}$  as the feedforward path controller and  $G_{FB}$  as

the feedback path controller.

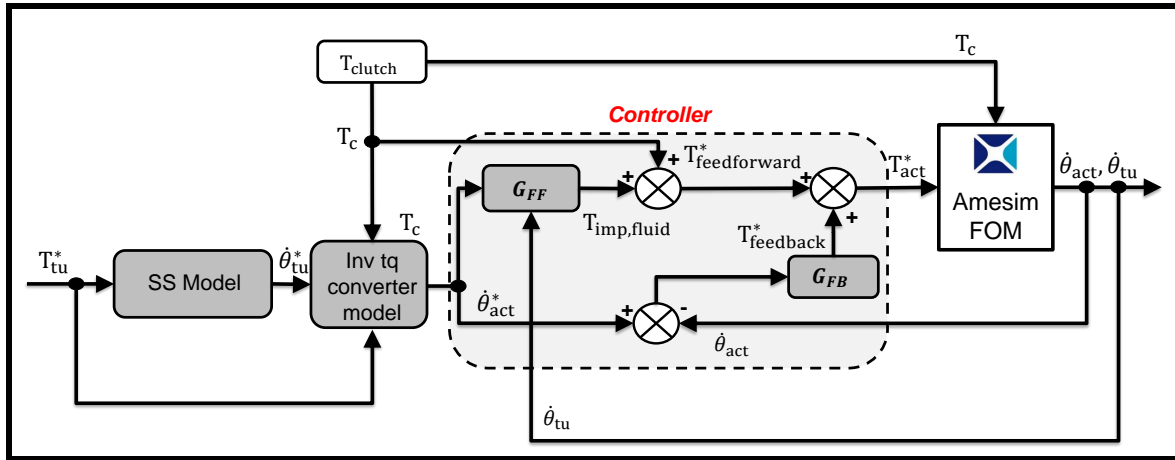


**Figure 3.15:** Anti-lag torque control - modified strategy layout

Thus, from Figure 3.15, for a known reference impeller speed,  $\dot{\theta}_{act}^*$ , the proposed feed-forward and feedback based control structure indicates that the controller is required to match the impeller speed of the torque converter with the generated reference. The inputs to the controller are: (1) generated reference speed signal,  $\dot{\theta}_{act}^*$ , (2) known clutch capacity,  $T_c$ , and (3) plant's impeller speed and turbine speed feedback,  $\dot{\theta}_{imp}$  and  $\dot{\theta}_{tu}$ , and its output is the shaped actuator torque request,  $T_{act}$ , that is input to the plant FOM (see Figure 3.15).

### 3.5.1 Feedforward path

The feedforward path of the controller incorporates a function that takes in the speed reference of impeller,  $\dot{\theta}_{act}^*$ , FOM turbine speed,  $\dot{\theta}_{tu}$ , and clutch capacity,  $T_c$ , as input

and provide, the feedforward actuator torque command,  $T_{\text{feedforward}}$ , as output. This feedforward torque command comprises of torques through the fluid path as well as the friction path. For this overall feedforward actuator torque request, the fluid path section can be computed in a similar way as shown in equation (3.18) or (3.20), i.e.,

$$T_{\text{act,fluid}}^* = \frac{\left(\frac{60}{2\pi}\right)^2 \dot{\theta}_{\text{act}}^{*2}}{K_{\text{cap}}\left(\frac{\dot{\theta}_{\text{tu}}}{\dot{\theta}_{\text{act}}^*}\right)}, \quad (3.30)$$

or,

$$T_{\text{act,fluid}}^* = \alpha_{1,\text{act}} \dot{\theta}_{\text{act}}^{*2} + \alpha_{2,\text{act}} \dot{\theta}_{\text{act}}^* \dot{\theta}_{\text{tu}} + \alpha_{3,\text{act}} \dot{\theta}_{\text{tu}}^2, \quad (3.31)$$

where,  $\dot{\theta}_{\text{act}}^*$  is the impeller speed reference and  $\dot{\theta}_{\text{tu}}$  is the FOM turbine speed.

The other part of the overall feedforward torque request, is the clutch friction element required in order to compensate for the mechanical friction resistance between the impeller and turbine.

The known clutch capacity ( $T_c$ ) for the converter slip is added to the fluid path actuator torque request, from equations (3.30) or (3.31), to obtain the overall feedforward path component of the shaped actuator torque request. This can be written mathematically as,

$$T_{\text{feedforward}}^* = T_{\text{act,fluid}}^* + T_c. \quad (3.32)$$

### 3.5.2 Feedback path

This portion of the proposed controller provides a feedback check on the generated speed at the impeller. The torque output of this feedback control path provides part of the actuator torque request to overcome the speed difference generated after the feedforward path torque implementation. This can be represented as,

$$T_{\text{feedback}}^* = \left(k_p + \frac{k_i}{s}\right)(\dot{\theta}_{\text{act}}^* - \dot{\theta}_{\text{act}}), \quad (3.33)$$

where  $k_p$  and  $k_i$  represents the tuned proportional and integral gains respectively. Thus, the overall shaped actuator torque request provided as the output by the controller is given by,

$$T_{\text{act}}^* = T_{\text{feedforward}}^* + T_{\text{feedback}}^*, \quad (3.34)$$

or,

$$T_{\text{act}}^* = T_{\text{act,fluid}}^* + T_c^* + \left(k_p + \frac{k_i}{s}\right)(\dot{\theta}_{\text{act}}^* - \dot{\theta}_{\text{act}}). \quad (3.35)$$

## 3.6 Results, validation and limitations

Figure 3.16 shows the overall response of the driveline with the implemented control strategy. In Figure 3.16(a), the actuator torque response corresponding to the desired shaped torque request and known clutch capacity has been shown. The plot also shows the torque requested by the driver. Figure 3.16(b) shows the comparison of the torque at the turbine for locked torque converter clutch, and slipping torque converter clutch with and without the control strategy implementation. The average difference between turbine torque values for the locked and slipping torque converter clutch without implementing the control strategy is computed to be around 13.1%. This gets reduced to 3.5% on implementing the control strategy, thus showcasing an improvement of around 73.1% in the performance of the driveline. Correspondingly, Figure 3.16(c) demonstrates the propeller shaft torque response of the driveline. It can be observed that the torque at the propeller shaft is more close to its locked case performance with the control strategy being active. The average error in the propeller shaft torque response was observed to be 13.1% without any control strategy implementation. However, this was reduced to 3.5% when the discussed control scheme was implemented.

### Limitations

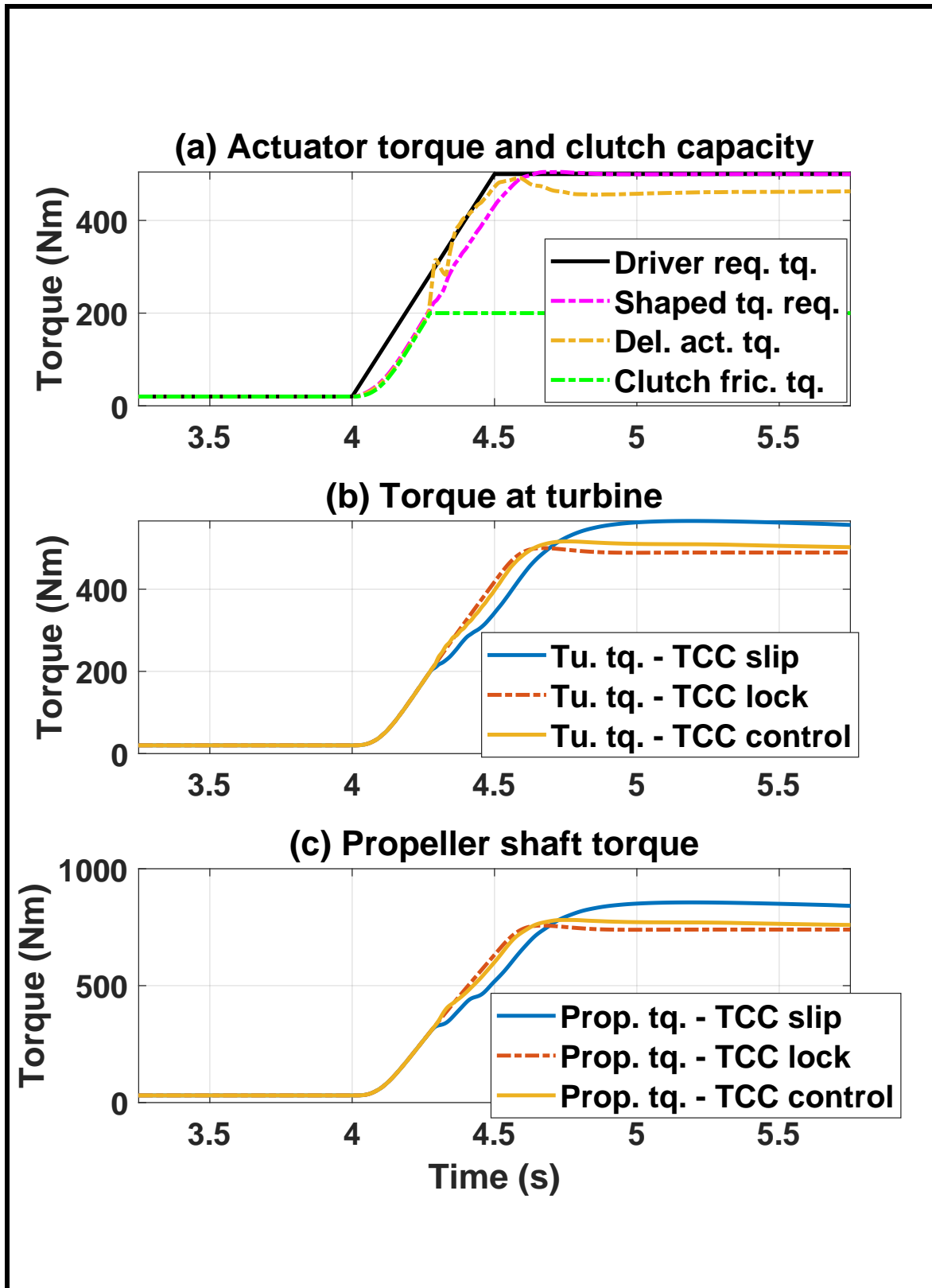


Figure 3.16: Driveline response after implementing the designed model-based ALTC

Though the implemented strategy shows a positive response by the controller, there are still some limitations in this approach which are discussed in this section.

As it is known, the actuator under consideration provides the torque in a bounded domain, and also has restriction on the rate at which it can deliver the torque, as has been discussed in Section 2.3.1.1 in the previous chapter. The controller developed with this strategy is not aware of the constraints under which the actuator operates. This governs the response of how closely the impeller speed from the FOM model matches the reference impeller speed output from the inverse torque converter model discussed in Section 3.4.

Figure 3.17 shows the performance of the proposed feedforward-feedback controller for matching the FOM plant output (impeller speed) with its reference. Further, the difference between the impeller speed reference,  $\dot{\theta}_{act}^*$ , and its counterpart from the FOM actuator  $\dot{\theta}_{act}$ , is accounted for the limitation on magnitude and rate of the torque that can be delivered by the actuator. To address these limitations, in the next chapter, a model predictive control based anti-lag torque controller is designed and evaluated. The operational constraints of the actuator are included in an optimization function to improve the overall performance of the controller.

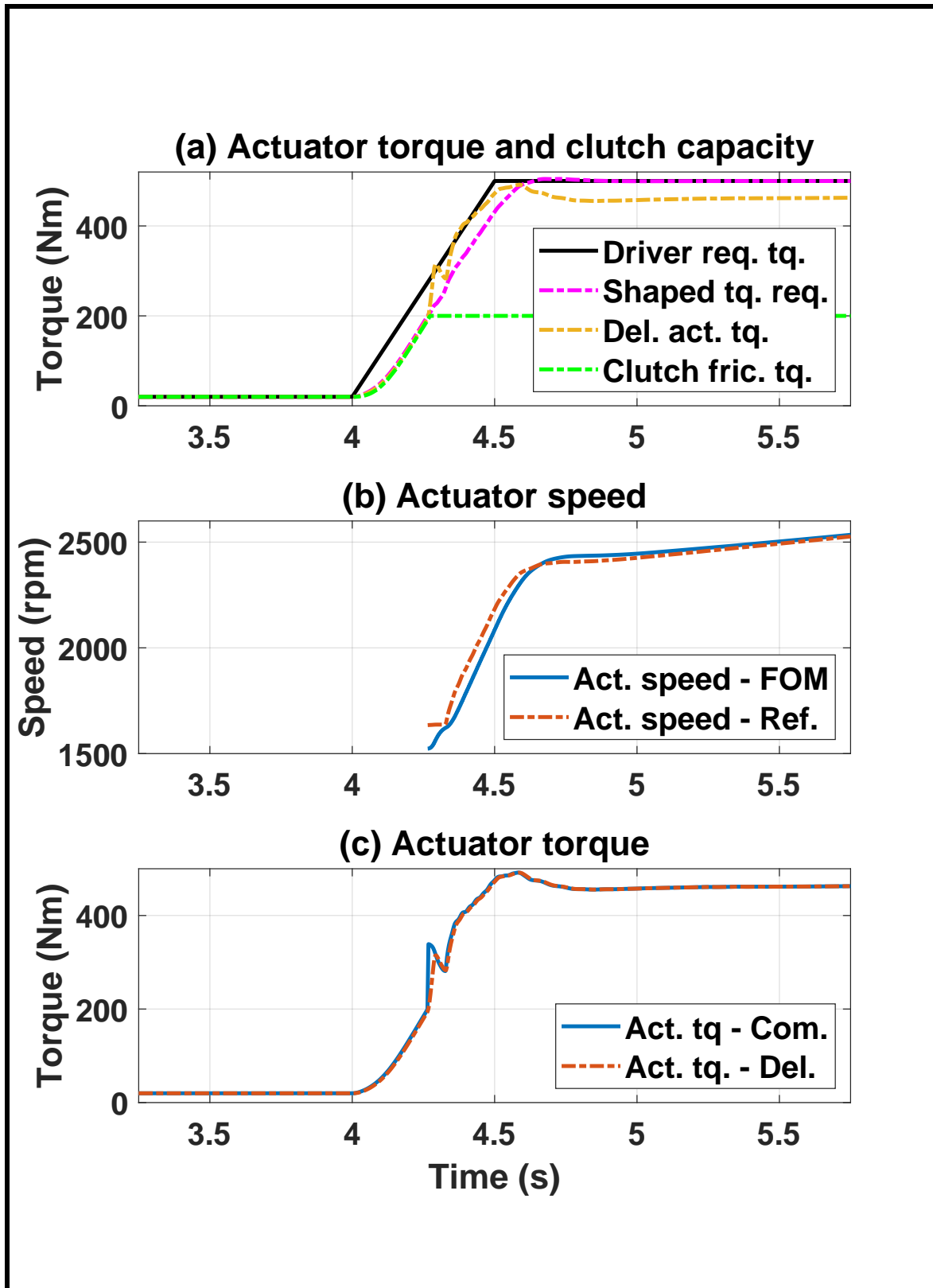


Figure 3.17: Controller performance evaluation - reference speed tracking and actuator constraints

### 3.6.1 Processor-In-the-Loop validation

The developed controller is run with the PIL setup previously shown in Figure 2.11 of Chapter 2. The results are shown in Figure 3.18. The ‘shaped torque request’ and ‘Delivered actuator torque’ output from the PIL setup and from the simulink model are shown in Figure 3.18(a). The two PIL based torques are found to be in good agreement with their Simulink based counterparts, within an error margin of 0.3 %. Further, the ‘turbine torques’ and ‘propeller shaft torques’ from the two sources are shown in Figure 3.18(b) and 3.18(c), respectively. The average error of two torques w.r.t. their simulink counterparts is found to be within 0.4 %.

Furthermore, the processor performance is tabulated in Table 3.3. For this validation, the controller is run at a time step of 10 ms. The turn-around time of the MABx processor is found to be 0.04 ms. Further, the overall run time for this validation experiment is 7 s.

**Table 3.3**  
PIL performance parameters

<b>Parameter</b>	<b>Value</b>
Controller sample time	10 ms
Turn-around time	0.04 ms
Run time	7 s

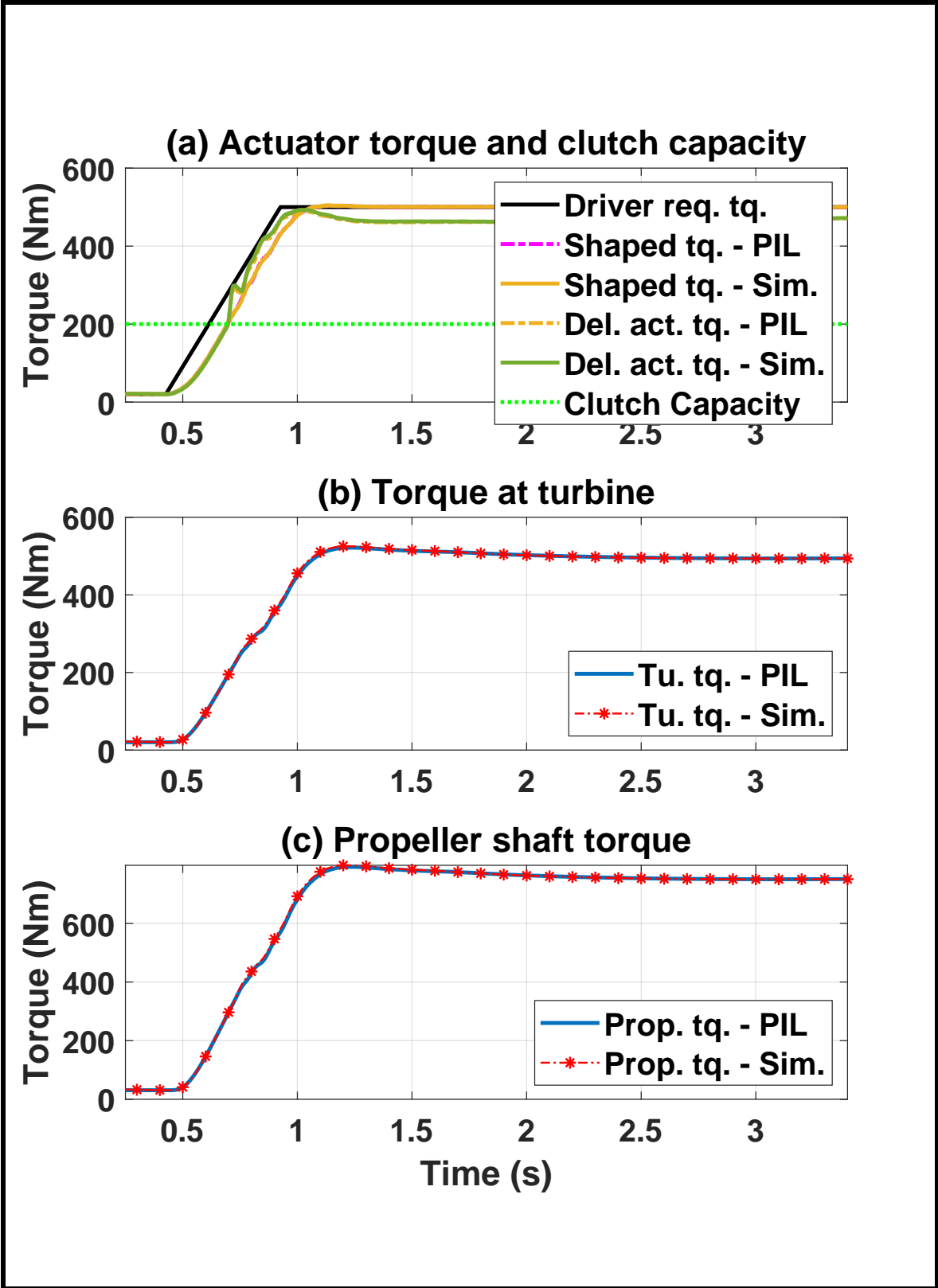


Figure 3.18: Performance of the model-based ALTC in the PIL setup

## Chapter 4

# Model predictive control of TCC capacity and actuator torque to deliver requested torque during torque converter slip

It is known that a plant representing a physical subsystem always operates in a confined domain of inputs and outputs. The control strategy implemented to monitor a certain performance aspect of any plant will show improved results if it is made aware of such operation boundations and actuator constraints. This is ensured by optimising the output commands from the controller to avoid violating the plant and

actuator constraints.

For the driveline plant considered in this work, the actuation system has a limitation on the magnitude and rate of torque delivery at which it can control the drivetrain performance against the lag induced due to TCC slip. If the proposed ALTC approach optimises its response over the operating range of the actuator, the overall performance of the driveline system, to overcome the torque lag due to TCC slip, can be improved.

A model predictive control (MPC) approach uses a prediction model to predict the future outcomes of the plant and correspondingly optimises the present controller outputs, making sure that the actuator always runs in its defined operating range. In this chapter, the proposed ALTC control strategy is designed based on a model prediction control approach.

For the work conducted in this chapter, studies in [55] and [56], were referred to. In reference [55], an in-depth explanation on an MPC control algorithm is provided. Its discussion on the setting up of an MPC controller in discrete time domain and further addition of constraints to the MPC problem have been utilized in this work. Further, the study in reference [56] is another source that discusses in detail on MPC control algorithm development. The section with a discussion on setting of an MPC control problem with a causal system, where the output has a direct feed-through contribution from the input, is particularly found useful.

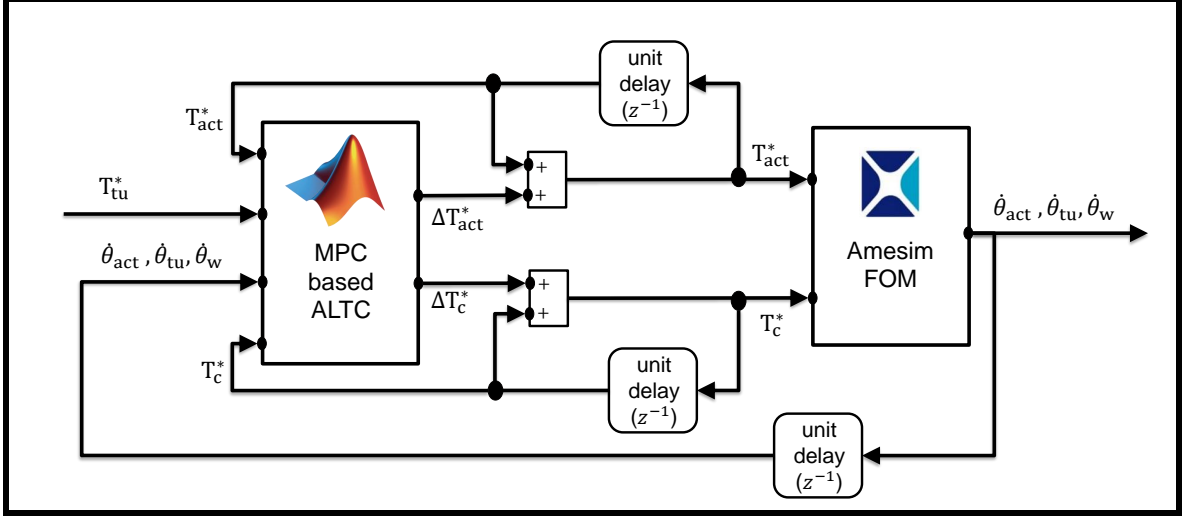


Figure 4.1: Schematic of MPC based control strategy

## 4.1 Control Strategy

The proposed schematic of a control strategy for model prediction based ALTC is shown in Figure 4.1. The inputs to the model predictive controller (MPC) are the reference turbine torque,  $T_{tu}^*$ , actuator torque command,  $T_{act}^*$ , clutch capacity command,  $T_c^*$ , FOM impeller speed,  $\dot{\theta}_{act}$ , FOM turbine speed,  $\dot{\theta}_{tu}$ , and FOM wheel speed,  $\dot{\theta}_w$ . Recall that the actuator is a primary torque source such as an engine or an emulator. The actuator parameters assumed for this work are mentioned in Section 2.3.1.1 of Chapter 2 of this thesis. The outputs from the MPC are commanded changes to the actuator torque,  $\Delta T_{act}^*$ , and clutch capacity,  $\Delta T_c^*$ . These outputs from the MPC are then added to the actuator torque command and clutch capacity command that

in turn are defined as inputs to the Amesim FOM. Further, the FOM delivers impeller, turbine and wheel speeds as the output. An important point to make note of is that with this MPC based approach, the clutch capacity input can also be controlled, unlike the earlier approach discussed in Chapter 3.

The outputs from the FOM, provided as feedback to the MPC, are required for linearisation of the nonlinear driveline model and for further development of the state space model, as discussed in detail in Section 4.2. In turn, the developed state space model is used for setting up the prediction model. This has been described in Section 4.3. Furthermore, the remaining inputs to the MPC, namely, the actuator torque command, the clutch capacity, and the reference turbine torque are used in framing of the MPC optimisation problem. This is explained in detail in sections 4.4 and 4.5.

## **4.2 Mathematical modeling of driveline with torque converter slipping**

A prediction model is required to set-up an MPC based control scheme. The prediction approach proposed for this work, involves the development of a linearised state space model of the drivetrain with slipping TCC. In this section, the state space model is developed and is later used in the setting up of the prediction model for this work.

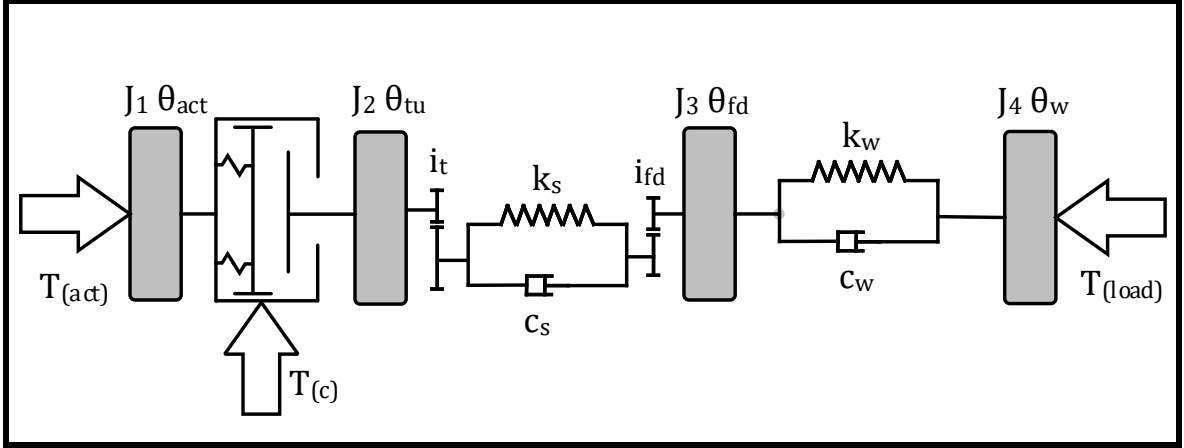


**Figure 4.2:** Reduced order model with torque converter slipping

Initial portion of this section explains in detail the redistribution of rotational inertia in the ROM with locked torque converter, discussed in Section 2.1, to make it compatible with the slipping torque converter clutch scenarios (Section 4.2.1). Further, the physics behind the transfer of torque from the actuator to the wheels through the slipping torque converter, that includes the nonlinear dynamics of the fluid coupling has been described (Section 4.2.2). This is followed by the linearization of the physics based subsystem (Section 4.2.4), developed based on the ROM with slipping TCC. This in turn paves the way for the formulation of state space model (Section 4.2.5)

### 4.2.1 Reduced order model with redistributed inertia

The reduced order model prepared in [4] and [5] was developed for the locked state of the torque converter lock-up clutch. However, for this work, in order to include the torque converter slipping dynamics in the ROM, the lumped inertia at the actuator

(for locked torque converter) was redistributed around the torque converter assembly (see Figure 4.2). Table 4.1 shows the changes made in the ROM used for this work with respect to the one developed earlier in [4] and [5].

**Table 4.1**  
Comparison of lumped inertia distribution for ROM with locked and slipping torque converter lockup clutch

Lumped Inertia	ROM with Torque Converter lockup clutch	
	Locked	Slipping
$J_1$	$J_{\text{act}} + J_{\text{tc}} + \frac{J_{\text{trans}} + J_{\text{prop shaft}}}{i_t^2} + \frac{J_{\text{fd}}}{i_t^2 i_{\text{fd}}^2}$	$J_{\text{act}} + J_{\text{tc},1}$
$J_2$	$J_{\text{tire}} + J_{\text{axle}}$	$J_{\text{tc},2} + \frac{J_{\text{trans}} + J_{\text{prop shaft}}}{i_t^2}$
$J_3$	$J_{\text{wheel}}$	$+ \frac{J_{\text{fd}}}{i_t^2 i_{\text{fd}}^2}$
$J_4$	-	$J_{\text{tire}} + J_{\text{axle}}$
		$J_{\text{wheel}}$

where,  $J_{\text{act}}$  is the actuator inertia,  $J_{\text{tc}}$  is the total inertia of the torque converter assembly,  $J_{\text{trans}}$  is the transmission inertia,  $J_{\text{prop shaft}}$  is the inertia of the propeller shaft,  $J_{\text{fd}}$  is the inertia of the final drive,  $J_{\text{tc},1}$  is the impeller inertia of the torque converter,  $J_{\text{tc},2}$  is the turbine inertia of the torque converter,  $J_{\text{tire}}$  is the tire inertia,  $J_{\text{axle}}$  is the axle shaft inertia, and  $J_{\text{wheel}}$  is the wheel inertia.

Figure 4.3 shows the validation of the modified reduced order model. The outputs of the ROM are compared with their counterparts from the FOM and the respective percentage errors are tabulated in Table 4.2.

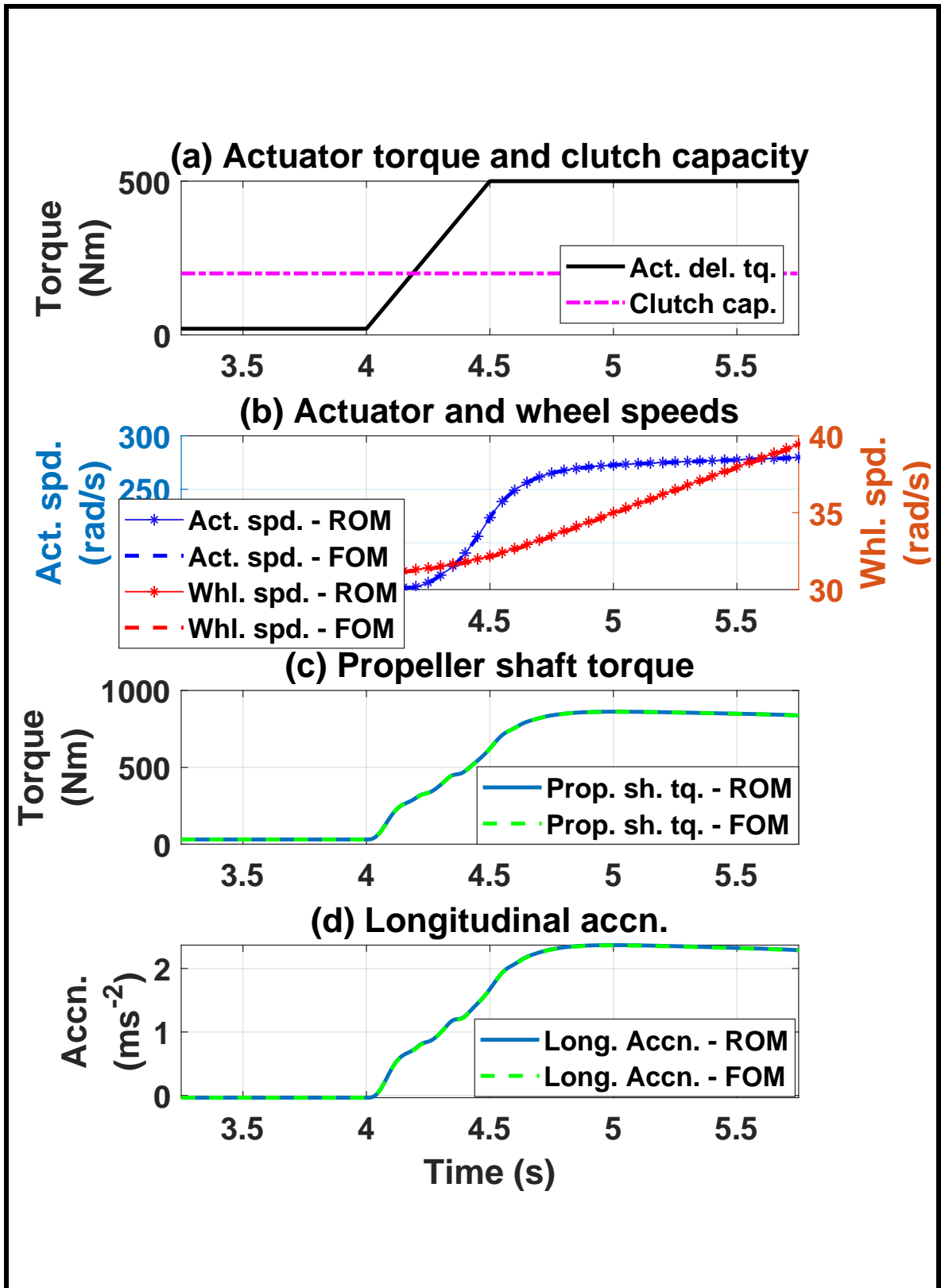


Figure 4.3: Comparison of modified ROM with FOM for slipping TCC

**Table 4.2**

Percentage error for modified ROM validation

Parameter	% error
Actuator speed	0.10
Wheel speed	0.22
Propeller shaft torque	0.11
Vehicle longitudinal acceleration	0.21

### 4.2.2 Equations of motion

Using the modified ROM developed in the Section 4.2.1, the equations for the system based on Newton's laws of motion can be framed as

$$T_{\text{act}} - T_{\text{imp,fluid}} - T_{\text{c}} = J_1 \ddot{\theta}_{\text{act}}, \quad (4.1)$$

$$T_{\text{tu,fluid}} + T_{\text{c}} - \frac{T_{\text{s}}}{i_{\text{t}}} = J_2 \ddot{\theta}_{\text{tu}}, \quad (4.2)$$

$$T_{\text{s}} = k_{\text{s}} \left( \frac{\theta_{\text{tu}}}{i_{\text{t}}} - \theta_{\text{fd}} i_{\text{fd}} \right) + c_{\text{s}} \left( \frac{\dot{\theta}_{\text{tu}}}{i_{\text{t}}} - \dot{\theta}_{\text{fd}} i_{\text{fd}} \right), \quad (4.3)$$

$$T_{\text{s}} i_{\text{fd}} - T_{\text{w}} = J_3 \ddot{\theta}_{\text{fd}}, \quad (4.4)$$

$$T_{\text{w}} = k_{\text{w}} (\theta_{\text{fd}} - \theta_{\text{w}}) + c_{\text{w}} (\dot{\theta}_{\text{fd}} - \dot{\theta}_{\text{w}}), \quad (4.5)$$

$$T_{\text{w}} - T_{\text{load}} = (J_4 + M r_{\text{T}}^2) \ddot{\theta}_{\text{w}}, \quad (4.6)$$

where  $T_{\text{act}}$  is the actuator torque,  $T_{\text{imp,fluid}}$  is the fluid path torque acting at the impeller,  $T_c$  is the clutch capacity,  $J_1$  is the lumped inertia at the actuator,  $\ddot{\theta}_{\text{act}}$  is the angular acceleration of the lumped actuator assembly,  $T_{\text{tu,fluid}}$  is the fluid path torque acting at the turbine,  $T_s$  is the lumped shaft torque,  $i_t$  is the transmission gear ratio,  $J_2$  is the lumped inertia at the turbine,  $\ddot{\theta}_{\text{tu}}$  is the acceleration of the lumped turbine assembly,  $k_s$  and  $c_s$  represent the stiffness and damping coefficients, respectively, of the lumped shaft,  $\theta_{\text{tu}}$  and  $\dot{\theta}_{\text{tu}}$  are the angular position and angular velocity, respectively, of the lumped turbine side assembly,  $\theta_{\text{fd}}$  and  $\dot{\theta}_{\text{fd}}$  are the angular position and angular velocity of tire and axle lumped inertia represented by  $J_3$ ,  $i_{\text{fd}}$  is the final drive ratio,  $T_w$  is the torque acting at lumped axle shaft,  $k_w$ , and damping,  $c_w$ ,  $\ddot{\theta}_{\text{fd}}$  is the angular acceleration of lumped inertia  $J_3$ ,  $\theta_w$ ,  $\dot{\theta}_T$  and  $\ddot{\theta}_w$  are the angular rotation, angular velocity and angular acceleration of the wheel lumped inertia,  $J_4$ ,  $T_{\text{load}}$  is the road load resistance,  $r_T$  is the tire radius, and  $M$  is the mass of the vehicle.

### 4.2.3 Nonlinear torque converter model

As has been discussed in sections 3.4.1.2 and 3.4.1.3 of the previous chapter, the torque  $T_{\text{imp,fluid}}$  in Equation (4.1) and the torque  $T_{\text{tu,fluid}}$  in Equation (4.2) have nonlinearity because of the fluid coupling dynamics of the torque converter. These torques can be represented as quadratic equations in terms of impeller and turbine speeds (Equation 3.20 and 3.21) on the basis of Kotwicki's proposed torque converter

model. An important point to note is that the clutch capacity,  $T_c$ , is also an input to the driveline along with the actuator torque,  $T_{act}$ , when the converter is slipping.

Also, it is important to note that, as the data available for the torque converter was only for the torque multiplication mode, the prepared Kotwicki based nonlinear model and its linear approximation (Section 4.2.3.1) is considered for this mode only.

#### 4.2.3.1 Kotwicki approximation

In this subsection, the equations of motion (Equation 4.1 - 4.6) are used along with the Kotwicki based torque converter model (Equation 3.20 and Equation 3.21) to attain the set of equations capturing the torque converter dynamics of the drivetrain. This set of equations is linearised later and subsequently a state space model is developed.

Using Equations (3.20) and (3.21) from Section 3.4.1.3, the Equation (4.1) can be expanded as

$$T_{act} - (\alpha_{1,act}\dot{\theta}_{act}^2 + \alpha_{2,act}\dot{\theta}_{act}\dot{\theta}_{tu} + \alpha_{3,act}\dot{\theta}_{tu}^2) - T_c = J_1\ddot{\theta}_{act}, \quad (4.7)$$

and Equation (4.2) can be expanded as

$$(\alpha_{1,tu}\dot{\theta}_{act}^2 + \alpha_{2,tu}\dot{\theta}_{act}\dot{\theta}_{tu} + \alpha_{3,tu}\dot{\theta}_{tu}^2) + T_c - \frac{T_s}{i_t} = J_2\ddot{\theta}_{tu}, \quad (4.8)$$

where the respective Kotwicky coefficients in the above equations were previously mentioned in Table 3.1 and Table 3.2.

#### 4.2.4 Linearisation of the torque converter model

In this section, the nonlinear system, discussed in Section 4.2.3, is linearised using the Kotwicky model approach. Correspondingly a state space representation of this linear approximation is developed.

The Equations (4.7) and (4.8) defined in Section 4.2.3 can be used for the linearisation of the nonlinear torque transfer across the torque converter through the fluid path. The equilibrium point for linearisation is considered at each time step for which the FOM based measured signals are available.

Therefore, linearising Equations (4.7) and (4.8) for the equilibrium point yields:

$$\delta T_{\text{act}} - (2\alpha_{1,\text{act}}\dot{\theta}_{\text{act,eq}} + \alpha_{2,\text{act}}\dot{\theta}_{\text{tu,eq}})\delta\dot{\theta}_{\text{act}} - (2\alpha_{3,\text{act}}\dot{\theta}_{\text{tu,eq}} + \alpha_{2,\text{act}}\dot{\theta}_{\text{act,eq}})\delta\dot{\theta}_{\text{tu}} - \delta T_{\text{c}} = J_1\delta\ddot{\theta}_{\text{act}}, \quad (4.9)$$

$$(2\alpha_{1,\text{tu}}\dot{\theta}_{\text{act,eq}} + \alpha_{2,\text{tu}}\dot{\theta}_{\text{tu,eq}})\delta\dot{\theta}_{\text{act}} + (2\alpha_{3,\text{tu}}\dot{\theta}_{\text{tu,eq}} + \alpha_{2,\text{tu}}\dot{\theta}_{\text{act,eq}})\delta\dot{\theta}_{\text{tu}} + \delta T_{\text{c}} - \frac{\delta T_{\text{s}}}{i_T} = J_2\delta\ddot{\theta}_{\text{tu}}, \quad (4.10)$$

where  $\dot{\theta}_{\text{act,eq}}$  and  $\dot{\theta}_{\text{tu,eq}}$  are the equilibrium point values of the actuator and turbine speeds, respectively. Also, prefix  $\delta$  used in the above equation represents the small

linear change of the variable from its respective equilibrium point value, i.e.,

$$\delta X_{k+1} = X_{k+1} - X_{eq}, \quad (4.11)$$

$$\delta Y_{k+1} = Y_{k+1} - Y_{eq}, \quad (4.12)$$

where subscript ‘k’ represents the k<sup>th</sup> time step and subscript ‘eq’ represents the equilibrium point.

#### 4.2.5 Development of linearised mathematical model of driveline

Considering the linear variation from the given equilibrium point for the subsystem as discussed above in Section 4.2.4, the set of equations (4.1 - 4.6) can be re-written in the linearised form similar to Equation (4.9) and (4.10) and the above complete subsystem can further be represented as a discrete state space model as shown below

$$\delta X_{k+1} = A\delta X_k + B\delta u_k + G\delta d_k, \quad (4.13)$$

$$\delta Y_{k+1} = C\delta X_{k+1} + D\delta u_{k+1}, \quad (4.14)$$

where

$$\delta \mathbf{X} = \left[ \delta \dot{\theta}_{\text{act}} \quad \delta \dot{\theta}_{\text{tu}} \quad \left( \frac{\delta \theta_{\text{tu}}}{i_t} - \delta \theta_{\text{fd}} i_{\text{fd}} \right) \quad (\delta \theta_{\text{fd}} - \delta \theta_{\text{w}}) \quad \delta \dot{\theta}_{\text{fd}} \quad \delta \dot{\theta}_{\text{w}} \right]^{\text{T}}, \quad (4.15)$$

$$\delta \mathbf{Y} = \left[ \delta T_{\text{tu}} \right], \quad (4.16)$$

$$\delta \mathbf{u} = \left[ \delta T_{\text{act}} \quad \delta T_{\text{c}} \right]^{\text{T}}, \quad (4.17)$$

$$\delta \mathbf{d} = \left[ \delta T_{\text{load}} \right], \quad (4.18)$$

where all the notations used have their regular meanings as discussed throughout this thesis. Furthermore, the matrices A, B, G, C and D from Equations 4.13 and 4.14 are shown below as

$$\mathbf{A} = \begin{bmatrix} -\frac{a_{1,\text{act}}}{J_1} & -\frac{a_{2,\text{act}}}{J_1} & 0 & 0 & 0 & 0 \\ \frac{b_{1,\text{tu}}}{J_2} & \frac{b_{2,\text{tu}}}{J_2} - \frac{c_s}{J_2 i_t^2} & -\frac{k_s}{J_2 i_t} & 0 & \frac{c_s i_{\text{fd}}}{J_2 i_t} & 0 \\ 0 & \frac{1}{i_t} & 0 & 0 & -i_{\text{fd}} & 0 \\ 0 & 0 & 0 & 0 & 1 & -1 \\ 0 & \frac{c_s i_{\text{fd}}}{J_3 i_t} & \frac{k_s i_{\text{fd}}}{J_3} & -\frac{k_w}{J_3} & -\frac{c_s i_{\text{fd}}^2}{J_3} - \frac{c_w}{J_3} & \frac{c_w}{J_3} \\ 0 & 0 & 0 & \frac{k_w}{b} & \frac{c_w}{b} & -\frac{c_w}{b} \end{bmatrix}, \quad (4.19)$$

$$\mathbf{B} = \begin{bmatrix} \frac{1}{J_1} & 0 & 0 & 0 & 0 & 0 \\ -\frac{1}{J_1} & \frac{1}{J_2} & 0 & 0 & 0 & 0 \end{bmatrix}^{\text{T}}, \quad (4.20)$$

$$\mathbf{G} = \begin{bmatrix} 0 & 0 & 0 & 0 & 0 & -\frac{r_T}{b} \end{bmatrix}^\top, \quad (4.21)$$

$$\mathbf{C} = \begin{bmatrix} b_{1,tu} & b_{2,tu} & 0 & 0 & 0 & 0 \end{bmatrix}, \quad (4.22)$$

$$\mathbf{D} = \begin{bmatrix} 0 & 1 \end{bmatrix}, \quad (4.23)$$

where  $a_{1,act}$ ,  $a_{2,act}$ ,  $b_{1,tu}$ ,  $b_{2,tu}$  and  $b$  are defined as:

$$a_{1,act} = 2\alpha_{1,act}\dot{\theta}_{act,eq} + \alpha_{2,act}\dot{\theta}_{tu,eq}, \quad a_{2,act} = 2\alpha_{3,act}\dot{\theta}_{tu,eq} + \alpha_{2,act}\dot{\theta}_{act,eq},$$

$$b_{1,tu} = 2\alpha_{1,tu}\dot{\theta}_{act,eq} + \alpha_{2,tu}\dot{\theta}_{tu,eq} \quad b_{2,tu} = 2\alpha_{3,tu}\dot{\theta}_{tu,eq} + \alpha_{2,tu}\dot{\theta}_{act,eq},$$

$$b = J_4 + Mr_T^2.$$

#### 4.2.6 Performance comparison of nonlinear model with linear approximation

This section discusses the comparison of nonlinear model of the driveline with its linear approximation developed in the previous section. Figure 4.4 shows the turbine torque output from the nonlinear model against its linearly approximated values, for known equilibrium points. The turbine torque from the linear model output is observed to comply with the nonlinear model with an error of 0.02%. For this

comparative study, the inputs to the linear model,  $\delta T_{\text{act}}$ , and,  $\delta T_{\text{c}}$ , were chosen considering a ramp actuator torque input and a constant clutch capacity input. The output from the nonlinear model were also obtained for the same input profiles. Moreover, the road load disturbance,  $\mathbf{d}$ , was assumed to be constant for the linear model.

## **4.3 Prediction based on developed linear model**

Based on the linear model developed in the Section 4.2, the next task realised was to set up the state space (SS) prediction model to predict the output and further optimise the actuator input command from the controller. This section discusses the development of the SS prediction model and setting up of the optimisation problem. In the later part of this section, the results obtained using the prediction model are discussed.

### **4.3.1 Overview**

The developed linear model, discussed in Section 4.2, is intended to be used for framing an SS prediction model. In this section, an overview is provided about the basic control scheme and parameters chosen while setting up the prediction model.

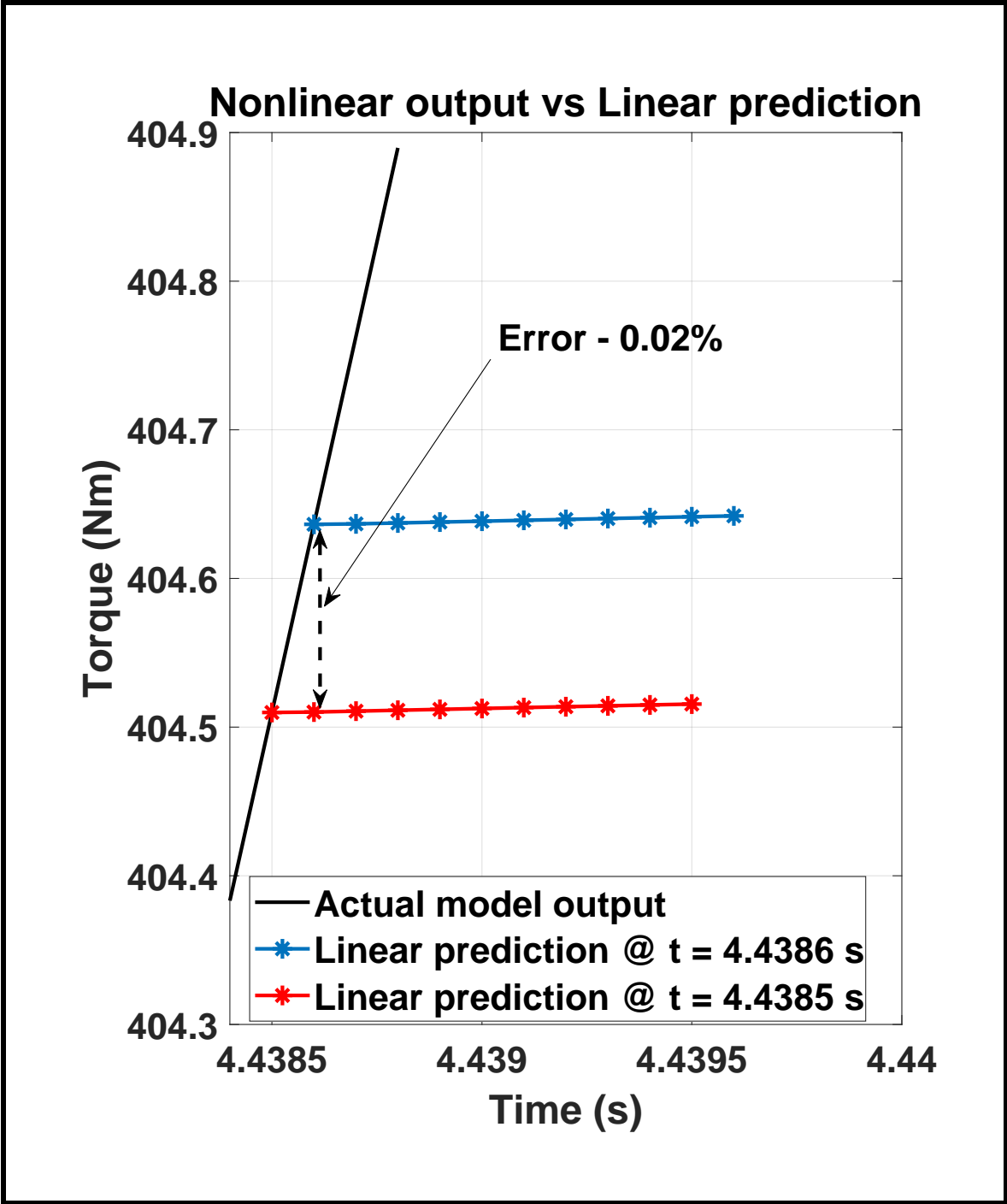


**Figure 4.4:** Comparison of the nonlinear model output with its linearised prediction at equilibrium points

Also, along with it, relevant definitions have been discussed.

Note that the design requirement of the prediction control scheme is based on the optimisation of the changes of inputs,  $\Delta u$ . At any time instant  $(k|i)$ , the designed controller is required to predict the outputs into the future time steps,  $(k|i + 1), (k|i + 2), \dots, (k|i + N_p)$ , over optimised values of change of inputs,  $\Delta u_{k|i+1}, \Delta u_{k|i+2}, \dots, \Delta u_{k|i+N_c}$ . The notation  $N_p$  and  $N_c$  used here denotes the prediction horizon and control horizon, respectively. Further, these optimised change of inputs, provided by the controller, are added to the respective plant inputs at the current time step to determine the plant inputs for the next time step. This can be shown as

$$u_{k+1|i} = u_{k|i} + \Delta u_{k|i+1}, \quad (4.24)$$

where, elements of vector  $u_{k|i}$  are the inputs to the plant at current time step, elements of vector  $\Delta u_{k|i+1}$  are the optimised change of inputs for the predicted outputs of the future time step, and the elements of vector  $u_{k+1|i}$  are the inputs for the next time step.

### 4.3.2 Augmentation of the model under consideration

For this work, the interest while framing the MPC based control lies in determining the optimised change in the input rather than the directly optimised input value at

each time step where linearisation is performed for model prediction and control, [55]. Hence, further augmentation of the state space model (Equations 4.13 - 4.14) is conducted to rewrite the state space model in terms of change of the input,  $\Delta u$ .

It is known from Section 4.2.5, that the state space model developed is based on the linearisation for a known equilibrium point and all the variables are represented in terms of linear variation from that equilibrium point. Mathematically,

$$\delta X_{k+n} = X_{k+n} - X_{eq}, \quad (4.25)$$

$$\delta Y_{k+n} = Y_{k+n} - Y_{eq}, \quad n = 1, 2, 3, \dots, \quad (4.26)$$

where for the time step,  $k+n$ ,  $X_{k+n}$  represents the state value at this time step and  $X_{eq}$  represents the equilibrium value of the state, that is measured from the full order model. Note that Equations (4.25) and (4.26) represent the general interpretation of the linearisation, and do not depend on whether the said  $X$  and  $Y$  are being predicted or not.

As it is known that the relation of the intermediate point variable in the linear model with the equilibrium point value is linear; thus, the change in the same variable at two adjacent points shall follow the same linear relationship. This can be mathematically represented as,

$$\Delta X_k = \delta X_k - \delta X_{k-1}, \quad (4.27)$$

$$\Delta Y_k = \delta Y_k - \delta Y_{k-1}, \quad (4.28)$$

using the Equations (4.25) - (4.28), it is obtained

$$\Delta X_k = \delta X_k - \delta X_{k-1} = X_k - X_{k-1} \quad (4.29)$$

$$\Delta Y_k = \delta Y_k - \delta Y_{k-1} = Y_k - Y_{k-1} \quad (4.30)$$

Thus, based on this deduction and assuming the change in road load disturbance to be negligible over the prediction window, Equations (4.13) and (4.14) can be rewritten as

$$\Delta X_{k+1} = A\Delta X_k + B\Delta u_k \quad (4.31)$$

and

$$\Delta Y_{k+1} = C\Delta X_{k+1} + D\Delta u_{k+1}, \quad (4.32)$$

respectively, where Equation (4.32) can be rewritten as

$$Y_{k+1} = C\Delta X_{k+1} + D\Delta u_{k+1} + Y_k. \quad (4.33)$$

Further, the above two equations can be written in the augmented form with a modified state vector as

$$X_{ag,k+1} = A_{ag}X_{ag,k} + B_{ag}\Delta u_k \quad (4.34)$$

and output vector as

$$Y_{k+1} = C_{ag}X_{ag,k} \quad (4.35)$$

where

$$X_{ag,k} = \begin{bmatrix} \Delta X_k \\ Y_k \end{bmatrix},$$

$$A_{ag} = \begin{bmatrix} A & 0 \\ CA & I \end{bmatrix},$$

$$B_{ag} = \begin{bmatrix} B \\ CB \end{bmatrix},$$

$$C_{ag} = \begin{bmatrix} 0 & I \end{bmatrix}.$$

The developed augmented state space model is based on the assumption of neglecting the D matrix. This can be justified by looking at the contribution of the D matrix to the output, Y, in Equation (4.33), for the maximum possible  $\Delta u$ . The contribution through the D matrix to the output is observed to be negligible as neglecting the contribution of direct feed-through input (from D matrix) generated a maximum difference of 0.1%, approximately. The D matrix was neglected to make the system a causal system i.e., where the output was dependent only on the past input and state values of the augmented model. This was done to simplify the optimisation problem.

Also, at the start of prediction, i.e., at the point of equilibrium at time instant,  $k$ , the initial states for  $X_{ag,k}$  can be defined as

$$X_{ag,k} = \begin{bmatrix} 0 & 0 & 0 & 0 & 0 & 0 & Y_{eq} \end{bmatrix}^T. \quad (4.36)$$

### 4.3.3 Development of prediction matrices

Using the augmented matrix form from Section 4.3.2 (Equation 4.34 - 4.35), the output prediction matrices can be set up over the prediction horizon of  $\mathbf{Np}$  and control horizon of  $\mathbf{Nc}$  as

$$\begin{bmatrix} Y_{k+1} \\ Y_{k+2} \\ \vdots \\ Y_{k+Np} \end{bmatrix} = \begin{bmatrix} C_{ag}A_{ag} \\ C_{ag}A_{ag}^2 \\ \vdots \\ C_{ag}A_{ag}^{Np} \end{bmatrix} X_{ag,k} + \begin{bmatrix} C_{ag}B_{ag} & 0 & \dots & 0 \\ C_{ag}A_{ag}B_{ag} & C_{ag}B_{ag} & \dots & 0 \\ \vdots & \vdots & \vdots & \vdots \\ C_{ag}A_{ag}^{Np-1}B_{ag} & C_{ag}A_{ag}^{Np-2}B_{ag} & \dots & C_{ag}A_{ag}^{Np-Nc}B_{ag} \end{bmatrix} \begin{bmatrix} \Delta u_k \\ \Delta u_{k+1} \\ \vdots \\ \Delta u_{k+Nc-1} \end{bmatrix}, \quad (4.37)$$

rewriting the equation in a shortened notation

$$Y = PX_{ag,k} + H\Delta U \quad (4.38)$$

### 4.3.4 Unconstrained optimisation problem

This section discusses the framing of the optimisation problem for the case when there is no constraint to be considered on the system. The objective function,  $J$ , is defined as a quadratic function as shown

$$J = (T_{tu}^* - T_{tu})^2 + \Delta U^T \bar{S} \Delta U \quad (4.39)$$

where  $T_{tu}^*$  is the reference output generated from the AJC,  $T_{tu}$  is the turbine torque output from the linearised state space model discussed above, and as mentioned in [55],  $\bar{S}$  represents a diagonal block matrix defined as  $s.I_{N_c \times N_c}$  where,  $s$  is a diagonal matrix shown as

$$s = \begin{bmatrix} s_1 & 0 \\ 0 & s_2 \end{bmatrix}$$

where  $s_1$  and  $s_2$  are the tuning parameters for the two inputs  $\Delta T_{act}^*$  and  $\Delta T_c^*$ , respectively. Also, as has been mentioned in [55], the second term in Equation (4.39) is added in order to reflect the consideration given to the value of elements of  $\Delta U$  while

minimising the cost function.

Further, the cost function given in Equation (4.39) can further be rewritten using the Equation (4.38) as

$$J = (\mathbf{T}_{\text{tu}}^* - (\mathbf{P}\mathbf{X}_{\text{ag},k} + \mathbf{H}\Delta\mathbf{U}))^T \mathbf{Q} (\mathbf{T}_{\text{tu}}^* - (\mathbf{P}\mathbf{X}_{\text{ag},k} + \mathbf{H}\Delta\mathbf{U})) + \Delta\mathbf{U}^T \bar{\mathbf{S}} \Delta\mathbf{U}, \quad (4.40)$$

where matrix  $\mathbf{Q}$  represents the weight consideration on the difference between the reference and the predicted turbine torques. Thus, the above discussed MPC optimisation problem can be written in a simplified mathematical version as

$$\mathbf{minimize} \quad \sum_k^{k+N_p-1} J(\mathbf{T}_{\text{tu}}^*, \mathbf{T}_{\text{tu}}) \quad (4.41)$$

$$\Delta\mathbf{T}_{\text{act}}^*, \Delta\mathbf{T}_{\text{c}}^*$$

where the cost function  $J$ , from Equation (4.39) is the function of reference turbine torque,  $\mathbf{T}_{\text{tu}}^*$ , and predicted turbine torque  $\mathbf{T}_{\text{tu}}$ . Further, if the above optimisation problem is considered to be unconstrained, Equation (4.41) can be solved for the minima of  $J$  by simply differentiating it w.r.t.  $\Delta\mathbf{U}$  and equating to 0, as also mentioned in [55]. The obtained solution for minima is

$$\Delta\mathbf{U} = (\mathbf{H}^T \mathbf{Q} \mathbf{H} + \bar{\mathbf{S}})^{-1} \mathbf{H}^T \mathbf{Q} (\mathbf{T}_{\text{tu}}^* - \mathbf{P}\mathbf{X}_{\text{ag},k}) \quad (4.42)$$

### 4.3.5 Results for unconstrained optimisation

This section discusses the results obtained for the above unconstrained optimisation problem, solving for a known equilibrium point. The known parameters that define the equilibrium point at a time instant,  $k$ , are provided in Table 4.3. Note that the

**Table 4.3**  
Known parameters for equilibrium point

Parameters	Value
$T_{tu,k}^*$	300.00 Nm
$\dot{\theta}_{act,k}$	167.60 rad/s
$\dot{\theta}_{tu,k}$	159.11 rad/s
$T_{c,k}$	200.00 Nm
$N_p$	10
$N_c$	10

impeller speed,  $\dot{\theta}_{act,k}$ , turbine speed,  $\dot{\theta}_{tu,k}$ , and, clutch capacity,  $T_{c,k}$ , in Table 4.3 are used to determine the equilibrium point value of the total torque acting at the turbine.

Figure 4.5 shows the prediction outputs for the unconstrained optimisation problem. Notice the unbounded optimised input changes,  $\Delta T_{act}^*$  and  $\Delta T_c^*$ , in sub-figures 4.5(a) and 4.5(b) respectively. For these values of the inputs, the predicted output obtained over the prediction horizon is shown in 4.5(c). The output is observed to converge to the reference value of 300 Nm at around the 7<sup>th</sup> time step, where correspondingly, the two inputs,  $\Delta T_{act}^*$  and  $\Delta T_c^*$ , converges to zero.

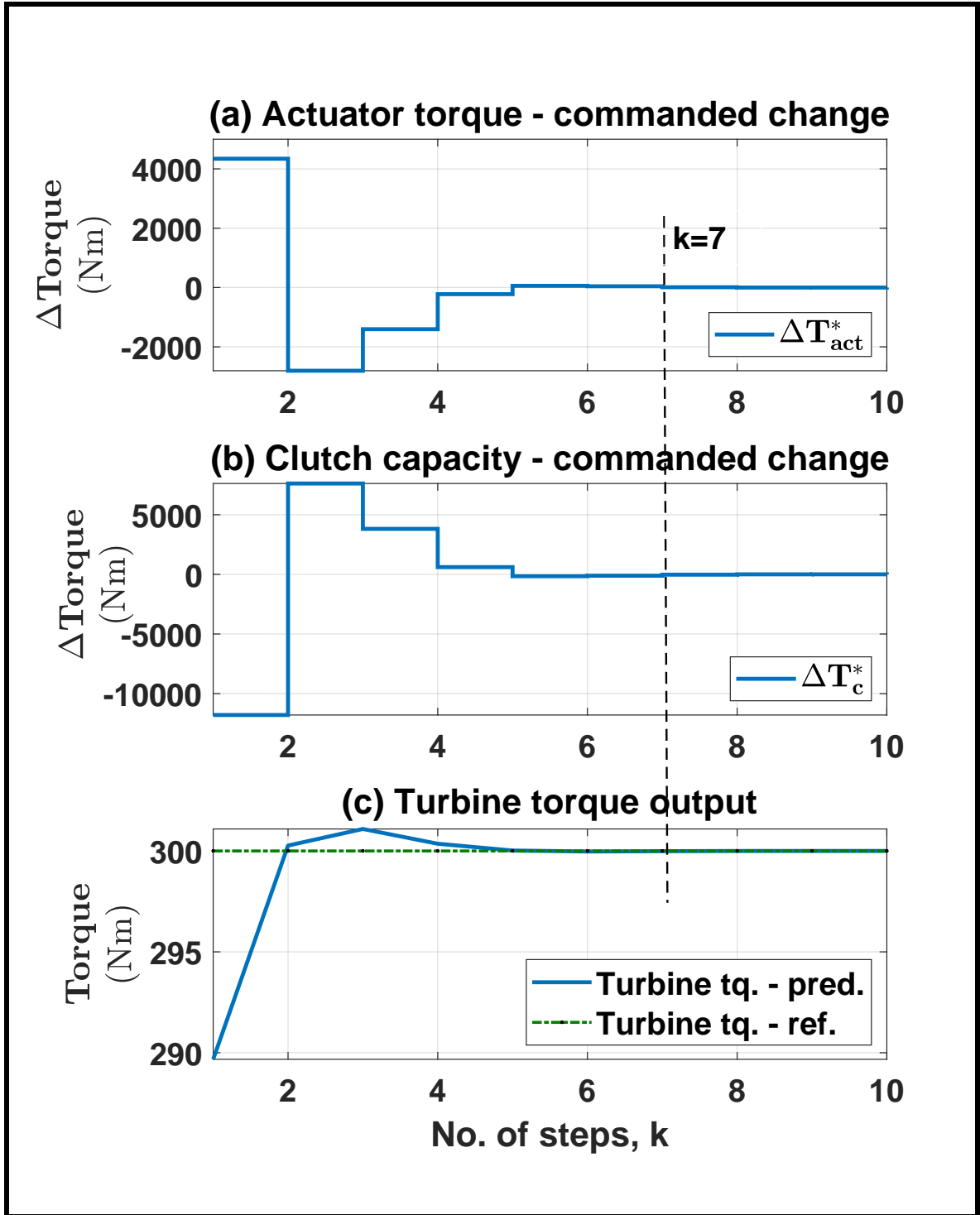


Figure 4.5: Unconstrained optimisation of inputs at a known equilibrium point

## 4.4 Constraints set-up

The actuator (i.e., engine or e-motor) is limited by its architecture as to the highest and lowest values of torque it can deliver. Thus, in order to ensure realistic application where the actuator torque is within the known bounds, and state constraints are met, the unconstrained optimisation problem discussed in the previous section is to be combined with the physical constraints in such a way that the optimised input references obtained from the controller are within the physical limits of the system. This section discusses the formulation of the actuator and state constraints and further their inclusion in the optimisation problem.

The major constraints for the system are identified as limit on the actuator delivered torque, and limit the rate of actuator delivered torque. Apart from these two, another constraint of the developed system is that while slipping of the torque converter clutch, the speed ratio defined by Equation (3.15) should be within the limits of torque multiplication mode. The formulation of each of these constraints is discussed in detail in the following subsections.

### 4.4.1 Constraint on rate of input

As has been discussed in previous chapters, for the actuator under consideration, the upper and lower limit on the rate at which it can deliver the requested torque is defined by

$$- 6000 \text{ Nm/s} \leq \Delta T_{\text{act}} \leq 6000 \text{ Nm/s}, \quad (4.43)$$

and further for the clutch actuator the torque rate is constrained as

$$- 6000 \text{ Nm/s} \leq \Delta T_c \leq 6000 \text{ Nm/s} \quad (4.44)$$

Thus, the developed constraint matrix for rate of input change is

$$\begin{bmatrix} \mathbf{I} & 0 & 0 & \dots & 0 \\ 0 & \mathbf{I} & 0 & \dots & 0 \\ \vdots & \vdots & \vdots & \vdots & \vdots \\ 0 & 0 & 0 & \dots & \mathbf{I} \\ -\mathbf{I} & 0 & 0 & \dots & 0 \\ 0 & -\mathbf{I} & 0 & \dots & 0 \\ \vdots & \vdots & \vdots & \vdots & \vdots \\ 0 & 0 & 0 & \dots & -\mathbf{I} \end{bmatrix} \begin{bmatrix} \Delta \mathbf{u}_k \\ \Delta \mathbf{u}_{k+1} \\ \vdots \\ \Delta \mathbf{u}_{k+N_c-1} \end{bmatrix} \leq \begin{bmatrix} \Delta u_{\max} \\ \Delta u_{\max} \\ \vdots \\ \Delta u_{\max} \\ -\Delta u_{\min} \\ -\Delta u_{\min} \\ \vdots \\ -\Delta u_{\min} \end{bmatrix}, \quad (4.45)$$

where the upper and lower limits on the rate of torque delivery for the two actuators are shown in the matrix form as

$$\Delta \mathbf{u} = \begin{bmatrix} \Delta T_{\text{act}}^* & \Delta T_{\text{c}}^* \end{bmatrix}^{\text{T}}, \quad (4.46)$$

$$\Delta \mathbf{u}_{\text{max}} = \begin{bmatrix} 6000 & 6000 \end{bmatrix}^{\text{T}}, \quad (4.47)$$

$$\Delta \mathbf{u}_{\text{min}} = \begin{bmatrix} -6000 & -6000 \end{bmatrix}^{\text{T}}. \quad (4.48)$$

Further, Equation (4.45) can be written in a shortened notation as

$$\mathbf{M}_1 \Delta \mathbf{U} \leq \Gamma_1, \quad (4.49)$$

where

$$\mathbf{M}_1 = \begin{bmatrix} \mathbf{I} & 0 & 0 & \dots & 0 \\ 0 & \mathbf{I} & 0 & \dots & 0 \\ \vdots & \vdots & \vdots & \vdots & \vdots \\ 0 & 0 & 0 & \dots & \mathbf{I} \\ -\mathbf{I} & 0 & 0 & \dots & 0 \\ 0 & -\mathbf{I} & 0 & \dots & 0 \\ \vdots & \vdots & \vdots & \vdots & \vdots \\ 0 & 0 & 0 & \dots & -\mathbf{I} \end{bmatrix}, \quad (4.50)$$

$$\Delta U = \begin{bmatrix} \Delta u_k & \Delta u_{k+1} & \dots & \Delta u_{k+N_c-1} \end{bmatrix}^\top, \quad (4.51)$$

$$\Gamma_1 = \begin{bmatrix} \Delta u_{\max} & \Delta u_{\max} & \dots & \Delta u_{\max} & -\Delta u_{\min} & -\Delta u_{\min} & \dots & -\Delta u_{\min} \end{bmatrix}^\top. \quad (4.52)$$

#### 4.4.2 Constraint on magnitude of input

The upper and lower bounds of the actuator torque are defined as,

$$0 \leq T_{\text{act}} \leq 500 \text{ Nm}. \quad (4.53)$$

Further, the upper bound on the clutch capacity is considered to be a dynamic constraint where it is always expected to be lower than the actuator torque. At its maximum value, the clutch capacity can be equal to the actuator delivered torque for the particular equilibrium point considered at that instant. Hence, the constraint equation for the clutch capacity input is framed as

$$0 \leq T_c \leq T_{\text{act,eq}} \text{ Nm}. \quad (4.54)$$

Thus, the constraint matrix for the magnitude of the input can be written as

$$\begin{bmatrix}
 \mathbf{I} & 0 & 0 & \dots & 0 \\
 0 & \mathbf{I} & 0 & \dots & 0 \\
 \vdots & \vdots & \vdots & \vdots & \vdots \\
 0 & 0 & 0 & \dots & \mathbf{I} \\
 -\mathbf{I} & 0 & 0 & \dots & 0 \\
 0 & -\mathbf{I} & 0 & \dots & 0 \\
 \vdots & \vdots & \vdots & \vdots & \vdots \\
 0 & 0 & 0 & \dots & -\mathbf{I}
 \end{bmatrix}
 \begin{bmatrix}
 \mathbf{u}_k \\
 \mathbf{u}_{k+1} \\
 \vdots \\
 \mathbf{u}_{k+N_c-1}
 \end{bmatrix}
 \leq
 \begin{bmatrix}
 \mathbf{u}_{\max} \\
 \mathbf{u}_{\max} \\
 \vdots \\
 \mathbf{u}_{\max} \\
 -\mathbf{u}_{\min} \\
 -\mathbf{u}_{\min} \\
 \vdots \\
 -\mathbf{u}_{\min}
 \end{bmatrix}, \quad (4.55)$$

where

$$\begin{bmatrix}
 \mathbf{u}_k \\
 \mathbf{u}_{k+1} \\
 \vdots \\
 \mathbf{u}_{k+N_c-1}
 \end{bmatrix}
 =
 \begin{bmatrix}
 \mathbf{I} \\
 \mathbf{I} \\
 \vdots \\
 \mathbf{I}
 \end{bmatrix}
 \mathbf{u}_{\text{eq}}
 +
 \begin{bmatrix}
 \mathbf{I} & 0 & 0 & \dots & 0 \\
 \mathbf{I} & \mathbf{I} & 0 & \dots & 0 \\
 \vdots & \vdots & \vdots & \vdots & \vdots \\
 \mathbf{I} & \mathbf{I} & \mathbf{I} & \dots & \mathbf{I}
 \end{bmatrix}
 \begin{bmatrix}
 \Delta \mathbf{u}_k \\
 \Delta \mathbf{u}_{k+1} \\
 \vdots \\
 \Delta \mathbf{u}_{k+N_c-1}
 \end{bmatrix}, \quad (4.56)$$

$$\mathbf{u}_{\text{eq}} = \begin{bmatrix} \mathbf{T}_{\text{act,eq}} & \mathbf{T}_{\text{c,eq}} \end{bmatrix}^T, \quad (4.57)$$

$$\mathbf{u}_{\max} = \begin{bmatrix} 500 & \mathbf{T}_{\text{act,eq}} \end{bmatrix}^T, \quad (4.58)$$

$$\mathbf{u}_{\min} = \begin{bmatrix} 0 & 0 \end{bmatrix}^T. \quad (4.59)$$

The Equation (4.55) can further be expanded using Equation (4.56) and written in a shortened notation as

$$\mathbf{M}_2 \mathbf{L} \Delta \mathbf{U} \leq \Gamma_2 - \mathbf{M}_2 \mathbf{E} \mathbf{u}_{\text{eq}}, \quad (4.60)$$

where

$$\mathbf{M}_2 = \begin{bmatrix} \mathbf{I} & 0 & 0 & \dots & 0 \\ 0 & \mathbf{I} & 0 & \dots & 0 \\ \vdots & \vdots & \vdots & \vdots & \vdots \\ 0 & 0 & 0 & \dots & \mathbf{I} \\ -\mathbf{I} & 0 & 0 & \dots & 0 \\ 0 & -\mathbf{I} & 0 & \dots & 0 \\ \vdots & \vdots & \vdots & \vdots & \vdots \\ 0 & 0 & 0 & \dots & -\mathbf{I} \end{bmatrix}, \quad (4.61)$$

$$\mathbf{L} = \begin{bmatrix} \mathbf{I} & 0 & 0 & \dots & 0 \\ \mathbf{I} & \mathbf{I} & 0 & \dots & 0 \\ \vdots & \vdots & \vdots & \vdots & \vdots \\ \mathbf{I} & \mathbf{I} & \mathbf{I} & \dots & \mathbf{I} \end{bmatrix}, \quad (4.62)$$

$$\Gamma_2 = \begin{bmatrix} \mathbf{u}_{\max} & \mathbf{u}_{\max} & \dots & \mathbf{u}_{\max} & -\mathbf{u}_{\min} & -\mathbf{u}_{\min} & \dots & -\mathbf{u}_{\min} \end{bmatrix}^T, \quad (4.63)$$

$$\mathbf{E} = \begin{bmatrix} \mathbf{I} & & & \\ & \mathbf{I} & & \\ & & \dots & \\ & & & \mathbf{I} \end{bmatrix}^{\top}. \quad (4.64)$$

### 4.4.3 Constraint on model impeller and turbine speeds

The constraint discussed in this section is implemented in the optimisation problem as a soft constraint, unlike the other two constraints discussed before, which were implemented as hard constraints. The purpose of this constraint was to ensure that the operation of torque converter is in the torque multiplication mode. This is formulated over the prediction horizon as follows:

$$\dot{\theta}_{\text{act},k+1} \geq \frac{\dot{\theta}_{\text{tu},k+1}}{0.95}, \quad (4.65)$$

$$\dot{\theta}_{\text{act},k+2} \geq \frac{\dot{\theta}_{\text{tu},k+2}}{0.95}, \quad (4.66)$$

⋮

$$\dot{\theta}_{\text{act},k+N_p} \geq \frac{\dot{\theta}_{\text{tu},k+N_p}}{0.95}, \quad (4.67)$$

Further, the predicted impeller and turbine speed at each future step can be expanded as

$$\dot{\theta}_{\text{act},k+n} = \dot{\theta}_{\text{act,eq}} + \Delta\dot{\theta}_{\text{act},k+1} + \Delta\dot{\theta}_{\text{act},k+2} + \dots + \Delta\dot{\theta}_{\text{act},k+n}, \quad (4.68)$$

$$\dot{\theta}_{tu,k+n} = \dot{\theta}_{tu,eq} + \Delta\dot{\theta}_{tu,k+1} + \Delta\dot{\theta}_{tu,k+2} + \dots + \Delta\dot{\theta}_{tu,k+n}, \quad (4.69)$$

where  $n = 1, 2, 3, \dots, N_p$ .

Writing the above mentioned inequalities, (4.65) - (4.67), in matrix form using the relation mentioned in Equations (4.68) - (4.69), yields:

$$\begin{bmatrix} 1 \\ 1 \\ \vdots \\ 1 \end{bmatrix} \dot{\theta}_{act,eq} + \begin{bmatrix} 1 & 0 & \dots & 0 \\ 1 & 1 & \dots & 0 \\ \vdots & \vdots & \vdots & \vdots \\ 1 & 1 & \dots & 1 \end{bmatrix} \begin{bmatrix} \Delta\dot{\theta}_{act,k+1} \\ \Delta\dot{\theta}_{act,k+2} \\ \vdots \\ \Delta\dot{\theta}_{act,k+N_p} \end{bmatrix} \geq \begin{bmatrix} 1 \\ 1 \\ \vdots \\ 1 \end{bmatrix} \dot{\theta}_{tu,eq} + \begin{bmatrix} 1 & 0 & \dots & 0 \\ 1 & 1 & \dots & 0 \\ \vdots & \vdots & \vdots & \vdots \\ 1 & 1 & \dots & 1 \end{bmatrix} \begin{bmatrix} \frac{\Delta\dot{\theta}_{tu,k+1}}{0.95} \\ \frac{\Delta\dot{\theta}_{tu,k+2}}{0.95} \\ \vdots \\ \frac{\Delta\dot{\theta}_{tu,k+N_p}}{0.95} \end{bmatrix}, \quad (4.70)$$

The Equation (4.70) can be further simplified to

$$\begin{bmatrix} 1 \\ 1 \\ \vdots \\ 1 \end{bmatrix} \left( \dot{\theta}_{\text{act,eq}} - \frac{\dot{\theta}_{\text{tu,eq}}}{0.95} \right) + \begin{bmatrix} 1 & 0 & \dots & 0 \\ 1 & 1 & \dots & 0 \\ \vdots & \vdots & \vdots & \vdots \\ 1 & 1 & \dots & 1 \end{bmatrix} \begin{bmatrix} \Delta \dot{\theta}_{\text{act},k+1} - \frac{\Delta \dot{\theta}_{\text{tu},k+1}}{0.95} \\ \Delta \dot{\theta}_{\text{act},k+2} - \frac{\Delta \dot{\theta}_{\text{tu},k+2}}{0.95} \\ \vdots \\ \Delta \dot{\theta}_{\text{act},k+n} - \frac{\Delta \dot{\theta}_{\text{tu},k+Np}}{0.95} \end{bmatrix} \geq 0, \quad (4.71)$$

which can further be written in a shortened notation a

$$\mathbf{E}_1 \dot{\theta}_{\text{eq}} + \mathbf{L}_1 \Delta \Theta \geq 0, \quad (4.72)$$

where

$$\mathbf{E}_1 = \begin{bmatrix} 1 & 1 & \dots & 1 \end{bmatrix}^\top, \quad (4.73)$$

$$\dot{\theta}_{\text{eq}} = \left( \dot{\theta}_{\text{act,eq}} - \frac{\dot{\theta}_{\text{tu,eq}}}{0.95} \right), \quad (4.74)$$

$$\mathbf{L}_1 = \begin{bmatrix} 1 & 0 & \dots & 0 \\ 1 & 1 & \dots & 0 \\ \vdots & \vdots & \vdots & \vdots \\ 1 & 1 & \dots & 1 \end{bmatrix}, \quad (4.75)$$

$$\Delta\Theta = \begin{bmatrix} \Delta\dot{\theta}_{\text{act},k+1} - \frac{\Delta\dot{\theta}_{\text{tu},k+1}}{0.95} \\ \Delta\dot{\theta}_{\text{act},k+2} - \frac{\Delta\dot{\theta}_{\text{tu},k+2}}{0.95} \\ \vdots \\ \Delta\dot{\theta}_{\text{act},k+n} - \frac{\Delta\dot{\theta}_{\text{tu},k+n}}{0.95} \end{bmatrix}. \quad (4.76)$$

Moreover, the matrix  $\Delta\Theta$  can be expanded using the state Equation (4.34) as

$$\begin{bmatrix} \Delta\dot{\theta}_{\text{act},k+1} - \frac{\Delta\dot{\theta}_{\text{tu},k+1}}{0.95} \\ \Delta\dot{\theta}_{\text{act},k+2} - \frac{\Delta\dot{\theta}_{\text{tu},k+2}}{0.95} \\ \vdots \\ \Delta\dot{\theta}_{\text{act},k+N_p} - \frac{\Delta\dot{\theta}_{\text{tu},k+N_p}}{0.95} \end{bmatrix} = \begin{bmatrix} VA_{\text{ag}} \\ VA_{\text{ag}}^2 \\ \vdots \\ VA_{\text{ag}}^{N_p} \end{bmatrix} X_{\text{ag},k} + \begin{bmatrix} VB_{\text{ag}} & 0 & \dots & 0 \\ VA_{\text{ag}}B_{\text{ag}} & VB_{\text{ag}} & \dots & 0 \\ \vdots & \vdots & \vdots & \vdots \\ VA_{\text{ag}}^{N_p-1}B_{\text{ag}} & VA_{\text{ag}}^{N_p-2}B_{\text{ag}} & \dots & VA_{\text{ag}}^{N_p-N_c}B_{\text{ag}} \end{bmatrix} \begin{bmatrix} \Delta u_k \\ \Delta u_{k+1} \\ \vdots \\ \Delta u_{k+N_c-1} \end{bmatrix}, \quad (4.77)$$

where matrix  $V$  is given by,

$$V = \begin{bmatrix} 1 & -\frac{1}{0.95} & 0 & 0 & 0 & 0 & 0 \end{bmatrix}. \quad (4.78)$$

This Equation (4.77) is further represented by a shortened notation as

$$\Delta\Theta = P_1 X_{\text{ag},k} + \Psi \Delta U, \quad (4.79)$$

where

$$P_1 = \left[ VA_{ag} \quad VA_{ag}^2 \quad \dots \quad VA_{ag}^{N_p} \right]^T, \quad (4.80)$$

$$\Psi = \begin{bmatrix} VB_{ag} & 0 & \dots & 0 \\ VA_{ag}B_{ag} & VB_{ag} & \dots & 0 \\ \vdots & \vdots & \vdots & \vdots \\ VA_{ag}^{N_p-1}B_{ag} & VA_{ag}^{N_p-2}B_{ag} & \dots & VA_{ag}^{N_p-N_c}B_{ag} \end{bmatrix}. \quad (4.81)$$

Thus, Equation (4.72) can be written using Equation (4.79) and simplifying further as,

$$-L_1\Psi\Delta U \leq (E_1\dot{\theta}_{eq} + L_1P_1X_{ag,k}). \quad (4.82)$$

In order to implement this constraint as a soft constraint to avoid infeasibility of the optimisation problem, a slack variable is added to allow relaxation to the framed constraint inequality. Thus, rewriting the above Equation (4.82) as

$$-L_1\Psi\Delta U \leq (E_1\dot{\theta}_{eq} + L_1P_1X_{ag,k} + \Phi), \quad (4.83)$$

where  $\Phi$  represents a slack variable relaxing the inequality constraint.

Therefore, the overall constraint inequality can be framed using Equations (4.49),

(4.60) and (4.83) as

$$\begin{bmatrix} M_1 \\ M_2 L \\ -L_1 \Psi \end{bmatrix} \Delta U \leq \begin{bmatrix} \Gamma_1 \\ \Gamma_2 - M_2 E u_{\text{eq}} \\ E_1 \dot{\theta}_{\text{eq}} + L_1 P_1 X_{\text{ag},k} + \Phi \end{bmatrix}, \quad (4.84)$$

## 4.5 Formulation of model predictive control problem

Based on the discussions in sections 4.3 and 4.4, the overall model predictive control problem architecture can be developed as shown in Figure 4.6. Further, for the development of the MPC controller, we can define the attributes of the observed optimisation problem as:

**Cost function:**

$$J = (T_{\text{tu}}^* - T_{\text{tu}})^2 + \Delta U^T \bar{S} \Delta U, \quad (4.85)$$

which is rewritten as

$$J = (T_{\text{tu}}^* - (P X_{\text{ag},k} + H \Delta U))^T Q (T_{\text{tu}}^* - (P X_{\text{ag},k} + H \Delta U)) + \Delta U^T \bar{S} \Delta U, \quad (4.86)$$

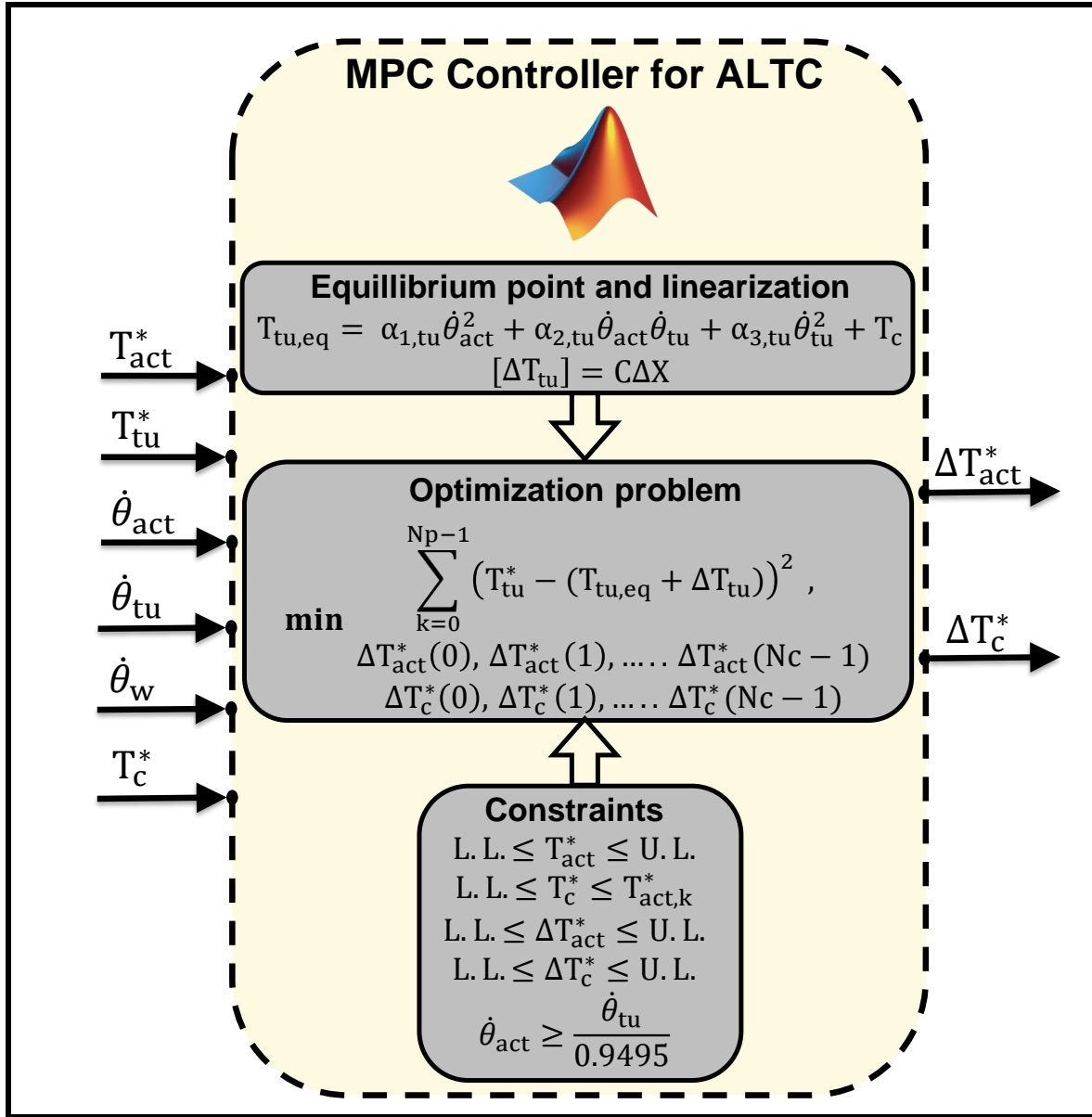


Figure 4.6: Designed MPC architecture for ALTC

and is subjected to **constraints**:

$$M' \Delta U \leq \Gamma, \tag{4.87}$$

where from Equation (4.84)

$$M' = \begin{bmatrix} M_1 & M_2 L & -L_1 \Psi \end{bmatrix}^T, \quad (4.88)$$

$$\Gamma = \begin{bmatrix} \Gamma_1 \\ \Gamma_2 - M_2 E u_{eq} \\ E_1 \dot{\theta}_{eq} + L_1 P_1 X_{ag,k} + \Phi \end{bmatrix}. \quad (4.89)$$

Thus, the overall MPC problem can be formulated as

$$\begin{aligned} \text{minimize} \quad & \sum_k^{k+N_p-1} J(T_{tu}^* - T_{tu}), \\ & \Delta T_{act}^*, \Delta T_c^* \end{aligned} \quad (4.90)$$

such that:

$$M' \Delta U \leq \Gamma. \quad (4.91)$$

For this work, the developed optimisation problem for the MPC was solved using the MATLAB ‘*quadprog*’ function. The developed model was set up for a ‘*Fixed step discrete*’ solver.

### 4.5.1 Results and discussions

The results obtained after the implementation of the discussed MPC control strategy are shown in Figure 4.7. Figure 4.7(b) shows the response of turbine torque for the locked and slipping torque converter cases with and without MPC. The average percentage error for the torques with no control for slipping TC was observed to be 13.0 %, while on implementation of MPC control this error was observed to reduce to 2.1 %, thereby improving the performance by 83.6 %. Conducting a similar analysis for the propeller shaft torque responses, shown in 4.7(c), an improvement of 83.7 % in the propeller shaft torque response was observed, where the controller reduced the percentage error between the locked and slipping torque converter scenario performances from 13.2 % to 2.2 %.

Table 4.4 shows the comparison of the developed anti-lag torque controllers from chapter 3 and chapter 4. The chosen driveline parameters for performance comparison of the two control strategies are the turbine torque and the propeller shaft torque. The error percentages are computed with respect to the locked torque converter performance of the respective parameters.

Comparing the response of the MPC based ALTC with that of the model based feedforward-feedback ALTC discussed in the Chapter 3, the performance of MPC

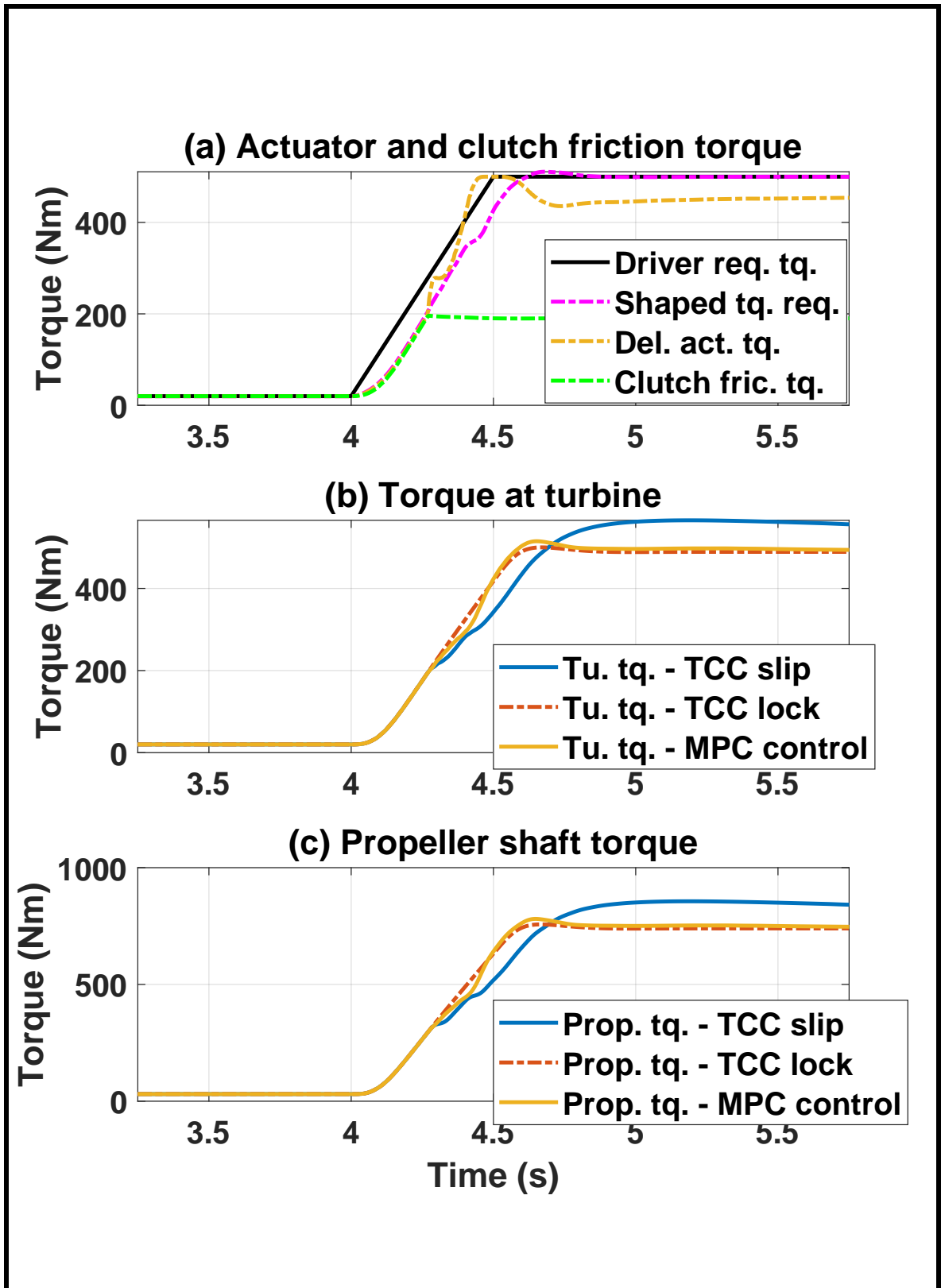


**Figure 4.7:** MPC controlled driveline response for slipping torque converter clutch

**Table 4.4**  
Performance comparison of developed ALTC strategies

Parameter	Error % w.r.t. locked TCC		
	Without ALTC	Model based feedforward-feedback ALTC	MPC based ALTC
Turbine torque	13.03	3.51	2.14
Propeller shaft torque	13.14	3.53	2.16

based ALTC is found to be 15.3 % better. Another important point to note is that adoption to the MPC controlling method overcame the limitation of the model based controller (Chapter 3), where the constraint of torque multiplication mode operation was implemented through saturation blocks and was not included in the control designing strategy. Thus, it can be ascertained that the optimisation of the torque commands from the controller, through model prediction over the system constraints, improved the desired performance of the driveline.

#### 4.5.2 Effect of transient fluid dynamics of torque converter

The torque converter models used in this work are steady state models. However, in this section, the designed controller's response to the torque converter's transient behaviour is discussed. Referring to the studies in [57] and [58], the effect of transient fluid dynamics during the slipping of TCC was analysed using a first order lag induced in the torque converter of FOM. The lag was introduced on the torque transfer through the fluid path, between impeller and turbine of torque converter assembly. Figure 4.8

shows the response of the controller for a torque converter with first order lag, having a 10 ms time constant.

The obtained results are compared for their average error w.r.t. the locked TCC case. The turbine torque shown in Figure 4.8(b) is observed to have an error of 2.3% w.r.t. to locked TCC case. Further, Figure 4.8(c) shows the response comparison of the propeller shaft torque with the locked TCC case. The average error computed in this case is observed to be 2.3 %.

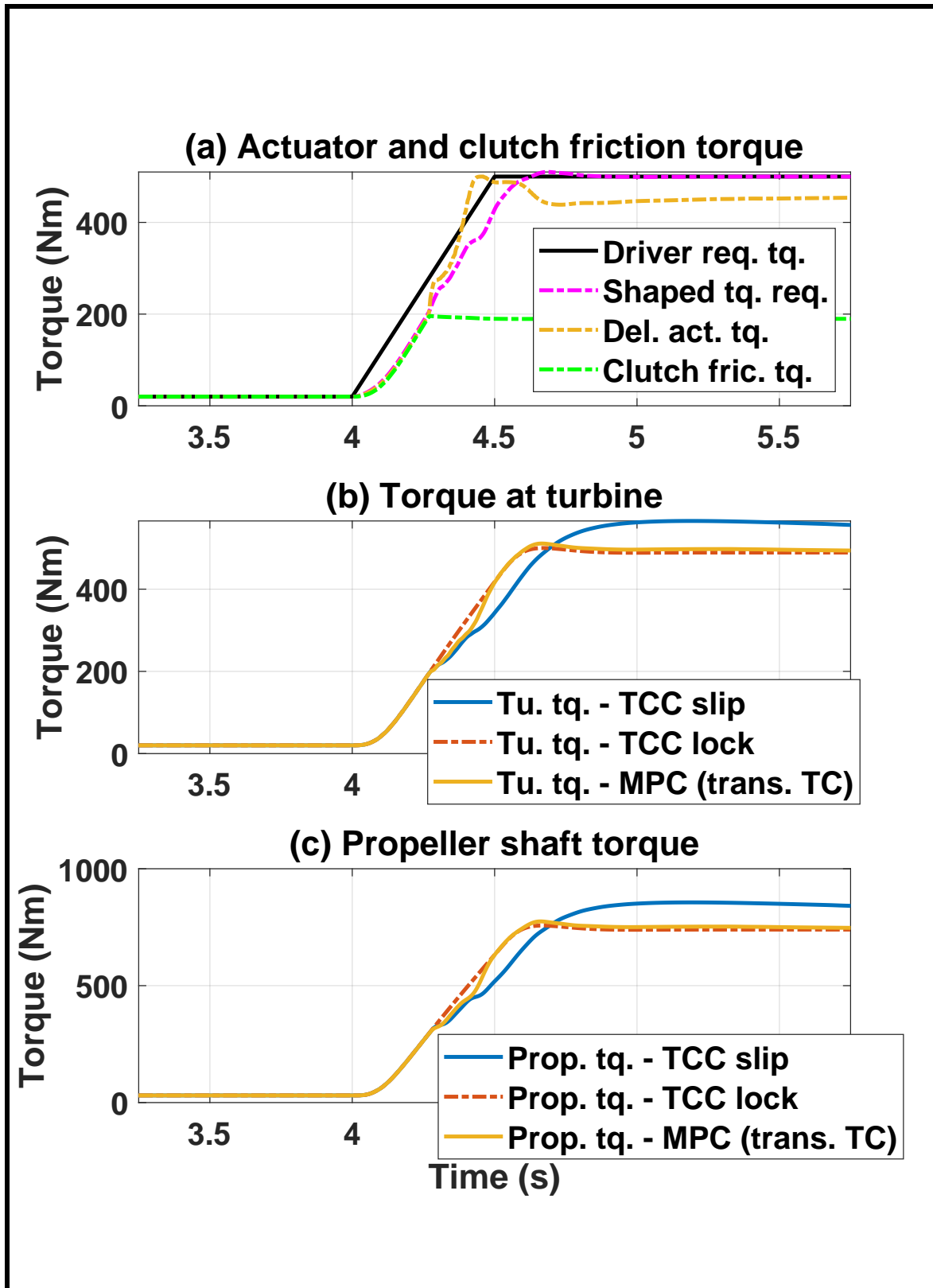


Figure 4.8: MPC response to torque converter with first order transient fluid dynamics

# Chapter 5

## Conclusion and Future Work

### 5.1 Conclusion

The main outcomes from this work are categorised as follows:

1. Design of an Anti-jerk controller (AJC) to control the shuffle oscillations during contact mode tip-in scenarios.
2. Design of a model based feedforward and feedback anti-lag torque controller (ALTC) to meet the shaped driver requested torque overcoming the lag induced in the drivetrain due to the slipping of torque converter lockup clutch.
3. Design of an MPC based controller of TCC capacity and actuator torque to

meet the shaped driver requested torque overcoming the lag induced in the drivetrain due to the slipping of torque converter lockup clutch.

In the following, the main activities and findings are explained

† Design of an AJC to control shuffle oscillations during the torque tip-in from positive to positive actuator torque.

- The Amesim based FOM model developed in [4] was subjected to a positive to positive actuator torque tip-in and the shuffle oscillations in the model were observed through the propeller shaft torque.
- Computationally light state space model for contact mode was developed from the corresponding ROM. In doing so, the equations of motion were realised for the elements of the ROM. The state space model delivered the lumped propeller shaft torque as the output for the actuator torque input. The model was further validated with Amesim based ROM and the propeller shaft torque torques were observed to comply within an average error of 1.3%.
- The state space model was used to develop the plant transfer function with actuator torque command as input and lumped propeller shaft torque as the output. The prepared transfer function was then used to study the frequency response of the plant. The bode plot showed the shuffle

frequency of the drivetrain plant.

- A pre-compensator and feedback controller based control strategy was designed for positive to positive torque tip-ins in contact mode, in order to address the shuffle oscillations in the drivetrain. The TCC was considered locked for this case to specifically address the shuffle oscillations. The pre-compensator was realised as a butterworth low-pass filter. The step response of a plant transfer function having shaft torque derivative as the output to the commanded actuator torque input was analysed in combination with multiple butterworth low-pass filters. The butterworth filters for this analysis were developed for multiple combinations of pass band and stop band frequencies. Further, to improve the rise time response of the pre-compensator, a zero was added to the filter.
- The poles and zeros of the plant transfer function were obtained to find the lightly damped poles responsible for shuffle oscillations in the plant. To add damping to these poles in the closed loop performance of the plant, the feedback controller was realised as a lead compensator. The lead compensator was developed such that the compensator's zero and pole added damping to the closed loop performance of the plant.
- Transfer function for pre-compensator and lead compensator based controller was obtained. This transfer function was representative of the commanded actuator torque as output and the negative propeller shaft torque

derivative as input. The controller performance was subjected to bode plot analysis and a dip in the magnitude plot of frequency response was observed. This dip was found to be in the range of the shuffle frequency of the drivetrain plant.

- The developed controller was further subjected to a Processor-in-the-loop (PIL) based evaluation where its performance was found to be in good agreement with the simulated results. The error between the generated results from the two sources was found to be within 0.6 %.

† Design of a model-based feedforward and feedback ALTC to meet the shaped driver requested torque overcoming the torque lag due to slipping TCC

- For a contact mode positive to positive torque tip-in request, the TCC was made to slip and the lag in the torque delivery at the turbine and propeller shaft was observed through the FOM. A control strategy for the ALTC was designed and Implemented in MATLAB/Simulink with co-simulation in Amesim. The development process of the controller was divided into three phases.

- \* In the first phase, a state space model representing the driveline with locked TCC was developed. The turbine speed was realised as the required output from the model. Further, the state space model was validated for its output with the FOM model. The average prediction error in the turbine speeds from the state space model and the FOM

was computed to be 2.2%.

\* In the second phase, the inversion of torque converter model was performed to generate a reference impeller speed signal for a known fluid path torque and turbine speed. In this phase, two inverted torque converter models were developed, first was based on the K-factor lookup table model and second was based on the Kotwicki's quadratic equation model. The approximated Kotwicki model for the torque multiplication mode was developed using the tabulated data of K-factor lookup table model. Later, the outputs from the two models were compared for validation of Kotwicki model that was chosen for reference impeller speed generation.

\* In the third phase, the controller was developed to track the reference impeller speed generated from the inverted torque converter model. In the developed controller, feedforward and feedback path torques were formulated. The feedforward path torque was obtained from the torque converter model equations and the feedback path torque was generated through a proportional integrator (PI) controller.

– The controller was able to improve the propeller shaft torque performance reducing the average error w.r.t. locked TCC, from 13.1% (with no ALTC implementation) to 3.5% (with ALTC implementation). Later, a limitation of the controller was analysed where it was not aware of the actuator

constraints while generating the output actuator torque command.

† Design of a model predictive ALTC controller of TCC capacity and actuator torque to deliver requested torque during TCC slip.

- The earlier developed ROM for contact mode was modified with addition of torque converter and the rotational inertia was redistributed across it. The outputs of ROM and FOM were compared and found in good agreement with an average error of 0.1% between the propeller shaft torques.
- The equations of motion were analysed for the modified ROM that included the nonlinear torque equations of the fluid path torque. The equations were linearised at the equilibrium point. The equilibrium point was found at each sampling time step and linearization was done at that point. A state space model was developed using the linearised equations. Further, for known equilibrium points, the outputs of the linear model were compared with the nonlinear model.
- A prediction model development algorithm was set-up based on the linearised state space model for the known equilibrium point. For setting up the prediction model, the linearised model was augmented. Further, based on the prediction model, an unconstrained optimisation problem was set-up and analyzed.
- The constraints on the magnitude of actuator torque and clutch capacity and on their respective delivery rates were established over the control

horizon. Another soft constraint on the model impeller and turbine speeds was set-up to ensure the operation of the torque converter in torque multiplication mode.

- An optimisation problem was set-up with prediction model subjected to the framed constraints. The problem was framed in the form of a quadratic equation and MATLAB's 'quadprog' function was used for its solution.
  
- The results of the controller performance were discussed. The MPC based controller overcome the propeller shaft torque lag by 83.7% when compared with no ALTC implementation for TCC slipping. Further, the performance of the MPC based ALTC was found to be 15.3% better than the model based feedforward and feedback ALTC controller in overcoming the torque lag at propeller shaft.
  
- The controller's performance with the transient behaviour of the torque converter fluid dynamics was discussed. A first order lag was introduced between the impeller and turbine of the torque converter model. The average error of the turbine torque and propeller shaft torque w.r.t. the locked TCC case was found to be within 2.3% and so the two torques were observed to be in good agreement with the controller performance for steady state torque converter.

## 5.2 Future work

The work presented through this thesis shall further be subjected to the proposed future works listed below:

- † The designed controller is to be experimentally validated on either a test bed in a laboratory or on an actual vehicle.
- † The AJC controller developed in this work is for the contact mode. Its collaboration with the developed backlash mode controller is to be considered in future.
- † The development of the ALTC control strategies are based on the approximated Kotwicki model developed for the torque multiplication mode. However, for the robust implementation of the controller, the Kotwicki model is to be approximated for the fluid coupling mode as well. This would further require to update and evaluate the Amesim model of the torque converter.
- † The ALTC developed based on the model prediction is to be worked upon in future to frame the optimisation problem covering multiple objective functions.
- † Robustness analysis of the MPC based ALTC for different torque ramp rates, different TCC slipping stages, etc., can be performed.

# References

- [1] Organisation Internationale des Constructeurs d'Automobiles (OICA), 2019. Sales of passenger cars in selected countries worldwide from 2005 to 2019. <https://www.statista.com/statistics/257660/passenger-car-sales-in-selected-countries/>. Accessed on 26 July 2020, [Online].
- [2] Bureau of Economic Analysis, 2019. U.S. light truck retail sales from 1980 to 2019. <https://www.statista.com/statistics/199980/us-truck-sales-since-1951/>. Accessed on 24 January 2020, [Online].
- [3] Lakhani, P., 2017. "Modeling and analysis for driveline jerk control". Tech. rep. Michigan Technological University.
- [4] Reddy, P., 2018. "Control oriented modeling of an automotive drivetrain for anti-jerk control". Master's thesis, Michigan Technological University.
- [5] Darokar, K. K., 2019. "Automotive driveline backlash state and size estimator

- design for Anti-Jerk Control”. Master’s thesis, Michigan Technological University.
- [6] Muller, D., 2019. Light trucks take a record 69 % of U.S. market. <https://www.autonews.com/sales/light-trucks-take-record-69-us-market>. Accessed on 25 January 2020, [Online].
- [7] National Center for Environmental Economics, 2009. “Evaluating the consumer response to fuel economy: A review of the literature”. Tech. Rep. 2168-2018-8113.
- [8] Choksey, J. S., 2019. The 7 Criteria for Car Buying. <https://www.autotrader.com/car-shopping/7-criteria-car-buying-281474979927978>. Accessed on 22 January 2020, [Online].
- [9] List, H. O., and Schoeggl, P., 1998. “Objective evaluation of vehicle driveability”. SAE Technical Paper No. 980204.
- [10] Sandberg, U., Goubert, L., and Mioduszewski, P., 2010. “Are vehicles driven in electric mode so quiet that they need acoustic warning signals”. In 20th International Congress on Acoustics. Sydney, Australia.
- [11] Hertzke, P., Müller, N., Schaufuss, P., Schenk, S., and Wu, T., 2019. Expanding electric-vehicle adoption despite early growing pains. <https://www.mckinsey.com/industries/automotive-and-assembly/our-insights/expanding-electric-vehicle-adoption-despite-early-growing-pains>. Accessed on 24 January 2020, [Online].

- [12] Higashimata, A., Adachi, K., Segawa, S., Kurogo, N., and Waki, H., 2004. “Development of a slip control system for a lock-up clutch”. SAE Technical Paper No. 2004-01-1227.
- [13] Kono, K., Itoh, H., Nakamura, S., Yoshizawa, K., and Osawa, M., 1995. “Torque converter clutch slip control system”. SAE Technical Paper No. 950672.
- [14] Krenz, R., 1985. “Vehicle response to throttle tip-in/tip-out”. pp. 45–52. SAE Technical Paper No. 850967.
- [15] Lagerberg, A., 2001. “A literature survey on control of automotive powertrains with backlash”. *Technical report no R013/2001; Department of Signals and Systems, Chalmers University of Technology, Gothenburg, Sweden*, pp. 1–15.
- [16] Lagerberg, A., and Egardt, B., 2002. “Evaluation of control strategies for automotive powertrains with backlash”. In 6th International Symposium on Advanced Vehicle Control. Hiroshima, Japan.
- [17] Lagerberg, A., and Egardt, B., 2003. “Estimation of backlash with application to automotive powertrains”. In 42nd IEEE International Conference on Decision and Control, Vol. 5, IEEE, pp. 4521–4526.
- [18] Lagerberg, A., and Egardt, B., 2005. “Model predictive control of automotive powertrains with backlash”. In IFAC Proceedings Volumes, Vol. **38**, pp. 1–6.
- [19] Lagerberg, A., and Egardt, B., 2007. “Backlash estimation with application to

- automotive powertrains”. *IEEE Transactions on Control Systems Technology*, **15**(3), pp. 483–493.
- [20] Templin, P., and Egardt, B., 2009. “An LQR torque compensator for driveline oscillation damping”. In 2009 IEEE Control Applications(CCA) & Intelligent Control(ISIC), IEEE, pp. 352–356.
- [21] Templin, P., and Egardt, B., 2011. “A powertrain LQR-torque compensator with backlash handling”. *Oil & Gas Science and Technology–Revue d’IFP Energies nouvelles*, **66**(4), pp. 645–654.
- [22] Karikomi, T., Itou, K., Okubo, T., and Fujimoto, S., 2006. “Development of the shaking vibration control for electric vehicles”. In 2006 SICE-ICASE International Joint Conference, IEEE, pp. 2434–2439.
- [23] Kawamura, H., Ito, K., Karikomi, T., and Kume, T., 2011. “Highly-responsive acceleration control for the Nissan Leaf electric vehicle”. pp. 1–6. SAE Technical Paper No. 2011-01-0397.
- [24] Ravichandran, M., Doering, J., Johri, R., and Ruybal, K., 2020. “Design and evaluation of ev drivetrain clunk and shuffle management control system”. In 2020 American Control Conference (ACC), IEEE, pp. 4905–4912.
- [25] Baumann, J., Swarnakar, A., Kiencke, U., and Schlegl, T., 2005. “A robust controller design for anti-jerking”. SAE Technical Paper No. 2005-01-0041.

- [26] Baumann, J., Torkzadeh, D. D., Ramstein, A., Kiencke, U., and Schlegl, T., 2006. “Model-based predictive anti-jerk control”. *Control engineering practice*, **14**(3), pp. 259–266.
- [27] Formentini, A., Oliveri, A., Marchesoni, M., and Storace, M., 2016. “A switched predictive controller for an electrical powertrain system with backlash”. *IEEE Transactions on Power Electronics*, **32**(5), pp. 4036–4047.
- [28] Reddy, P., Darokar, K., Robinette, D., Shahbakhti, M., Ravichandran, M., and Doering, J., 2020. “Backlash size estimation in automotive drivelines”. In 2020 IEEE Conference on Control Technology and Applications (CCTA), IEEE.
- [29] Darokar, K., Reddy, P., Furlich, J., Robinette, D., Shahbakhti, M., Ravichandran, M., and Doering, J., 2020. “Automotive backlash position estimator for driveline jerk control”. In 2020 IEEE Conference on Control Technology and Applications (CCTA), IEEE.
- [30] Ishihara, T., and Emori, R. I., 1966. “Torque converter as a vibration damper and its transient characteristics”. SAE Technical Paper No. 660368.
- [31] Hrovat, D., and Tobler, W., 1985. “Bond graph modeling and computer simulation of automotive torque converters”. *Journal of the Franklin Institute*, **319**(1-2), pp. 93–114.
- [32] Tsangarides, M., and Tobler, W., 1985. “Dynamic behavior of a torque converter with centrifugal bypass clutch”. SAE Technical Paper No. 850461.

- [33] Adibi Asl, H., Azad, N. L., and McPhee, J., 2011. “Math-based modeling and parametric sensitivity analysis of torque converter performance characteristics”. SAE Technical Paper No. 2011-01-0732.
- [34] Lee, J.-H., 2017. “Control oriented modeling of dynamic torque converter system”. In 2017 7th International Conference on Modeling, Simulation, and Applied Optimization (ICMSAO), IEEE, pp. 1–5.
- [35] Pohl, B., 2003. “Transient torque converter performance, testing, simulation and reverse engineering”. SAE Technical Paper No. 2003-01-0249.
- [36] Kotwicki, A. J., 1982. “Dynamic models for torque converter equipped vehicles”. SAE Technical Paper No. 820393.
- [37] Hebbale, K., Lee, C., Samie, F., Kao, C.-K., Chen, X., Horgan, J., and Hearld, S., 2011. “Model based torque converter clutch slip control”. SAE Technical Paper No. 2011-01-0396.
- [38] Mishra, K. D., and Srinivasan, K., 2017. “On-line identification of a torque converter model”. *IFAC-PapersOnLine*, **50**(1), pp. 4763–4768.
- [39] Cho, D., and Hedrick, J. K., 1989. “Automotive powertrain modeling for control”. *Journal of dynamic systems, measurement and control*, **111**(4), pp. 568–576.
- [40] Adibi Asl, H., Lashgarian Azad, N., and McPhee, J., 2012. “Modeling torque

- converter characteristics in automatic drivelines: lock-up clutch and engine braking simulation”. In International Design Engineering Technical Conferences and Computers and Information in Engineering Conference, American Society of Mechanical Engineers, pp. 359–367.
- [41] Adibi Asl, H., 2014. ““Acausal powertrain modelling with application to model-based powertrain control””. PhD thesis, University of Waterloo.
- [42] Li, J., and Wang, X., 2008. “Study on transfer function and dynamic characteristic of hydraulic converter”. In 2008 IEEE Vehicle Power and Propulsion Conference, IEEE, pp. 1–5.
- [43] Yang, B., Keqiang, L., Ukawa, H., and Handa, M., 2006. “Modelling and control of a non-linear dynamic system for heavy-duty trucks”. *Proceedings of the Institution of Mechanical Engineers, Part D: Journal of Automobile Engineering*, **220**(10), pp. 1423–1435.
- [44] Qin, S. J., and Badgwell, T. A., 2003. “A survey of industrial model predictive control technology”. *Control Engineering Practice*, **11**(7), pp. 733–764.
- [45] Atabay, O., Ötkür, M., and Ereke, İ. M., 2018. “Model based predictive engine torque control for improved drivability”. *Proceedings of the Institution of Mechanical Engineers, Part D: Journal of Automobile Engineering*, **232**(12), pp. 1654–1666.
- [46] Wang, Y., and Sun, Z., 2015. “Optimal slip control of a torque converter clutch”.

In Dynamic Systems and Control Conference, Vol. 57267, American Society of Mechanical Engineers, p. V003T41A002.

- [47] Bemporad, A., Bernardini, D., Livshiz, M., and Pattipati, B., 2018. “Supervisory model predictive control of a powertrain with a continuously variable transmission”. SAE Technical Paper No. 2018-01-0860.
  
- [48] Bemporad, A., Bernardini, D., Long, R., and Verdejo, J., 2018. “Model predictive control of turbocharged gasoline engines for mass production”. SAE Technical Paper No. 2018-01-0875.
  
- [49] Raut, A., Irdmoussa, B. K., and Shahbakhti, M., 2018. “Dynamic modeling and model predictive control of an RCCI engine”. *Control Engineering Practice*, **81**, pp. 129–144.
  
- [50] Caruntu, C. F., Balau, A. E., Lazar, M., van den Bosch, P., and Di Cairano, S., 2011. “A predictive control solution for driveline oscillations damping”. In Proceedings of the 14th international conference on Hybrid systems: computation and control, pp. 181–190.
  
- [51] Caruntu, C. F., Balau, A. E., Lazar, M., Bosch, P. P., and Di Cairano, S., 2016. “Driveline oscillations damping: A tractable predictive control solution based on a piecewise affine model”. *Nonlinear Analysis: Hybrid Systems*, **19**, pp. 168–185.

- [52] Reddy, P., Darokar, K., Robinette, D., Shahbakhti, M., Blough, J., Ravichandran, M., Farmer, M., and Doering, J., 2019. “Control-oriented modeling of a vehicle drivetrain for shuffle and clunk mitigation”. SAE Technical Paper No. 2019-01-0345.
- [53] Hage, A., Szatkowski, A., and Li, Z., 2007. “Improving low frequency torsional vibrations NVH performance through analysis and test”. SAE Technical Paper No. 2007-01-2242.
- [54] Hahn, J.-O., and Lee, K.-I., 2002. “Nonlinear robust control of torque converter clutch slip system for passenger vehicles using advanced torque estimation algorithms”. *Vehicle System Dynamics*, **37**(3), pp. 175–192.
- [55] Wang, L., 2009. *Model predictive control system design and implementation using MATLAB®*. Springer Science & Business Media. Chapter 1 and 2.
- [56] Maciejowski, J. M., 2002. *Predictive control with constraints*. Prentice Hall. Chapter 1 and 2.
- [57] Lee, J.-H., and Lee, H., 2004. “Dynamic simulation of nonlinear model-based observer for hydrodynamic torque converter system”. SAE Technical Paper No. 2004-01-1228.
- [58] Tugcu, A., Hebbale, K., Alexandridis, A., and Karmel, A., 1986. “Modeling and simulation of the powertrain dynamics of vehicles equipped with automatic

transmission". In Proceedings of Symposium on Simulation of Ground Vehicles and Transportation Systems, ASME Winter Annual Meeting, no. 2, pp. 39–61.

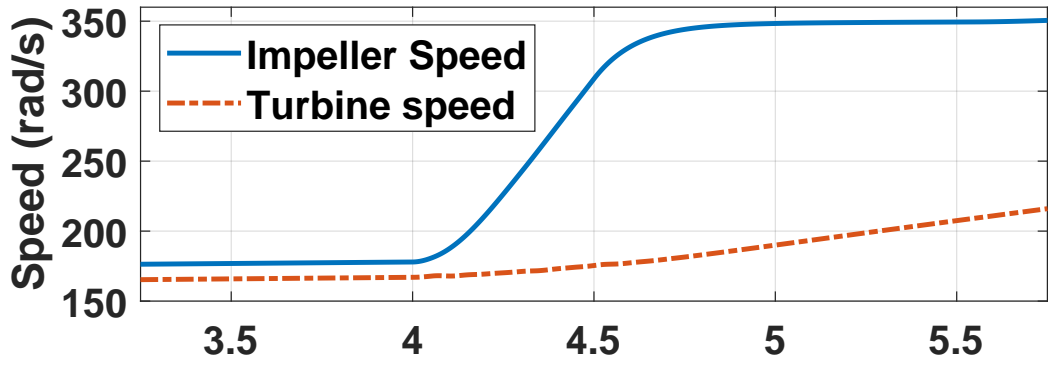
# Appendix A

## Validation of Kotwicki Model

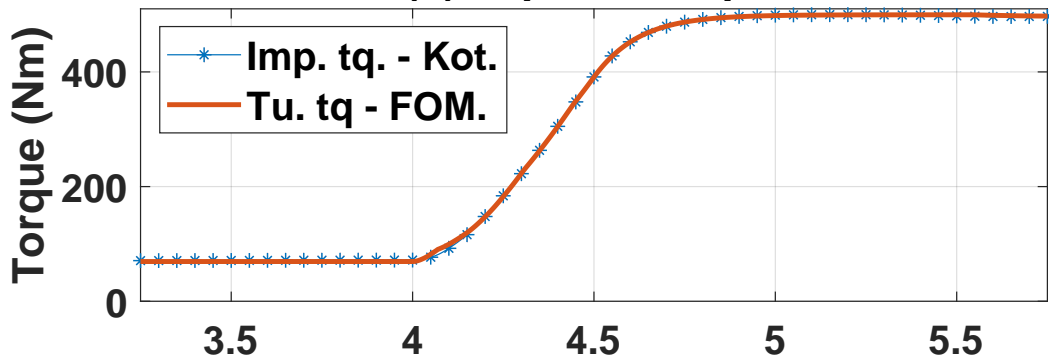
This section shows the validation of the obtained Kotwicki Model for different test cases. While developing the model, the Amesim FOM was used to run the torque converter for slipping mode and required signals were recorded. The torque inputs were so chosen such that the operation of torque converter was ensured in the torque multiplication mode. Table A.1 provides the details for the test cases that were used to record the Amesim FOM impeller and turbine speeds signals for the estimation of Kotwicki coefficients. The test cases were so chosen to cover maximum range of torque converter's operation.

For the obtained results for Kotwicki model coefficients, Table A.2 tabulates the percentage average error obtained for the different test cases.

(a) Impeller and turbine speeds  
(known dataset)



(b) Impeller torque



(c) Turbine torque

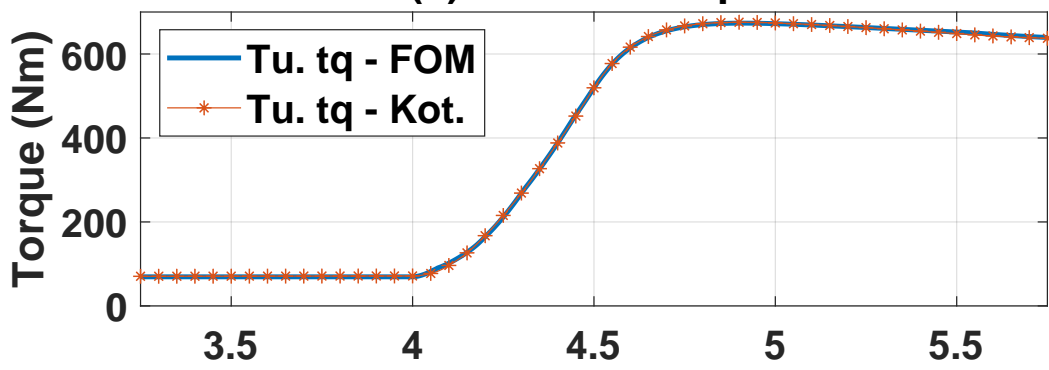


Figure A.1: Results obtained for Test-case:1

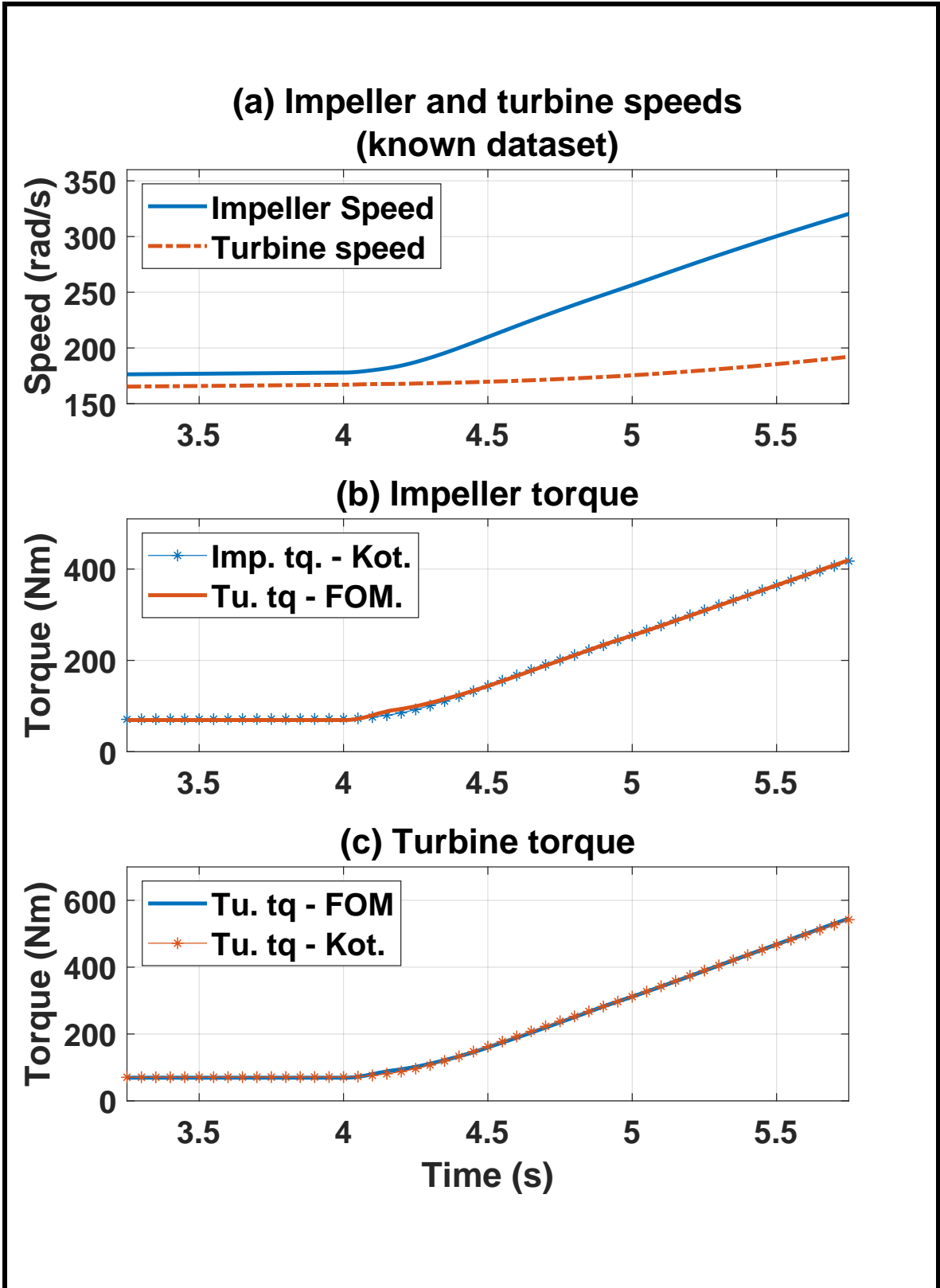


Figure A.2: Results obtained for Test-case:2

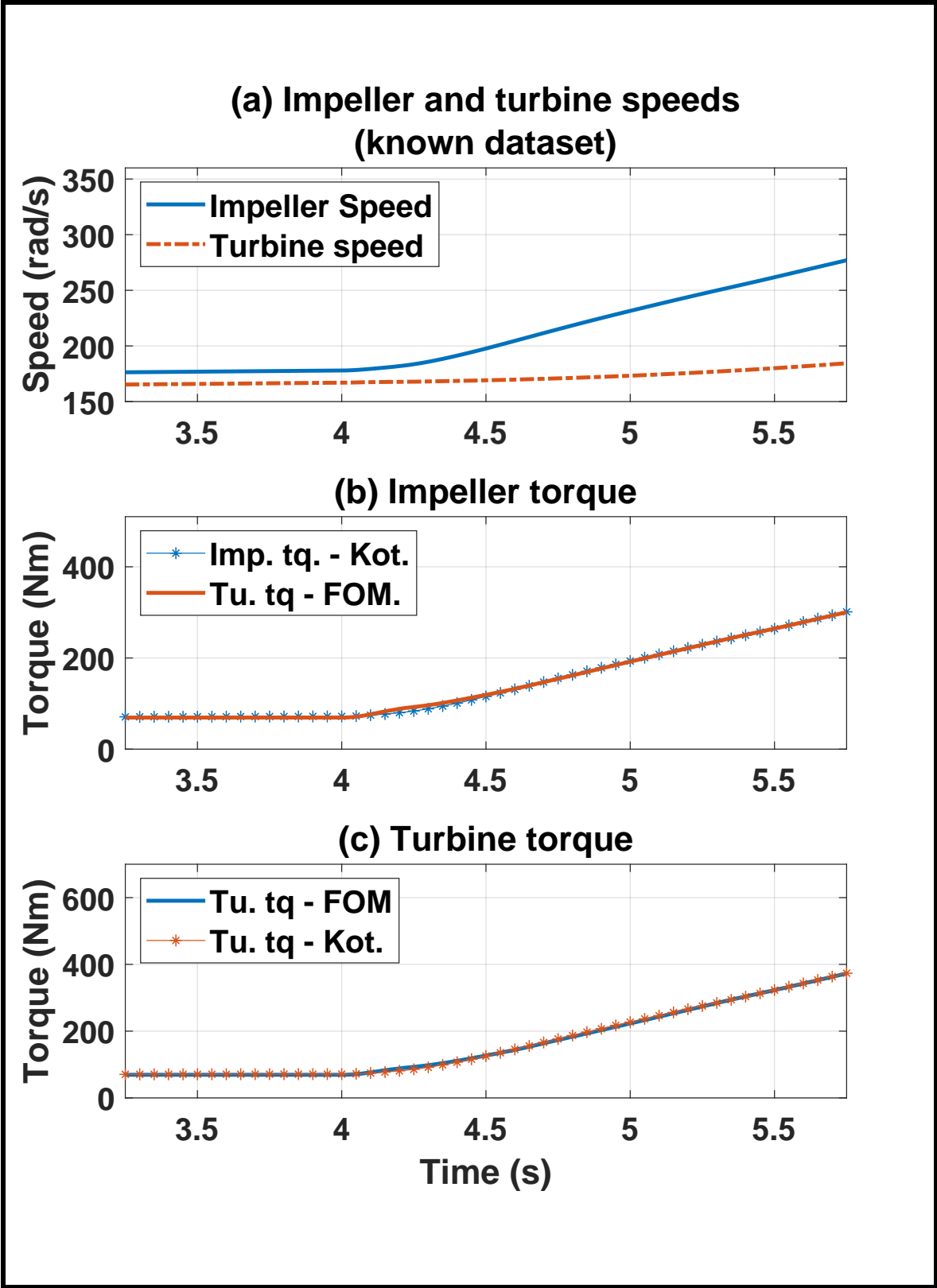


Figure A.3: Results obtained for Test-case:3

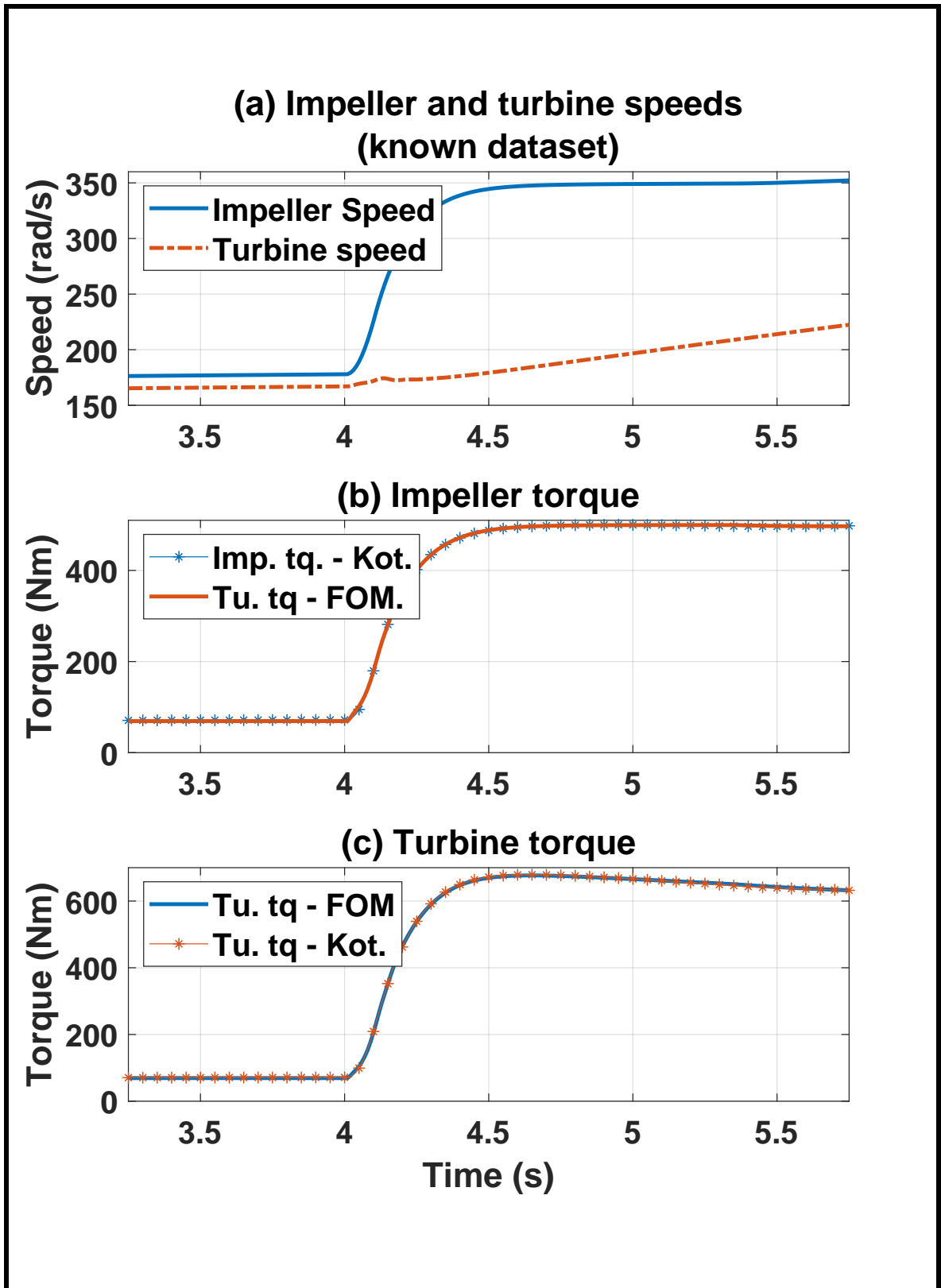


Figure A.4: Results obtained for Test-case:4

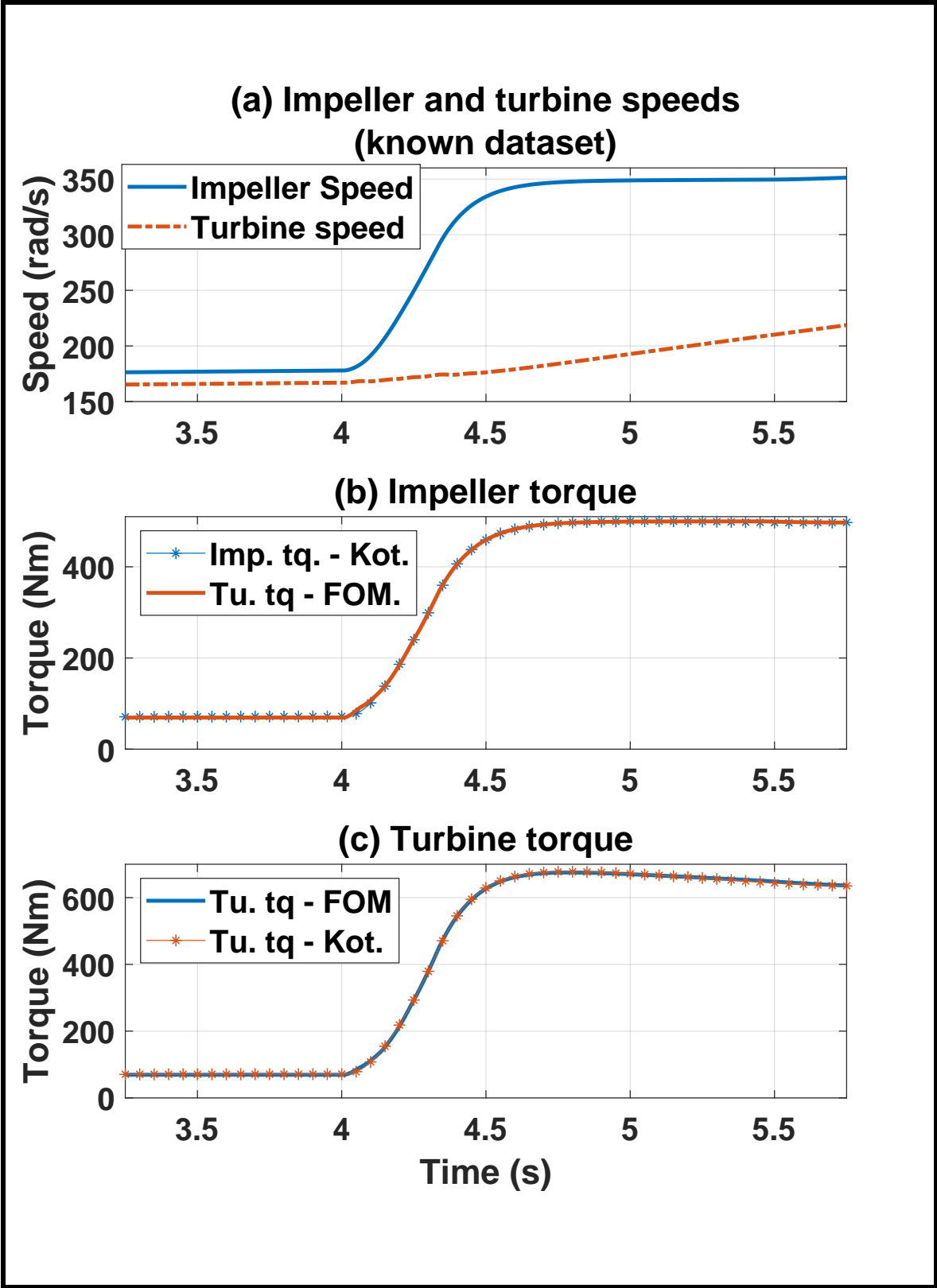


Figure A.5: Results obtained for Test-case:5

**Table A.1**

Test cases considered for Kotwicki model validation

<b>Test case No.</b>	<b>Torque input (Nm)</b>	<b>Torque rate (<math>\frac{\text{Nm}}{\text{s}}</math>)</b>
Test case 1	70 - 500	860
Test case 2	70 - 500	215
Test case 3	70 - 500	143
Test case 4	70 - 500	4300
Test case 5	70 - 500	1300

**Table A.2**

Percentage error observed for the Kotwicki model for different test cases

<b>Test case</b>	<b>Error % w.r.t. FOM results</b>	
	<b>Impeller torque</b>	<b>Turbine torque</b>
Test case 1	1.2	1.1
Test case 2	2.3	2.1
Test case 3	2.8	2.6
Test case 4	0.9	0.9
Test case 5	1.2	1.1



# Appendix B

## Software Versions

The software versions used for running the discussed simulation models in this work are mentioned in Table B.1.

**Table B.1**  
Software versions

<b>Software</b>	<b>Version</b>
MATLAB	R2018a (Version: 9.4.0.802882)
Simulink	R2018a (Version: 9.1)
Simcenter Amesim	Version: 2019.1
Operating system	Windows 10



# Appendix C

## Program and Data File Summary

This section lists the figure files, model files, script files, and data sets used to generate the results shown in this work.

### C.1 Chapter 1

**Table C.1**  
Figure files - Chapter 1

<b>File Name</b>	<b>File Description</b>
Fig_1_1.pdf	Figure 1.1
Fig_1_2.pdf	Figure 1.2
Fig_1_3.vsdX	Figure 1.3
Fig_1_4.vsdX	Figure 1.4
Fig_1_5.pdf	Figure 1.5
Fig_1_6.vsdX	Figure 1.6

## C.2 Chapter 2

This section contains model file and data files details in context of the contact mode

AJC designed in chapter 2.

**Table C.2**  
Figure files - Chapter 2

<b>File Name</b>	<b>File Description</b>
Fig_2_1.fig	Figure 2.1
Fig_2_2.vsdX	Figure 2.2
Fig_2_3.fig	Figure 2.3
Fig_2_4.pdf	Figure 2.4
Fig_2_5.fig	Figure 2.5
Fig_2_6.fig	Figure 2.6
Fig_2_7.fig	Figure 2.7
Fig_2_8.pdf	Figure 2.8
Fig_2_9.fig	Figure 2.9
Fig_2_10.fig	Figure 2.10
Fig_2_11.pdf	Figure 2.11
Fig_2_12.fig	Figure 2.12

**Table C.3**  
Simulink and Amesim model files - Chapter 2

<b>File Name</b>	<b>File Description</b>
AJC_contact_mode_test_cases.slx	Simulink model file with contact mode AJC with FOM and ROM
Vehicle_Model_trials_mod_lumpedbl_new_TCslip.ame	Full Order Model Amesim file
Driveline_model_ROM_with_TC_for_slip.ame	Reduced Order Model Amesim file

**Table C.4**  
Matlab script and dataset files - Chapter 2

File Name	File Description
PnLC_with_motor_dynamics_plot_for_PC_design.m	Matlab script file for contact mode AJC design
Pre_lead_compensators.mat	Dataset with pre and lead compensator

### C.3 Chapter 3

Relevant program and data files in context of chapter 3 are mentioned in this section:

**Table C.5**  
Figure files - Chapter 3

File Name	File Description
Fig_3_1.fig	Figure 3.1
Fig_3_2.vsdX	Figure 3.2
Fig_3_3.pdf	Figure 3.3
Fig_3_4.vsdX	Figure 3.4
Fig_3_5.fig	Figure 3.5
Fig_3_6.pdf	Figure 3.6
Fig_3_7.pdf	Figure 3.7
Fig_3_8.pdf	Figure 3.8
Fig_3_9.pdf	Figure 3.9
Fig_3_10.pdf	Figure 3.10
Fig_3_11.pdf	Figure 3.11
Fig_3_12.fig	Figure 3.12
Fig_3_13.fig	Figure 3.13
Fig_3_14.pdf	Figure 3.14
Fig_3_15.pdf	Figure 3.15
Fig_3_16.fig	Figure 3.16
Fig_3_17.fig	Figure 3.17
Fig_3_18.fig	Figure 3.18

**Table C.6**  
Simulink and Amesim model files - Chapter 3

File Name	File Description
TC_check_ch3_running_with_overall_results.slx	Simulink model file with model based feedforward and feedback controller
Vehicle_Model_trials_mod_lumpedbl_new_TCslip.ame	Full Order Model Amesim file
TC_check_ch3_PIL_cleaned_rate_transition_RTI.slx	PIL oriented simulink model
ROM_contactmode_TCC_updated.ame	PIL oriented Amesim model file

**Table C.7**  
Matlab script and dataset files - Chapter 3

File Name	File Description
TC_Turbine_torque_control_dvp.m	Matlab script file for state space model design
Pre_lead_compensators.mat	Dataset with pre and lead compensator
SR_TR_and_Kcap.mat	Dataset with capacity factor, torque ratio and speed ratio table

## C.4 Chapter 4

This section contains the description of model files used in the model predictive controller design approach in chapter 4.

**Table C.8**  
Figure files - Chapter 4

File Name	File Description
Fig_4_1.pdf	Figure 4.1
Fig_4_2.vsd	Figure 4.2
Fig_4_3.fig	Figure 4.3
Fig_4_4.fig	Figure 4.4
Fig_4_5.fig	Figure 4.5
Fig_4_6.pdf	Figure 4.6
Fig_4_7.fig	Figure 4.7
Fig_4_8.fig	Figure 4.8

**Table C.9**  
Simulink and Amesim model files - Chapter 4

File Name	File Description
MPC_model.check.slx	Simulink model file with MPC algorithm
MPC_model.check_TClag.slx	Simulink model file with MPC for transient Torque Converter
Vehicle_Model_trials_mod_lumpedbl_new_TCslip.ame	FOM Amesim file
Driveline_model_ROM_with_TC_for_slip.ame	ROM Amesim file
Vehicle_Model_trials_mod_lumpedbl_new_TCslip_TCLAG.ame	FOM Amesim file with first-order torque converter lag

**Table C.10**  
Matlab script and dataset files - Chapter 4

<b>File Name</b>	<b>File Description</b>
meas_vals_Linearization_check_visual_TC_MPC.mat	Dataset for equilibrium point values
Pre_lead_compensators.mat	Dataset with pre and lead compensator
unconstrained_opt_for_givn_eqbm_pt.m	Matlab code for unconstrained optimisation at known equilibrium points
Linearization_check_visual_TC_MPC.m	Matlab code for comparison of nonlinear output with linear model at equilibrium